

Finite Temperature Decay Rates and Thermal Field Theory

Studying the Behaviour of Thermal Systems in a Freeze-in Singlet Model

Bror Amund Flaten Hjemgaard

Theoretical Physics
60 ECTS study points

Department of Physics
Faculty of Mathematics and Natural Sciences

Spring 2023



Bror Amund Flaten Hjemgaard

Finite Temperature Decay Rates and Thermal Field Theory

Studying the Behaviour of Thermal Systems in a
Freeze-in Singlet Model

Supervisor:
Torsten Bringmann

Til Gomor, Gofar, Mormor og Bestefar.

Abstract

In the continuous endeavour to understand the origin of the paradoxically abundant substance known as *dark matter*, there are few particle theories who dominate the spotlight quite as much as the proposed mechanisms of *freeze-out* and *freeze-in*. Since freeze-in concerns processes within high-temperature plasmas in the early universe, it becomes critical to accurately account for the detailed thermal behaviour of in-medium effects. The following thesis studies one of these effects; namely that of resonant intermediate particle production.

Specifically, we consider the effects of intermediate Higgs bosons going on-shell in a scalar singlet model of dark matter. The question becomes, how do we distinguish internal Higgs bosons that go briefly on-shell from the physical Higgs bosons that are already present in the surrounding plasma? To address this, we turn to the *Breit-Wigner* scheme and use thermal quantum field theory to derive the *Breit-Wigner decay rate*, Γ_{BW} , at finite temperatures.

We show how to calculate two-loop corrections to Γ_{BW} for both final-state scalars and fermions. Through this, we establish several useful notions of how to perform higher-order thermal loop calculations – both analytically and numerically.

Although an expression for Γ_{BW} already exists in the literature, we show that our result corrects the existing one at leading order and beyond. We argue that the origin of these discrepancies lies in the conventional freeze-in/out collision operators featuring an inherently non-field-theoretical thermal structure. As such, we propose a new collision operator which is calculable through thermal quantum field theory.

Additionally, we present a new approach to real-time thermal quantum field theory. It is derived through an extension of a superselection rule from zero to finite temperatures and results in the same generating functional and observables as a conventional approach. It completely avoids the Keldysh contour while naturally explaining the origin of the doubling of degrees of freedom one encounters in real-time thermal field theory.

Preface

This thesis represents the work done by me for a Master of Science degree in theoretical physics, totalling 60 ECTS credits. I have aimed to write at a level accessible to a second year master’s student, while referring to existing literature whenever a more comprehensive description is needed. The [Reference Guide](#) gives an overview over the sources most relevant to this thesis. All figures are made by me.

I had a lot of fun writing this thesis! It is written from the perspective of someone exploring and uncovering the curious world of thermal physics for the first time, and I have tried to convey that feeling of discovery and curiosity.

Although filled with trials and tribulations, the past 2 – 3 years has been made ever more enjoyable due to the continuous support and insight from my supervisor, Prof. Torsten Bringmann – thank you for helping me de-stress during this very intense period, for grounding me when I get too excited, for teaching me proper L^AT_EX etiquette and for sharing with me your seemingly unlimited physical intuition and teaching me dimensional analysis. I would also like to lend a personal thanks to Nils Johannes Mikkelsen for endless late-night discussions regarding “the box” and for proofreading my thesis, to Carl Martin Fevang for teaching me that energy is not a vector and to the rest of the theory section at the University of Oslo for letting me partake in both the smartest and the dumbest conversations of my life.

During my 5 years at the University of Oslo, I always felt like at home due to the extraordinary community garnered by “Lillefy” and “Fysikkforeningen” – as an expression of my gratitude I have donated to you my 3D-printer. May it never stop printing. Of course, the largest thanks goes out to my wonderful, unconditionally supportive and silly parents – thank you for never giving up on me! Lastly, a thanks to my friends Maia Oline Wirgenes and Magnus Rønning who both demanded to be mentioned in my thesis.

Oslo
June 2023

Bror Amund Flaten Hjemgaard

Contents

1	Introduction	1
1.1	Thesis Overview	2
1.2	Notations and Conventions	3
2	Background	4
2.1	Dark Matter Relic Density	4
2.1.1	Qualitative Evolution	5
2.1.2	Freeze-out	6
2.1.3	Freeze-in	7
2.2	The Higgs Portal and Resonance	9
3	Breit-Wigner Decay Rates	15
3.1	Stable Particles and Their Mass	15
3.2	Unstable Particles and Their Mass	18
3.2.1	Determining $\bar{\epsilon}$	20
3.3	The Breit-Wigner Decay Rate	21
3.4	Rates at Finite Temperatures	23
4	Thermal Field Theory	27
4.1	Superselection Rules	27
4.1.1	SSR and CPT	30
4.2	Finite Temperature	31
4.2.1	The Thermal BW Decay Rate	34
4.3	Thermal Propagators	35
4.3.1	The Thermal BW Propagator	38
4.4	Cutting Rules at Finite Temperature	38
4.5	Thermal Quantum Field Theory	43
4.6	What is Cutting?	45
5	Calculating Decay Rates at $T \geq 0$	48
5.1	One-Loop Order	48
5.1.1	Different Final States: $\psi_1 \neq \psi_2$	48

5.1.2	Identical Final States: $\psi_1 = \psi_2$	51
5.2	Two-Loop Order	52
5.2.1	Vertex Corrections	52
5.2.2	Self-Energy Corrections	53
5.3	Numerical Calculations	55
5.3.1	Results	58
6	Discussion	63
6.1	The Many Formalisms of Thermal Quantum Field Theory	63
6.2	Understanding Rates	66
6.3	Branch versus Sector	68
6.4	Contextualizing Applications	69
6.4.1	Applying the BW Rate	70
6.4.2	The Collision Operator	71
7	Final Remarks	74
7.1	Summary of Work	74
7.2	Review of Key Results	75
7.3	Further Work	76
	Appendices	78
A	The Optical Theorem	78
A.1	Zero Temperature	78
A.2	Finite Temperature	79
B	Scalar Two-loop Vertex Calculations	81
B.1	Contributions from $\text{Re}\{\mathcal{N}_1\}$	82
B.2	Contributions from $\text{Re}\{\mathcal{N}_3\}$	83
C	Fermionic Two-loop Self-Energy Calculations	85
D	Regularization & Renormalization at Finite Temperature	87
E	Imaginary-Time Thermal Quantum Field Theory	91
F	Deriving Conventional Phase SpaceSuppressions	93
	References and Bibliography	96
	Reference Guide	96
	Bibliography	97

Chapter 1

Introduction

Out of the numerous challenges facing modern physics, few have been as elusive as the questions regarding the nature of dark matter (DM). The earliest hints towards the existence of this invisible substance were based on discrepancies between observed orbital velocities in galaxies compared to the amount of visible matter [1, 2]. Today there exists a plethora of sophisticated experimental evidence for dark matter on cosmological scales [3–8], like observations of large-scale structures and the cosmic microwave background, to name a few. Despite a scientific consensus of DM existence, extensive evidence and comprehensive experimental and theoretical endeavours, the questions of both the nature and origin of DM still remain unanswered. Some of the only qualities we can say for certain that DM possesses are:

- (i) Except through gravity, DM does not interact noticeably with Standard Model (SM) particles or itself.
- (ii) DM is stable on cosmological timescales [9].
- (iii) The DM must be “cold”, i.e. non-relativistic, in order to allow for the observed structures of today [10, 11].
- (iv) The DM *relic abundance* is large: $\Omega_{\text{DM}}h^2 = 0.120 \pm 0.001$ [6].

Although one can certainly appreciate the difficulties of trying to describe a substance subject to these restrictions, the search for a comprehensive DM model has not been a lost cause. For example, even though the DM conundrum is based in cosmological observations, this has not prevented the development of sophisticated models of DM as a particle theory. Since cosmological observations have previously been helpful in determining questions in particle physics, like constraining the masses and number of neutrino species in the Standard Model [12], a hope is that the accurately measured dark matter relic density may be used to address critical questions about physics beyond the Standard Model.

Of the numerous particle explanations for DM production, few have garnered as much attention as the *freeze-out* mechanism [13] and the *freeze-in* mechanism [14]. We will go into much more detail about them in Chapter 2, but their underlying idea is that DM belongs

to an “invisible sector” of particles which coupled noticeably with the visible SM sector in the early, hot universe. As space expanded and the universe cooled, these sectors eventually decoupled and the DM density “froze” at a constant value, which we today measure to be $\Omega_{\text{DM}}h^2 = 0.120 \pm 0.001$ [6].

Though the freeze-out scheme originally garnered much attention due to the so-called “WIMP miracle” [15], a lack of experimental evidence of freeze-out has recently shifted much of the focus onto the freeze-in mechanism [16–20]. Since the freeze-in process generally happens at much larger temperatures than freeze-out, the detailed high-temperature behaviour of the thermal medium (the *plasma*) itself must be properly accounted for. This will be the main focus of this thesis, as we show how to adapt the notion of a *Breit-Wigner decay rate* to finite temperatures, and use it to account for resonant *s*-channel behaviour of intermediate unstable Higgs bosons in a DM scalar singlet model of freeze-in [21–23].

Although the finite-temperature Breit-Wigner (BW) rate has previously been derived in the literature [23], this thesis presents an alternate approach based in thermal quantum field theory which gives corrections to the existing expression.

1.1 Thesis Overview

We begin Chapter 2 by introducing the necessary background. This includes an introduction to both the freeze-out and freeze-in mechanisms, and illustrations of how to apply them through the Boltzmann equation. We then show how to derive the BW decay rate found in ref. [23], which will serve as a benchmark for the BW decay rate we then set out to derive for ourselves.

In Chapter 3, we define the founding principles of the BW scheme by deriving the BW decay rate at zero temperature before extending these ideas to finite temperatures, $T > 0$. Since the BW rate will be used to account for resonant behaviour of unstable particles, Chapter 3 focuses on viewing the BW scheme through the lens of resonance and instability. Lastly, we show how the concept of a “decay rate” must be altered when working within a plasma compared to at zero temperature.

The goal of Chapter 4 is to calculate the BW decay rate at finite temperatures. We start out by considering quantum field theory (QFT) at $T = 0$: We show how the introduction of a superselection rule to the states satisfying the on-shell requirement $p^2 = m^2$ can be used to calculate decay rates at zero temperature. By extending this superselection rule to $T > 0$, we show how to perform the same calculations at finite temperatures, and use this to derive a master formula, Eq. (4.77), for the BW decay rate in a plasma. In a new heuristic approach to thermal field theory, we use this superselection rule to derive the entire formalism of real-time thermal QFT and associated concepts like the Kubo-Martin-Schwinger condition [24, 25], finite temperature cutting rules [26–28] and the doubling of degrees of freedom in the real-time formalism [29, 30].

In Chapter 5, we show that our master formula, Eq. (4.77), gives corrections to the results of ref. [23] at leading order (LO) in the case of final-state particles of different masses. At next-to-leading order (NLO) and beyond, our result are fundamentally different from

theirs. In Section 5.3 we perform numerical two-loop calculations of the BW decay rate.

We discuss our results in Chapter 6, and address the analytical aspects of our approach. Here, we show that our approach to real-time thermal QFT reproduces the results of Weldon [31], and we discuss what is “wrong” with the derivation of the BW rate in ref. [23]. Using the insight gained from this discussion, we conclude the chapter by proposing a new field-theoretic collision operator, Eq. (6.13), to be used in freeze-in/out calculations. Finally, we present our conclusions and an outlook in Chapter 7.

1.2 Notations and Conventions

We will use natural units:

$$c = \hbar = k_B \equiv 1, \quad (1.1)$$

i.e. $c = 299792458 \text{ m} \cdot \text{s}^{-1} = 1$, $\hbar = h/2\pi = 1.054572 \times 10^{-34} \text{ m}^2 \cdot \text{s}^{-1} \cdot \text{kg} = 1$ and $k_B = 1.380649 \times 10^{-23} \text{ m}^2 \cdot \text{s}^{-2} \cdot \text{kg} \cdot \text{K}^{-1} = 1$. In this system, the mass of a particle is equal to its rest energy, and

$$[\text{time}] = [\text{length}] = [\text{energy}]^{-1} = [\text{mass}]^{-1} = [\text{temperature}]^{-1}. \quad (1.2)$$

Energy will be given in electronvolts (eV), wherein $1 \text{ eV} = 1.60218 \times 10^{-19}$ joules.

The conventions for the tensors used in this thesis are

- 3-vectors are written in lower case boldface, \mathbf{v} , and 3-vector components as v^i (Latin indices).
- 4-vectors are written in lower case, p , with components $p^\mu = (p_0, \mathbf{p})$ (Greek indices).
- Matrix components are denoted $M_{\mu\nu}$ (Latin or Greek indices).

We use the $(+, -, -, -)$ signature such that the product between four-vectors is denoted $p \cdot q \equiv g^{\mu\nu} p_\mu q_\nu = p_0 q_0 - \mathbf{p} \cdot \mathbf{q}$.

Since position, x^μ , and momentum, p^μ , are conjugate variables under the Fourier transform, the Fourier transformed of a spatial function $F(x)$ will implicitly be denoted $F(p)$. In d dimensions, this becomes

$$F(p) = \int d^d x F(x) e^{ip \cdot x} \quad \text{and} \quad F(x) = \int \frac{d^d p}{(2\pi)^d} F(p) e^{-ip \cdot x}. \quad (1.3)$$

The *unit step function* (also known as the *Heaviside function*) and the *sign function* are defined as

$$\theta(x) \equiv \begin{cases} 1 & x \geq 0, \\ 0 & x < 0, \end{cases} \quad \text{and} \quad \epsilon(x) \equiv \begin{cases} +1 & x > 0, \\ -1 & x < 0, \end{cases}, \quad (1.4)$$

respectively.

Chapter 2

Background

In this chapter, we outline the relevant background for the remainder of the thesis; primarily that of dark matter production in an expanding universe, the freeze-out and freeze-in mechanisms and the scalar singlet model [21, 22, 32–34]. Then, by utilizing the Boltzmann equation and following the procedure outlined by ref. [23], we show how to implement the freeze-in process for a scalar singlet model and how to derive their expression for the BW decay rate, will serve as a benchmark for our own derivation in later chapters.

We will not go into extensive detail about the thermal and statistical aspects of the background material. For a more detailed introduction to these topics, please refer to the [Reference Guide](#).

2.1 Dark Matter Relic Density

Here, we show the procedure for calculating the DM relic density, $\Omega_{\text{DM}}h^2$, through the *Boltzmann equation*:

$$\frac{d}{dt}(a^3 n_\chi) = a^3 C[f_\chi], \quad (2.1)$$

where χ is a DM particle, $C[f_\chi]$ is the *collision operator* for all processes that do not conserve the number of χ particles, a is the *scale factor*¹ and n_χ is the DM number density which is related to the DM phase space density, f_χ , through

$$n_\chi(t) = \int d\Pi_p f_\chi(p, t), \quad (2.2)$$

for $d\Pi_p$ being the phase space measure which accounts for all physical degrees of freedom. The quantity $a^3 n_\chi(t)$, which appears on the LHS of the Boltzmann equation in Eq. (2.1), is known as the *comoving* DM number density, and accounts for the number of particles

¹For example, $a = 0$ corresponds to an infinitely dense, singular universe, while $a \rightarrow \infty$ to a universe where curvature and matter becomes negligible.

present in a region of expanding spacetime. On the RHS of the Boltzmann equation, we have the collision operator

$$C[f_\chi] = -\langle\sigma_{\text{ann}}v\rangle(n_\chi^2 - n_{\chi,\text{eq}}^2), \quad (2.3)$$

where $\langle\sigma_{\text{ann}}v\rangle$ is the velocity averaged total DM annihilation cross-section and $n_{\chi,\text{eq}}$ is the DM number density in equilibrium (found by integrating Eq. (2.6)). We can actually re-write the Boltzmann equation of Eq. (2.1) into a more convenient form by introducing the unitless parameter $x \equiv m_\chi/T$ as a measurement of time in an expanding (and cooling) universe and defining the *Hubble rate* as $H \equiv \frac{1}{a} \frac{da}{dt}$, giving:

$$\frac{dY_\chi}{dx} = \frac{-sx}{H} \langle\sigma_{\text{ann}}v\rangle (Y_\chi^2 - Y_{\chi,\text{eq}}^2), \quad (2.4)$$

where $s \propto a^{-3}$ is the DM entropy density, and we changed variables to the DM *abundance* $Y_\chi \equiv n_\chi/s$. If this is integrated up to $x \rightarrow \infty$, we get the DM abundance of today, Y_χ^0 , which is related to the observable DM relic density through

$$\Omega_{\text{DM}} h^2 = 2.755 \times 10^{10} \frac{m_\chi}{100\text{GeV}} \frac{2}{N_\chi} Y_\chi^0, \quad (2.5)$$

where $N_\chi = 2$ (1) for self-conjugate (not self-conjugate) DM particles [23].

2.1.1 Qualitative Evolution

By simply studying the Boltzmann equation, we can actually say a lot about the qualitative evolution of $n_\chi(x)$. We start by noting the phase space distribution of a thermalized particle

$$f_{\chi,\text{eq}}(\omega) \equiv \frac{1}{e^{\omega/T} - \varepsilon_\chi}, \quad (2.6)$$

where ω is the χ -energy measured in the plasma rest frame and $\varepsilon_A \equiv +1(-1)$ if A is a boson (fermion). From Eq. (2.2), it follows that the number density in a thermalized (equilibrium) system, $n_{\chi,\text{eq}}(x)$, decreases exponentially as temperature decreases, as illustrated by the red line in Figure 2.1. Next, from the collision operator in Eq. (2.3), the Boltzmann equation in Eq. (2.1) tells us that $n_{\chi,\text{eq}}$ acts as an “attractor” – if $n_\chi^2 > n_{\chi,\text{eq}}^2$, the comoving density decreases, while if $n_\chi^2 < n_{\chi,\text{eq}}^2$, it increases. Since $n_{\chi,\text{eq}}(x)$ eventually decreases exponentially as x increases, it follows (regardless of initial conditions) that $n_\chi(x)$ is always an upper bounded function and that its bound decreases as x grows. The size of the RHS of Eq. (2.1) is therefore doomed to diminish as x grows. Depending on the size of $\langle\sigma_{\text{ann}}v\rangle$, the RHS of Eq. (2.1) eventually vanishes compared to the LHS.² The point at which the RHS starts to vanish compared to the LHS is called the point of “chemical decoupling”, x_f . At x_f , the change in $a^3 n_\chi$ quickly ceases and the comoving density becomes constant, i.e. “frozen”. The

²To be more accurate, this argument is actually made by writing the LHS of Eq. (2.1) as $a^3 \dot{n}_\chi + 3H n_\chi$ and comparing the scale of H to the RHS.

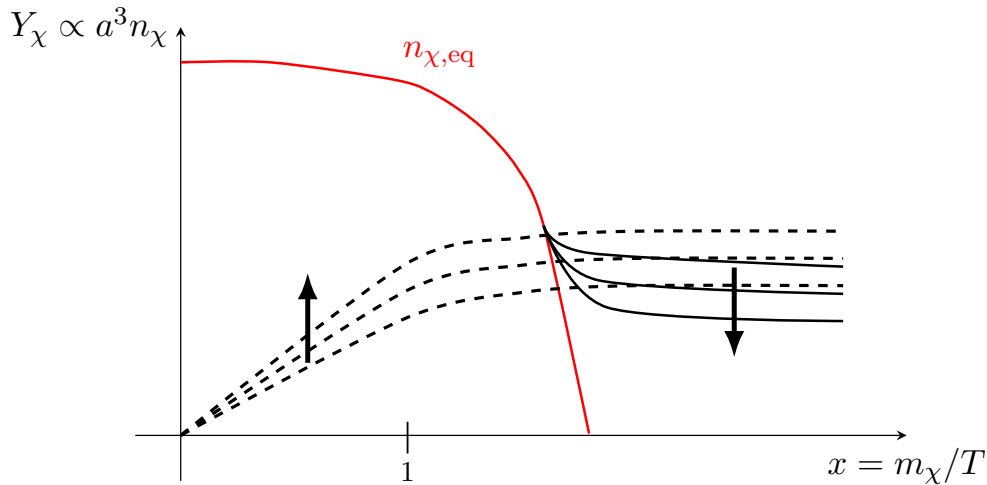


Figure 2.1: Qualitative illustration of DM comoving number densities as a function of x . The red line shows the evolution of the equilibrium density, which eventually decreases exponentially. The freeze-out process is illustrated by the solid lines: The dark sector starts out in equilibrium and follows the equilibrium curve until the point of chemical decoupling, whereafter it freezes. In freeze-in (as illustrated by the dashed line), the DM starts out with a negligible number density, but since DM is produced via the visible sector, the density is slowly drawn towards equilibrium. Before it manages to equilibrate, chemical decoupling happens – freezing the DM value. For both the freeze-out and freeze-in curves, the arrows indicate the effect of increasing the cross-section $\langle\sigma_{\text{ann}}v\rangle$.

Boltzmann equation therefore predicts that the DM density of an expanding and cooling universe necessarily freezes at a constant value.

This is an inevitable quality of a thermal system in a cooling universe and has nothing to do with the inherent properties of the system in question. We have made no assumptions about the particle populations, their detailed interaction picture, energy scales or even the initial conditions on n_χ , yet the comoving density necessarily freezes. This is the origin behind the naming of *freeze-out* and *freeze-in*, and the primary difference between the two processes are simply which assumptions they make regarding the initial value of $n_\chi(x)$ and the size of the SM-DM coupling g .

2.1.2 Freeze-out

In the freeze-out scheme, it is assumed that in the early, hot universe, the SM sector the DM sector were in thermal equilibrium, i.e. $n_\chi = n_{\chi,\text{eq}}$. Since equilibrium acts as an “attractor”, the comoving DM density therefore initially followed the red curve in Figure 2.1. Per the analysis in the previous subsection, the larger the cross-section $\langle\sigma_{\text{ann}}v\rangle$, the later the unavoidable point of chemical decoupling. This means that for larger SM-DM couplings,

$n_\chi(x)$ stays on the equilibrium curve longer before it freezes – as illustrated by the arrow and solid lines in Figure 2.1. By comparing to the observed DM relic density, one can determine a value for the SM-DM coupling g .

It turns out that if one lets g and m_χ be on the scale of the weak force, then even the simplest of freeze-out models predict a DM relic density within the order of magnitude of the observed value [35]. This explanation of the relic density through a freeze-out process and weakly interacting massive particles (WIMPs) is known as the *WIMP-miracle* and has served as a large motivating factor for the freeze-out mechanism. The WIMP-miracle has sparked a large scale search for so-called “WIMP candidates” as any particle theory that featured WIMPs could seemingly get DM production for free. Unfortunately, a null-result from direct, indirect and collider WIMP searches has cast doubt on the applicability of freeze-out [15, 16]. Although initially promising, the freeze-out mechanism has yet to prevail as the *de facto* explanation of DM production.

2.1.3 Freeze-in

Originally proposed as an alternative to freeze-out [14], the freeze-in mechanism has proven itself as a worthy candidate in the pursuit of the DM origin. In the freeze-in scheme, it is assumed that the DM density in the very early universe is negligibly small; $n_\chi \ll n_{\chi,\text{eq}}$, to the point where we can take $n_\chi \approx 0$ at early times. Additionally, one assumes that the SM and DM sectors couple so feebly that they were never in equilibrium.³ These two assumptions imply that the dominating process in the early universe, although feeble, is $\text{SM} \rightarrow \text{DM}$. This causes the DM density to increase, as shown by the dashed lines in Figure 2.1. The larger $\langle\sigma_{\text{ann}}v\rangle$ is, the faster the DM density will increase, as indicated by the arrow on the dashed lines in Figure 2.1. For small enough cross-sections, the RHS of Eq. (2.1) vanishes *before* DM manages to reach equilibrium; freezing the density earlier than in a typical freeze-out process. For this reason, DM produced via freeze-in is usually warmer than that produced via freeze-out.

In the cases where the SM-DM coupling g (and hence, $\langle\sigma_{\text{ann}}v\rangle$) is *not* small enough, the DM density may actually manage to reach equilibrium before x_f , effectively putting it back on the freeze-out path. It is therefore imperative that g is sufficiently small for the freeze-in scheme to be applicable. Due to the feeble strength at which the two sectors couple, the DM particles within the freeze-in scheme are referred to as feebly interacting massive particles (FIMPs).

In many ways, freeze-in can be viewed as the opposite process to freeze-out. For example, as illustrated in Figure 2.1, increasing g will give a smaller freeze-out relic abundance, but a larger freeze-in abundance. Additionally, freeze-out is not dependent on the conditions of the DM prior to the freeze mechanism due to thermal equilibrium, while freeze-in assumes the initial condition $n_\chi = 0$. Furthermore, due to the small x at which freeze-in production (mostly) happens, the freeze-in scheme is often highly sensitive to large temperatures [36,

³From the anisotropies of the CMB, it has been confirmed that the visible sector indeed was in thermal equilibrium with itself at early times [12], but there is no such evidence to suggest the same for the dark sector.

37]. As previously stated, in-medium plasma corrections become especially relevant at these temperatures, and accounting for such corrections will be the main focus of this thesis.

In order to illustrate the implementation of a freeze-in process, we will initially be following the procedure outlined in ref. [23]. In Section 6.4 we will present an alternative approach. The DM production processes of interest in ref. [23] are those of $2 \rightarrow 2$ processes $\psi\psi \rightarrow \chi\chi$, where ψ and χ are SM and DM particles, respectively.⁴ We take the two DM particles to have the on-shell 4-momenta $p^\mu = (E_{\mathbf{p}}, \mathbf{p})$ and $p'^\mu = (E'_{\mathbf{p}}, \mathbf{p}')$ and the SM particles to have $k^\mu = (E_{\mathbf{k}}, \mathbf{k})$ and $k'^\mu = (E'_{\mathbf{k}}, \mathbf{k}')$. The collision operator then takes the form [23]

$$C[f_\chi] = \frac{1}{N_\psi} \int d\Pi_{\text{tot}} (2\pi)^4 \delta^{(4)}(p + p' - k - k') \times \left[|\mathcal{M}_{\psi\psi \rightarrow \chi\chi}|^2 f_\psi(E_{\mathbf{k}}) f_\psi(E'_{\mathbf{k}}) \left(1 + \tilde{f}_\chi(E_{\mathbf{p}})\right) \left(1 + \tilde{f}_\chi(E'_{\mathbf{p}})\right) - |\mathcal{M}_{\chi\chi \rightarrow \psi\psi}|^2 f_\chi(E_{\mathbf{p}}) f_\chi(E'_{\mathbf{p}}) \left(1 + \tilde{f}_\psi(E_{\mathbf{k}})\right) \left(1 + \tilde{f}_\psi(E'_{\mathbf{k}})\right) \right], \quad (2.7)$$

where we have defined, for the sake of neatness,

$$d\Pi_{\text{tot}} \equiv \frac{d^3\mathbf{p}}{(2\pi)^3 2E_{\mathbf{p}}} \frac{d^3\mathbf{p}'}{(2\pi)^3 2E'_{\mathbf{p}}} \frac{d^3\mathbf{k}}{(2\pi)^3 2E_{\mathbf{k}}} \frac{d^3\mathbf{k}'}{(2\pi)^3 2E'_{\mathbf{k}}} \quad (2.8)$$

and $\tilde{f}_i \equiv \varepsilon_i f_i$, where f_i denotes the thermal phase space distribution of a particle i and $N_\psi = 2(1)$ if ψ is self-conjugate (not self-conjugate). We have also adopted a convention which sums over all internal degrees of freedom in the matrix elements. The second line in Eq. (2.7) accounts for the production of χ while the third subtracts the χ annihilation. The factors f and $(1 + \tilde{f})$ implement the statistical in-medium effects of Pauli blocking and Bose enhancement.

Since the SM bath is thermalized, ψ follows a Bose-Einstein or Fermi-Dirac distribution:

$$f_\psi(\omega) = \frac{1}{e^{\omega\beta} - \varepsilon_\psi}, \quad (2.9)$$

where $\beta \equiv 1/T$ and ω is the particle energy measured in the plasma rest frame. Though we do not know the distribution of the DM, the freeze-in scheme lets us infer that

1. $f_\chi \ll 1$: The DM phase space density remains very small.⁵
2. $f_\chi \ll g$: The DM abundance stays sub-thermal.

⁴In the case of fermion fields, we of course substitute for the appropriate conjugate fields.

⁵Recall $f_\chi = 0$ for very early times.

Collectively, these assertions let us set $f_\chi = 0$ in Eq. (2.7), giving:

$$C_{\text{freeze-in}}[f_\chi] = \frac{1}{N_\psi} \int d\Pi_{\text{tot}} (2\pi)^4 \delta^{(4)}(p + p' - k - k') |\mathcal{M}_{\psi\psi \rightarrow \chi\chi}|^2 f_\psi(E_{\mathbf{k}}) f_\psi(E'_{\mathbf{k}}). \quad (2.10)$$

Hence, the collision operator in the freeze-in regime is independent of the DM phase space distribution. Eq. (2.10) is distinguishably different from the form of the general collision operator, cf. Eq. (2.7), and since the latter is a more studied scenario, it would allow for a more model-independent implementation of the freeze-in collision operator if we could rewrite $C_{\text{freeze-in}}[f_\chi]$ in a way similar to a typical collision operator.

Ref. [23] proposes a solution to this predicament. It starts by employing the rewrite

$$f_\psi(E_{\mathbf{k}}) f_\psi(E'_{\mathbf{k}}) = f_\chi^{\text{MB}}(E_{\mathbf{p}}) f_\chi^{\text{MB}}(E'_{\mathbf{p}}) (1 + \tilde{f}_\psi(E_{\mathbf{k}})) (1 + \tilde{f}_\psi(E'_{\mathbf{k}})), \quad (2.11)$$

where we have defined the *Maxwell-Boltzmann* distribution $f_i^{\text{MB}}(\omega) \equiv \exp(-\omega\beta)$. Then, assuming CP invariance, $|\mathcal{M}_{\psi\psi \rightarrow \chi\chi}|^2 = |\mathcal{M}_{\chi\chi \rightarrow \psi\psi}|^2$, the freeze-in collision operator can be written as

$$C_{\text{freeze-in}}[f_\chi] = \frac{(2\pi)^4}{N_\psi} \int d\Pi_{\text{tot}} \delta^{(4)}(p + p' - k - k') |\mathcal{M}_{\chi\chi \rightarrow \psi\psi}|^2 f_\chi^{\text{MB}}(E_{\mathbf{p}}) f_\chi^{\text{MB}}(E'_{\mathbf{p}}) (1 + \tilde{f}_\psi(E_{\mathbf{k}})) (1 + \tilde{f}_\psi(E'_{\mathbf{k}})). \quad (2.12)$$

Comparing this to the third line of Eq. (2.7), we note that this collision operator takes the form of (minus) the contribution from DM annihilation to a collision operator where the DM follows a Maxwell-Boltzmann distribution. In other words, the conventional freeze-in scheme in Eq. (2.10) is equivalent to studying the collision operator for DM annihilation where the DM follows a Maxwell-Boltzmann distribution. Moving forward, we will therefore be working with Eq. (2.12).

2.2 The Higgs Portal and Resonance

So far, we have made very few assumptions – not even a model has been specified. Since a Lagrangian is required to calculate $|\mathcal{M}_{\chi\chi \rightarrow \psi\psi}|^2$, this is about to change.

Still following the approach of ref. [23], we will primarily concern ourselves with processes mediated by a *Higgs portal* – a scheme wherein the SM and DM sectors are linked via the Higgs field. One way of realizing a Higgs portal is through what is called a *scalar singlet DM model* [21, 22, 32–34]. This model follows from a pretty general setting wherein the dark sector contains a stable (obeying a \mathbb{Z}_2 symmetry) real singlet scalar, S . Since the Lagrangian contains all (renormalizable) terms obeying the symmetries of the theory, we necessarily have

$$\mathcal{L} \supset -\frac{1}{2} \mu_S^2 S^2 - \frac{1}{2} \lambda_{hS} S^2 |H|^2, \quad (2.13)$$

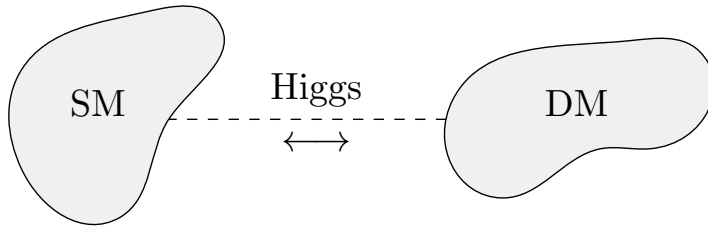


Figure 2.1: The idea behind the Higgs portal, where the Higgs field acts as a mediator between the two otherwise disconnected SM and DM sectors. The concept of “portals” and mediators connecting otherwise disconnected sectors is not unique to the scalar singlet DM model, e.g. supersymmetry breaking in the Minimal Supersymmetric Standard Model [38, 39]

where H is the complex scalar which obtains a vacuum expectation value, $v_0 = 246.2$ GeV, and induces electroweak symmetry breaking (EWSB). The two terms in Eq. (2.13) are in fact the only renormalizable terms allowed by general symmetry arguments [32]. After EWSB, the dark scalar, S , obtains the mass $m_S = \sqrt{\mu_S^2 + \frac{1}{2}\lambda_{hS}v_0^2}$ and couples to the Higgs boson, h , through

$$\mathcal{L}_{\text{EWSB}} \supset -\frac{1}{2}m_S^2 S^2 - \frac{1}{4}\lambda_{hS}S^2 h^2 - \frac{1}{2}\lambda_{hS}v_0 S^2 h. \quad (2.14)$$

Under the assumptions of the freeze-in mechanism, the dark and visible sectors couple extremely feebly, implying a very small λ_{hS} .

Since the Higgs field couples to most SM particles, it necessarily follows that a scattering process may have initial states in the dark sector and final states in the visible sector. This means that the scalar singlet DM model allows us to calculate matrix elements like $\mathcal{M}_{\chi\chi \rightarrow \psi\psi}$ required for the collision operator. These processes must be mediated by the Higgs field, as illustrated in Figure 2.1.

We will therefore primarily concern ourselves with the effective interaction-terms

$$\mathcal{L}_I = -g\phi\chi\chi - \lambda\phi\psi\psi, \quad (2.15)$$

where λ is some coupling, ϕ and χ are real scalars and ψ is a SM particle.⁶ The Higgs portal is then recovered in the case of $g = \frac{1}{2}\lambda_{hS}v_0$ and $\phi \rightarrow h$, $\chi \rightarrow S$. In sum, by only asserting the existence of a single DM scalar singlet, a theory compatible with DM production through freeze-in/out emerges.

In accordance with ref. [23], the $2 \rightarrow 2$ processes which we will be considering are therefore the ones of the form $\chi\chi \rightarrow \phi \rightarrow \psi\psi$. Letting \sqrt{s} be the c.o.m energy, we can write

⁶Again, in the fermionic case, an appropriate conjugation of ψ is required.

the Matrix element required for Eq. (2.12) as

$$\mathcal{M}_{\chi\chi\rightarrow\psi\psi}(s) = \text{Diagram} \quad (2.16)$$

$$= \mathcal{M}_{\chi\chi\rightarrow\phi}(s) iD(s) \mathcal{M}_{\phi\rightarrow\psi\psi}(s), \quad (2.17)$$

where a “blob” indicates a sum of all perturbative corrections, and

$$\mathcal{M}_{\chi\chi\rightarrow\phi}(s) = \text{Diagram} \quad , \quad \mathcal{M}_{\phi\rightarrow\psi\psi}(s) = \text{Diagram} \quad , \quad (2.18)$$

and

$$iD(s) = \text{Diagram} = \frac{i}{s - \tilde{m}_\phi^2 + \Pi(s)} \quad (2.19)$$

is the two-point correlator of ϕ , $\Pi(s)$ is the ϕ self-energy, i.e. sum of all 1PI diagrams and \tilde{m}_ϕ is the *bare mass* of ϕ . Not to be confused with the physical mass m_ϕ , the bare mass is the parameter of the quadratic ϕ term of the Lagrangian: $\mathcal{L} \supset \frac{1}{2} \tilde{m}_\phi^2 \phi^2$. The physical mass is related to the bare mass through any mass renormalization scheme of choice [40–42]. One such scheme is that of the *real pole mass*, which will be explored in Chapter 3. Using the real pole mass scheme, the physical mass is defined through $\tilde{m}_\phi^2 = m_\phi^2 + \text{Re} \Pi(m_\phi^2)$.

In ref. [23], the pole mass is used in conjunction with the *Breit-Wigner* (BW) framework wherein one defines a quantity known as the *Breit-Wigner decay rate*

$$m_\phi \Gamma_{\text{BW}} \equiv \text{Im} \Pi(m_\phi^2). \quad (2.20)$$

The extent to which Γ_{BW} is an actual decay rate will be discussed in Eq. (3.3), but for now it suffices to think of Γ_{BW} as the total decay rate of ϕ . The takeaway is that we can take $\Pi(s) \approx \Pi(m_\phi^2)$ in the domain $s \approx m_\phi^2$, meaning a good approximation to the correlator Eq. (2.19) in this domain is

$$iD(s) \stackrel{s \sim m_\phi^2}{\approx} iG_{\text{BW}}(s) \equiv \frac{i}{s - m_\phi^2 + im_\phi \Gamma_\phi}, \quad (2.21)$$

where iG_{BW} is known as the *Breit-Wigner propagator*. The BW propagator is an invaluable tool in theoretical particle physics, because by “simply” measuring the mass and decay rate of a particle, one can substitute the (otherwise complicated) correlator $D(s)$ for $G_{\text{BW}}(s)$. In the case of scalar particles, the square matrix element in Eq. (2.12) can therefore be approximated as⁷

$$|\mathcal{M}_{\chi\chi\rightarrow\psi\psi}|^2 = \frac{|\mathcal{M}_{\chi\chi\rightarrow\phi}|^2 |\mathcal{M}_{\phi\rightarrow\psi\psi}|^2}{(s - m_\phi^2)^2 + m_\phi^2 \Gamma_{\text{BW}}^2}, \quad (2.22)$$

⁷In the case of particles of non-zero spin, additional internal degrees of freedom must be accounted for when squaring the matrix elements – see ref. [43]. Also note that we are only considering s -channel processes, as the procedure differs in the t - and u -channels.

within the domain $s \sim m_\phi^2$. This domain is known as the *domain of resonance*, named so due to the similarities between Eq. (2.22) and the universal resonance curve [44]

$$I(\omega) \propto \frac{1}{(\omega - \Omega)^2 + (\sigma/2)^2}, \quad (2.23)$$

where Ω is the resonant frequency and σ is known as the width of the resonance. Note that $I(\omega)$ has its maximal values for $\omega \sim \Omega$ and that its maximal value increases as σ decreases. A similar behaviour is expressed in Eq. (2.22) for $s \sim m_\phi^2$, hence the naming of the “domain of resonance”. We will discuss further implications of resonance in Chapter 3.

In the limit $\Gamma_{\text{BW}} \rightarrow 0$, the denominator in Eq. (2.22) behaves like a Dirac δ -function

$$\frac{1}{(s - m_\phi^2)^2 + m_\phi^2 \Gamma_{\text{BW}}^2} \stackrel{\Gamma_{\text{BW}} \ll m_\phi}{\approx} \frac{\pi}{m_\phi \Gamma_{\text{BW}}} \delta(s - m_\phi^2), \quad (2.24)$$

which is known as the *narrow-width approximation* (NWA). The $\delta(s - m_\phi^2)$ tells us that resonant particles in the NWA are indistinguishable from on-shell particles.

This last remark is so important that we state it twice: highly stable⁸ off-shell resonant particles as just as physical as on-shell particles. At zero temperature this is an interesting piece of insight, but in a finite temperature plasma we encounter a complication: In the domain of resonance, how are we to distinguish intermediate resonant on-shell Higgs particles from existing Higgs particles within the plasma? Equivalently, how are we to distinguish the ψ produced in $\chi\chi \rightarrow \phi \rightarrow \psi\psi$ from those produced in a $1 \rightarrow 2$ process $\phi \rightarrow \psi\psi$? Are they different processes or is the former a concatenated version of the latter? Since the plasma is a soup of interacting particles, both processes will necessarily take place. If we wish to study the rate of DM production within a plasma, these questions must be addressed, otherwise we risk over- or underestimating the actual production rate.

Ref. [23] claims that these complications can be accounted for by adopting a BW propagator with an appropriate temperature-dependent Γ_{BW} . They also show how to derive this temperature-dependent Γ_{BW} through the freeze-in collision operator of Eq. (2.12): Assuming CP symmetry $|\mathcal{M}_{\chi\chi \rightarrow \phi}|^2 = |\mathcal{M}_{\phi \rightarrow \chi\chi}|^2$, we can write Eq. (2.12) in the plasma frame under the NWA as

$$\begin{aligned} & \frac{1}{N_\psi} \int \frac{d^3\mathbf{p}}{(2\pi)^3 2E_{\mathbf{p}}} \frac{d^3\mathbf{p}'}{(2\pi)^3 2E_{\mathbf{p}'}} |\mathcal{M}_{\phi \rightarrow \chi\chi}|^2 f_\chi^{\text{MB}}(E_{\mathbf{p}}) f_\chi^{\text{MB}}(E_{\mathbf{p}'}) \frac{\pi}{\omega} \delta(\omega - E_{\mathbf{p}} - E_{\mathbf{p}'}) \\ & \times \frac{1}{2m_\phi \Gamma_{\text{BW}}} \int \frac{d^3\mathbf{k}}{(2\pi)^3 2E_{\mathbf{k}}} \frac{d^3\mathbf{k}'}{(2\pi)^3 2E_{\mathbf{k}'}} \delta^{(4)}(p + p' - k - k') |\mathcal{M}_{\phi \rightarrow \psi\psi}|^2 (1 + \tilde{f}_\psi(E_{\mathbf{k}}))(1 + \tilde{f}_\psi(E_{\mathbf{k}'})), \end{aligned} \quad (2.25)$$

where ω is the ϕ energy. At this point, a discussion regarding the importance of reference frames is long overdue. We want to calculate amplitudes in the centre-of-mass (c.o.m) frame, because it is usually the easiest frame to work in, and it is the frame in which cross-sections are usually stated. Unfortunately, the energies which appears in the thermal bath distribution functions, f_A , are defined in the plasma rest frame. By Lorentz transforming to the frame

⁸In the sense that they satisfy $m\Gamma_{\text{BW}} \ll 1$

where the plasma moves with a relative 4-velocity u^μ , the correct thermal distribution to use for a particle A with 4-momentum k^μ is instead $f_A(k^\mu u_\mu)$, where

$$k^\mu u_\mu = \omega \cosh \eta + \cos \theta \sinh \eta |\mathbf{k}|. \quad (2.26)$$

Here, η is the rapidity (which is related to the Lorentz factor through $\gamma = \cosh \eta$) and θ is the spatial angle between \mathbf{u} and \mathbf{k} . If the spin-averaged amplitude $|\mathcal{M}_{\chi\chi \rightarrow \psi\psi}|^2$ has no angular dependence, it turns out that we can factorize the cross-section required for $C_{\text{freeze-in}}[f_\chi]$ in the plasma frame as [23]

$$\sigma_{\chi\chi \rightarrow \psi\psi}^{\text{plasma}} = I_{\psi\psi}(\gamma, s) \times \sigma_{\chi\chi \rightarrow \psi\psi}^{\text{c.o.m}}, \quad (2.27)$$

where

$$I_{\psi_1\psi_2}(\gamma, s) \equiv \frac{1}{2} \int_{-1}^1 d\cos \theta (1 + \tilde{f}_{\psi_1}(u \cdot k))(1 + \tilde{f}_{\psi_2}(u \cdot k)). \quad (2.28)$$

This factorization will allow us work with cross-sections defined in the c.o.m frame, while still respecting the fact that it is different from the plasma rest frame. Of the two amplitudes in Eq. (2.25), we need only concern ourselves with converting $|\mathcal{M}_{\phi \rightarrow \psi\psi}|^2$ to the c.o.m frame, as $|\mathcal{M}_{\phi \rightarrow \chi\chi}|^2$ only has relevant contributions at tree-level because we have assumed $g \propto \lambda_{hs}$ so small that the dark scalars never enter into equilibrium with the visible sector. Assuming $|\mathcal{M}_{\phi \rightarrow \psi\psi}|^2$ to be angularly independent, we can convert the second line in Eq. (2.25) to c.o.m quantities, giving

$$\begin{aligned} & \frac{1}{N_\psi} \int \frac{d^3\mathbf{p}}{(2\pi)^3 2E_{\mathbf{p}}} \frac{d^3\mathbf{p}'}{(2\pi)^3 2E'_{\mathbf{p}}} |\mathcal{M}_{\phi \rightarrow \chi\chi}|^2 f_\chi^{\text{MB}}(E_{\mathbf{p}}) f_\chi^{\text{MB}}(E'_{\mathbf{p}}) \frac{\pi}{\omega} \delta(\omega - E_{\mathbf{p}} - E'_{\mathbf{p}}) \\ & \times \frac{\Gamma_{\phi \rightarrow \psi\psi}}{\Gamma_{\text{BW}}} I_{\psi\psi}(\gamma, s), \end{aligned} \quad (2.29)$$

where

$$\Gamma_{\phi \rightarrow \psi_1\psi_2} = \frac{1}{2m_\phi} \int \frac{d^3\mathbf{k}}{(2\pi)^3 2E_{\mathbf{k}}} \frac{d^3\mathbf{k}'}{(2\pi)^3 2E'_{\mathbf{k}}} \delta^{(4)}(p + p' - k - k') |\mathcal{M}_{\phi \rightarrow \psi_1\psi_2}|^2 \quad (2.30)$$

is the standard decay rate for $\phi \rightarrow \psi_1\psi_2$, calculated with ordinary $T = 0$ QFT in the c.o.m frame.

Finally, in order to obtain an expression for Γ_{BW} , ref. [23] realizes that in the domain of resonance, the collision operator for $\psi\psi \rightarrow \phi \rightarrow \chi\chi$ should agree with the collision operator of $\phi \rightarrow \chi\chi$

$$\frac{1}{N_\chi} \int \frac{d^3\mathbf{p}}{(2\pi)^3 2E_{\mathbf{p}}} \frac{d^3\mathbf{p}'}{(2\pi)^3 2E'_{\mathbf{p}}} |\mathcal{M}_{\phi \rightarrow \chi\chi}|^2 f_\chi^{\text{MB}}(E_{\mathbf{p}}) f_\chi^{\text{MB}}(E'_{\mathbf{p}}) \frac{\pi}{\omega} \delta(\omega - E_{\mathbf{p}} - E'_{\mathbf{p}}) \times (1 + \tilde{f}_\phi(\omega)), \quad (2.31)$$

in a system where χ follows a Maxwell-Boltzmann distribution. By demanding Eq. (2.29) and Eq. (2.31) agree under the NWA, the authors get that

$$\Gamma_{\text{BW}} = \frac{1}{1 + f_\phi(\omega)} \sum_{\psi_1 \psi_2} \Gamma_{\phi \rightarrow \psi_1 \psi_2} I_{\psi_1 \psi_2}(\gamma, s), \quad (2.32)$$

where the sum is over all relevant heat bath particles, ψ_i .

This is a reasonable expression, as the thermal factors within the sum serve to include the effect of Bose enhancement/Pauli blocking while the overall factor of $1/(1 + f_\phi(\omega))$ is to account for the fact that the total decay rate is a difference between decay and production rates. Even though this lets us construct a BW decay rate at finite temperatures, there are some issues which must be addressed:

1. So far, we have not justified *why* the BW rate is a useful tool when accounting for intermediate particles going on-shell. Without motivation, we simply claimed that using the BW propagator equipped with a finite-temperature Γ_{BW} will help us avoid over- or underestimating the production rates in a plasma. For an accurate implementation of a freeze-in process, it would be highly beneficial if we had a detailed understanding of how the BW scheme works and what Γ_{BW} actually *is*.
2. According to Eq. (2.32), the finite-temperature BW decay rate can be written as a $T = 0$ rate multiplied by some thermal factors. Meanwhile, *thermal QFT* is an existing framework [29, 30, 45] which allows for the calculation of rates at finite temperature. Within this framework, loop-order processes have a highly non-trivial temperature dependence [26, 46]. It is therefore naïve to expect that such intricate temperature corrections can be accounted for by merely multiplying the $T = 0$ rate by some thermal factors. To tree-level, however, thermal QFT is structurally similar to QFT at $T = 0$, meaning there is a good chance that Eq. (2.32) at least holds at LO.

We will cover point 1 in the following chapter where we work intimately with the BW decay rate and the BW propagator in order to get an intuitive understanding of their affiliations to resonant particle behaviour. Point 2 will be addressed in Chapters 4 and 5 where we derive a different expression for Γ_{BW} which corrects the one derived by ref. [23] while staying true to thermal QFT. In Section 6.4 we will discuss what went “wrong” with the derivation of Eq. (2.32).

Chapter 3

Breit-Wigner Decay Rates

The aim of this chapter is to understand how unstable particles behave differently from stable particles, and how this is related to the BW propagator. Even though we are ultimately interested in Γ_{BW} at $T \geq 0$, we will start by exploring the case of $T = 0$. This will allow us to establish an intuition behind the general BW scheme and why it is related to the decay of resonant particles. Using this intuition, we will thereafter extend our results to finite temperatures and explore the behaviour of Γ_{BW} at $T \geq 0$.

While exploring the effects of off-shell resonant behaviour at $T = 0$, we will show that we naturally encounter the BW scheme, and we show why the Breit-Wigner propagator

$$G_{\text{BW}}(q^2) = \frac{1}{q^2 - m^2 + im\Gamma_{\text{BW}}}, \quad (3.1)$$

is a good approximation for the correlator near resonance. The purpose of our approach is primarily to illustrate exactly *how* the BW scheme accounts for the resonant behaviour of unstable particles. As a consequence, our derivation of the BW propagator will be much more tedious than a conventional procedure, like the one in Chapter 24 of ref. [40]. Conventionally, one firstly derives Eq. (3.1) and then proceed to illustrate how it expresses the resonant behaviour of unstable particles. Instead, we will do the opposite. We will start by studying how a stable particle differs from an unstable one and then attempt to express this behaviour through the lens of an approximated propagator, which in turn ends up matching Eq. (3.1).

The underlying idea of our approach will be to define an unstable particle as a perturbation of a stable particle. To do this, we must first understand the behaviour of stable particles.

3.1 Stable Particles and Their Mass

The Lorentz group, $\text{O}(1, 3)$, is the group of all Lorentz transformations on Minkowski-space. The (smaller) set of causally preserving Lorentz transformations is a subgroup known as the *proper orthochronous* Lorentz group $\text{SO}^+(1, 3)$. In addition to the Lorentz group, one is typically also interested in the group of spacetime translations: $\mathbb{R}(1, 3)$. These two groups

can be combined into the full symmetry group on spacetime, $\mathcal{P} \equiv \mathbf{SO}^+(1, 3) \ltimes \mathbb{R}(1, 3)$, known as the *Poincaré group* after Henri Poincaré.

In his seminal 1939 paper, Eugene Wigner showed that all fundamental particles may be identified as irreducible representations of the Poincaré group [47]. He showed that each such representation is uniquely identified by two numbers: a positive real number (mass) and a positive integer times 1/2 (spin). Hence, any type of particle is uniquely identified solely from its mass and spin! Mathematically, this two-number classification comes from the fact that the Poincaré algebra contains two Casimir operators, the eigenvalues of which uniquely identify a specific representation [48]. These operators are $P_\mu P^\mu$ and $W_\mu W^\mu$ where P_μ is the 4-momentum operator and

$$W_\mu \equiv \frac{1}{2} \varepsilon_{\mu\nu\rho\sigma} J^{\nu\rho} P^\sigma \quad (3.2)$$

is the Pauli-Lubanski pseudovector. Here, $\varepsilon_{\mu\nu\rho\sigma}$ is the four-dimensional antisymmetric Levi-Civita symbol and $J^{\nu\rho}$ is the relativistic angular momentum tensor [49]. Informally, one may say that $P_\mu P^\mu$ originates from $\mathbb{R}(1, 3)$ and corresponds to the on-shell requirement $p^2 = m^2$, while $W_\alpha W^\alpha$ originates from $\mathbf{SO}^+(1, 3)$ and corresponds to helicity or spin. For an introduction to viewing particles as representations of the Poincaré group, see ref. [42].

It must be emphasized that the values of mass and spin may not be derived from theory, but must be experimentally measured. A conventional approach to determining m^2 is through the pole mass: the mass of stable particles are experimentally measured through the poles of scattering amplitudes [40]. To motivate this, consider for example the tree-level contribution to the amplitude of forward scattering $\phi\phi \rightarrow \phi\phi$ in a ϕ^3 theory:

$$\sigma \sim \left| \begin{array}{c} \text{---} \\ \diagup \quad \diagdown \\ \text{---} \end{array} \begin{array}{c} q \\ \text{---} \\ \text{---} \end{array} \begin{array}{c} \diagdown \quad \diagup \\ \text{---} \\ \text{---} \end{array} \right|^2 \sim \frac{1}{|q^2 - m^2 + i\epsilon|^2}, \quad (3.3)$$

which clearly has a pole at $q^2 = m^2$. In order to experimentally measure the mass of ϕ , it appears that we need only locate the pole of its propagator through scattering amplitudes. However, measurements of scattering amplitudes contain contributions from all orders, not just tree-level. We must therefore instead define the mass through the pole of the full two-point correlator:

$$D(q^2) \equiv \text{---} \xrightarrow{q} \text{---} \text{---} \quad (3.4)$$

The celebrated *Källén-Lehmann spectral representation* [50, 51] lets us describe the singular behaviour of $D(q^2)$ through a real-valued and positive distribution $\rho(\mu^2)$ (called the *spectral density*) as

$$D(q^2) = \int_0^\infty d\mu^2 \frac{\rho(\mu^2)}{q^2 - \mu^2 + i\epsilon}. \quad (3.5)$$

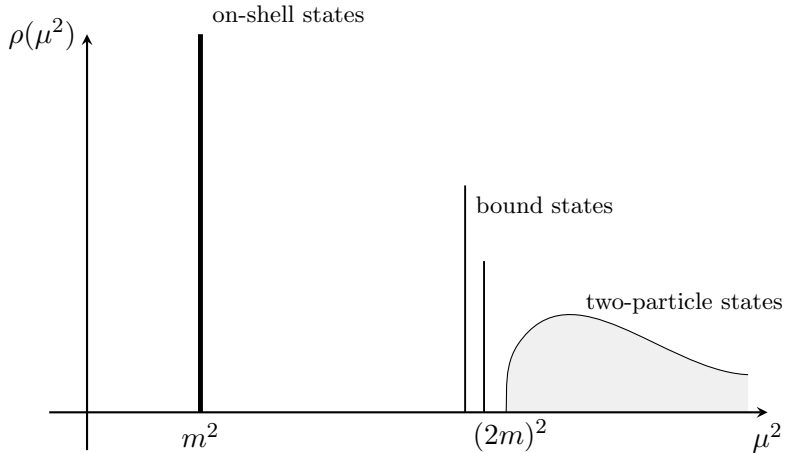


Figure 3.1: Singular behaviour of the spectral density $\rho(\mu^2)$. There is a single pole for on-shell particles at $\mu^2 = m^2$, a couple bound states just below $\sim (2m)^2$ and a spectrum of unbounded states above $(2m)^2$. This figure is inspired by Figure 7.2 in ref. [41].

The idea behind $\rho(\mu^2)$ is that it contains the locations where $D(q^2)$ is singular. According to the pole mass scheme, this means that ρ describes the locations of all physical on-shell states which the interacting theory may produce. Peskin and Schroeder [41] argue that the shape of the spectral density $\rho(\mu^2)$ is similar to that of Figure 3.1, with a pole at exactly $\mu^2 = m^2$, several poles at bound states just below $\mu^2 \sim (2m)^2$ and a continuum of poles for possible two-particle states at $\mu^2 \geq (2m)^2$. This continuous spectrum comes from the fact that in an unbounded two-particle system you can always take the particles to have opposite momenta, allowing the system to exist at any arbitrary c.o.m energy, μ^2 . Technically, this spectrum comes from a branch cut in the correlator D . Letting E_B be energy of the bound state with the lowest energy, Figure 3.1 shows that the singular behaviour of D may be modeled through ρ as

$$\rho(\mu^2) = \delta(\mu^2 - m^2) + (\text{nothing else until } \mu^2 \geq E_B^2). \quad (3.6)$$

The Källén-Lehmann spectral representation therefore implies that $D(q^2)$ always takes the form

$$D(q^2) = \frac{1}{q^2 - m^2 + i\epsilon} + \int_{E_B^2}^{\infty} d\mu^2 \frac{\rho(\mu^2)}{p^2 - \mu^2 + i\epsilon}, \quad (3.7)$$

where m^2 is the physical mass of the particle that appears as a pole in the amplitude of scattering experiments. This way, we define the physical mass of a particle to be the first pole of its two-point correlator.

3.2 Unstable Particles and Their Mass

Now that we have defined the mass of particles through the Poincaré group and the two-point correlator, we turn to consider unstable particles. The inherent randomness of particle decay means that a decay process is irreversible, meaning there must exist certain Poincaré transformations under which the field of an unstable particle is not symmetric. In contrast to a stable particle, an unstable particle can therefore, at best, be a representation of a semigroup of \mathcal{P} [52]. In making a particle unstable, we are therefore breaking the symmetry of the Poincaré group – specifically the translation symmetry from $\mathbb{R}(1, 3)$ is broken. Since $P_\mu P^\mu$ originates in $\mathbb{R}(1, 3)$, the only Casimir left in the broken Poincaré group is $W_\alpha W^\alpha$. Since $P_\mu P^\mu$ is no longer a Casimir, this effectively means that the on-shell requirement does not hold for unstable particles: $p^2 \neq m^2$, i.e. unstable particles are not associated with a specific mass.⁹

The probability for an unstable particle to exist decreases exponentially with time, and in this context it is commonly said that “the longer lifetime a particle has, the more precisely one can determine its mass”. Motivated by this, we can informally state that an unstable particle with lifetime τ has its mass “more sharply defined” than one of lifetime $< \tau$. A stable particle has an infinite lifetime and an infinitely sharp mass. Limiting our studies to unstable particles of large lifetimes, we should therefore be able to consider instability as a perturbation of stability by slightly decreasing the “sharpness” of the mass of a stable particle.

We can associate the “sharpness” of a stable particle mass with the $\delta(\mu^2 - m^2)$ in Eq. (3.6).¹⁰ We can reduce this “sharpness” by replacing the δ with a different distribution of finite width centred on $\mu^2 = m^2$. To do this, first take note of the *Sochocki-Plemelj theorem*, which says that

$$\lim_{\epsilon \rightarrow 0^+} \frac{1}{x \pm i\epsilon} = \mathcal{P} \frac{1}{x} \mp i\pi\delta(x), \quad (3.8)$$

where \mathcal{P} denotes the Cauchy principal value. From Eq. (3.5) we then get

$$\rho(q^2) = -\frac{1}{\pi} \text{Im} \{D(q^2)\}. \quad (3.9)$$

Since the infinitesimal width of $\rho(q^2)$ at $q^2 = m^2$ comes from the imaginary part of $D(q^2)$, and Eq. (3.7) tells us the imaginary component of $D(q^2)$ is introduced through the infinitesimal ϵ , we propose to make the distribution “less sharp” by considering the substitution $\epsilon \rightarrow \bar{\epsilon} \in \mathbb{R}$, where $0 < \bar{\epsilon} \ll 1$ is a small but finite value.

Effectively, we are creating a perturbed ρ , centred around a sharp particle mass $q^2 = m^2$. Hence, the approximation will only be accurate for $q^2 \sim m^2$, i.e. the domain of resonance

⁹Of course, since Wigner’s classification only holds for non-interacting particles, it comes as no surprise that the adaptation to unstable particles behaves differently.

¹⁰The “(nothing else until $\mu^2 \geq E_B^2$)” is irrelevant for this discussion as it lies outside the domain of resonance.

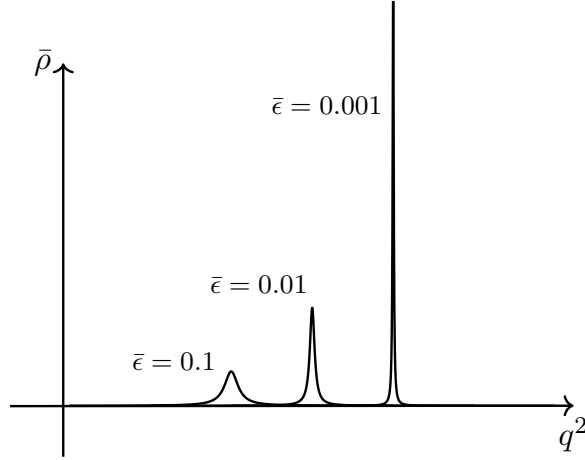


Figure 3.1: Plot of $\bar{\rho}(q^2; \bar{\epsilon})$ (centred on different q^2) for three different $\bar{\epsilon}$. The sharpness of $\bar{\rho}$ increases as $\bar{\epsilon}$ decreases.

discussed in Chapter 2. Since the effects of bound- and two-particle states are likely to lay outside the domain of resonance, we need only consider the first term of Eq. (3.7) as relevant to our perturbation, giving us the approximated two-point correlator for an unstable particle near resonance:

$$\bar{G}(q^2; \bar{\epsilon}) \equiv \frac{1}{q^2 - m^2 + i\bar{\epsilon}}, \quad 0 < \bar{\epsilon} \ll 1. \quad (3.10)$$

Similarly, we define the approximated (perturbed) spectral density as

$$\bar{\rho}(q^2; \bar{\epsilon}) \equiv -\frac{1}{\pi} \text{Im} \bar{G}(q^2; \bar{\epsilon}). \quad (3.11)$$

Figure 3.1 illustrates how the sharpness of $\bar{\rho}$ increases as $\bar{\epsilon}$ decreases. In the case of $\bar{\epsilon} \rightarrow 0$, we have $\bar{\rho} \rightarrow \delta(q^2 - m^2)$ – agreeing with the sharp mass case of Eq. (3.6). The domain of resonance can therefore be loosely identified as the domain where $\bar{\rho}(q^2; \bar{\epsilon}) \gtrsim \mathcal{O}(1)$. By Figure 3.1, the larger $\bar{\epsilon}$ is, the larger this domain is, but since our approach only holds for $\bar{\epsilon} \ll 1$, it must follow that only small domains are physically applicable to this model.

In our above discussion of stable particles, we said that “ ρ describes the locations of all physical on-shell states which the interacting theory may produce”. Since $\bar{\rho}$ is a generalization of ρ that accounts for resonant unstable particles, we claim that $\bar{\rho}$ implements the effect that off-shell states have within the interacting theory. As shown in Figure 3.1, this effect is largest in the domain of resonance. In other words, the fact that $\bar{\rho}(q^2; \bar{\epsilon}) \neq 0$ for $q^2 \neq m^2$ means that resonant particles can give physical contributions similarly to on-shell particles, but Figure 3.1 tells us that the size of this contribution diminishes rapidly outside the domain of resonance.

3.2.1 Determining $\bar{\epsilon}$

The goal of this subsection is to derive an expression for $\bar{\epsilon}$ which may be perturbatively determined such that the object $\bar{G}(q^2; \bar{\epsilon})$ can be used in calculations. To do so, we must first determine the properties of $\bar{\epsilon}$. The whole idea behind introducing $\bar{\epsilon}$ was for it to mimic the behaviour of the limit $\epsilon \rightarrow 0^+$, while still maintaining a finite value. As such, we will only keep terms up to $\mathcal{O}(\bar{\epsilon}^1)$, effectively taking $\bar{\epsilon}^2 = 0$. As a consequence, from the series expansion of a function $F(z)$ around some $x \in \mathbb{C}$, we have

$$F(x \pm i\bar{\epsilon}) = F(x) \pm i\bar{\epsilon}F'(x), \quad (3.12)$$

where $F'(x)$ denotes the derivative of F at x . Note that this only holds when F is analytic around x , which is a risky assumption when working with correlators. Luckily, the functions which we will apply Eq. (3.12) to are analytical in their respective domains. It should also be mentioned that $\bar{\epsilon}$ is necessarily real, because Eq. (3.10) tells us that a finite imaginary component would be interpreted as a shift of the mass of the particle, meaning the perturbation would no longer be centred on $q^2 = m^2$. We will also assume that $\bar{\epsilon}$ is constant in q^2 .

In order to determine $\bar{\epsilon}$, we will identify $\bar{G}(q^2; \bar{\epsilon})$ with the function that it aims to imitate: the two-point correlator $D(q^2)$. This correlator satisfies the Dyson equation [53]

$$D(q^2) = G_F(q^2) + G_F(q^2)\Pi(q^2)D(q^2) \quad (3.13)$$

$$\Rightarrow D(q^2) = \frac{1}{G_F^{-1}(q^2) + \Pi(q^2)}, \quad (3.14)$$

where $G_F(q^2)$ is the time-ordered (Feynman) propagator and $\Pi(q^2)$ is the self-energy. For reasons that will shortly become apparent, we will pass to the analytically continued $\bar{G}(z; \bar{\epsilon})$ and $D(z)$ for $z \in \mathbb{C}$, the former being a trivial extension of Eq. (3.10) while the latter always exists by the Osterwalder-Schrader theorem [54]. In order to assert $\bar{G}(z; \bar{\epsilon}) \stackrel{!}{=} D(z)$, we need only impose that they are equivalent Green's functions, i.e. that they solve the same system of equations, giving:

$$z - m^2 + i\bar{\epsilon} \stackrel{!}{=} G_F^{-1}(z) + \Pi(z). \quad (3.15)$$

The LHS is a first order polynomial in z , meaning the RHS must also be. Hence, we need only assert that the two sides share equal kernels and first derivative in z . The latter requirement yields that

$$1 \stackrel{!}{=} \frac{d}{dz} [G_F^{-1}(z) + \Pi(z)] \quad \forall z \in \mathbb{C}. \quad (3.16)$$

Requiring the kernels to match we get that the LHS of Eq. (3.15) is zero at $z = m^2 - i\bar{\epsilon}$,

giving

$$0 \stackrel{!}{=} G_F^{-1}(m^2 - i\bar{\epsilon}) + \Pi(m^2 - i\bar{\epsilon}) \quad (3.17)$$

$$\stackrel{(3.12)}{=} G_F^{-1}(m^2) + \Pi(m^2) - i\bar{\epsilon} \frac{d}{dz} [G_F^{-1}(z) + \Pi(z)]_{z=m^2} \quad (3.18)$$

$$\stackrel{(3.16)}{=} G_F^{-1}(m^2) + \Pi(m^2) - i\bar{\epsilon}. \quad (3.19)$$

This illustrates our need to pass to the analytically continued expressions. Since $\bar{\epsilon}$ and $G_F^{-1}(m^2)$ are real,¹¹ we end up with two equations:

$$0 = G_F^{-1}(m^2) + \text{Re } \Pi(m^2), \quad (3.20)$$

$$\bar{\epsilon} = \text{Im } \Pi(m^2). \quad (3.21)$$

We note that Eq. (3.20) is equivalent to the real pole mass definition which we briefly encountered in Chapter 2: Letting the free Lagrangian be $\mathcal{L}_0 = \frac{1}{2}\phi(\partial^2 + \tilde{m}^2)\phi$, with \tilde{m} being the bare mass, we get $G_F^{-1}(m^2) = m^2 - \tilde{m}^2$, giving

$$\tilde{m}^2 = m^2 + \text{Re } \Pi(m^2). \quad (3.22)$$

We have therefore extended the definition of the stable pole mass of Section 3.1 to hold for unstable particles. In accordance with resonance theory and Eq. (2.23), the resonant “frequency” of $\bar{G}(q^2; \bar{\epsilon})$ (i.e. $D(q^2)$) is the physical pole mass, m^2 . For a further discussion of the real pole mass, see ref. [40].

Through Eq. (3.21), we have finally illustrated the relationship that the self-energy has with unstable particles: The larger $\text{Im } \Pi(m^2)$ is, the more unstable the particle is. This hints at some relation between $\bar{\epsilon}$ and the decay rate of a particle. Indeed, by our definition in Section 3.4, we have

$$\bar{\epsilon} = \text{Im } \Pi(m^2) = m\Gamma_{\text{BW}}. \quad (3.23)$$

In other words, the approximated propagator becomes

$$\bar{G}(q^2; \bar{\epsilon} = m\Gamma_{\text{BW}}) = G_{\text{BW}}(q^2), \quad (3.24)$$

meaning we have showed that the BW scheme is the technique which naturally accounts for resonant unstable particles. Crucially, this result is non-perturbative! If we calculate the self-energy to any order $\mathcal{O}(\lambda^n)$, then $\bar{G}(q^2; m\Gamma_{\text{BW}})$ is the order-appropriate approximation to the correlator $D(q^2)$ which accounts for off-shell resonance.

3.3 The Breit-Wigner Decay Rate

This begs the question, what does $\text{Im } \Pi(m^2)$ have to do with a decay rate? Why have we defined it to be $m\Gamma_{\text{BW}}$? At first glance, there are some hints which point towards a relation

¹¹More specifically, $\text{Im } \{G_F^{-1}(m^2)\} = 0^+$ is not a finite, real number.

between Γ_{BW} and the decay rate of a particle. For example, we have already noted that our approximation is most accurate when $\bar{\epsilon} \ll 1$, which corresponded to a very long lifetime. Since the mean lifetime is inversely proportional to the total decay rate, it follows that a small $\bar{\epsilon}$ implies a small decay rate as well. In this section, we formalize this relationship.

Diagrammatically, we can write

$$m\Gamma_{\text{BW}} = \text{Im} \left\{ \text{---} \textcircled{\Pi} \text{---} \right\}. \quad (3.25)$$

This can be compared to the results of the optical theorem – derived in Appendix A.1, which, for an unstable scalar A , says

$$\text{Im} \mathcal{M}_{A \rightarrow A} = \text{Im} \left\{ \text{---} \textcircled{} \text{---} \right\} \quad (3.26)$$

$$= \text{Im} \left\{ \text{---} + \text{---} \textcircled{\Pi} \text{---} + \text{---} \textcircled{\Pi} \text{---} \textcircled{\Pi} \text{---} + \dots \right\}. \quad (3.27)$$

This tells us that Γ_{BW} is calculated by amputating the forward scattering diagram $\mathcal{M}_{A \rightarrow A}$ and taking the imaginary part. By “amputating” we mean in the sense of the LSZ reduction formula [55], which tells us that contributions to the S -matrix only come from diagrams whose external lines are amputated [40, 41]. Therefore, Γ_{BW} must be equivalent to the rate that is calculated through the S -matrix, i.e. the *physical* decay rate. For example, the probability of a state decays like $\exp(-t\Gamma_{\text{BW}})$ [42]. The claim made back in Section 2.2 of Γ_{BW} being the total decay rate is therefore perfectly accurate.

The natural question then becomes, what is the interpretation of the imaginary component of the *non*-amputated forward scattering diagram, $\text{Im} \mathcal{M}_{A \rightarrow A}$? Since we associate the amputated diagram with an externally connected process, it is reasonable to interpret $\text{Im} \mathcal{M}_{A \rightarrow A} \equiv m\Gamma_{\text{virt}}$ as the “decay rate” of an internal (virtual) particle. Of course, a virtual particle is not physical and is therefore not compatible with a real decay process, so Γ_{virt} may not be viewed as an inverse mean lifetime the way Γ_{BW} can. We can instead formalize the relationship that Γ_{virt} has with the physical Γ_{BW} through Eq. (3.27), which can be expressed as a geometric series:

$$\text{Im} \mathcal{M}_{A \rightarrow A} = \text{Im} \left\{ \Pi(m^2) + \Pi(m^2)(iG_F(m^2))\Pi(m^2) + \dots \right\} \quad (3.28)$$

$$= \text{Im} \left\{ \frac{\Pi(m^2)G_F^{-1}(m^2)}{G_F^{-1}(m^2) - i\Pi(m^2)} \right\}. \quad (3.29)$$

If $\Pi(m^2)$ contains terms of order $\mathcal{O}(\lambda^\ell)$ and higher, we have

$$\text{Im} \mathcal{M}_{A \rightarrow A} = \text{Im} \Pi(m^2) + \mathcal{O}(\lambda^{2\ell}), \quad (3.30)$$

meaning there always exists some order $\mathcal{O}(\lambda^{<2\ell})$ to which we have $\Gamma_{\text{virt}} = \Gamma_{\text{BW}}$. At this order, the virtual decay rate may be thought of as identical to the physical decay rate of the particle. This approximation holds particularly well in a weakly coupled theory with $\lambda \ll 1$, as higher order terms are heavily suppressed.

Having established how Γ_{BW} is related to the physical decay rate, it would next be highly beneficial if we could also interpret it through the lens of resonance. This would help us in our endeavour to understand the role of Γ_{BW} in accounting for the resonant behaviour of off-shell particles. To address this, we turn to $\bar{\rho}(q^2; \bar{\epsilon})$ as it is the object responsible for implementing the resonant behaviour of off-shell particles. From Eq. (3.11), we get

$$\bar{\rho}(q^2; \text{Im } \Pi(m^2)) = \frac{1}{\pi} \frac{\text{Im } \Pi(m^2)}{(q^2 - m^2) + (\text{Im } \Pi(m^2))^2}. \quad (3.31)$$

In the limit $\bar{\epsilon} \rightarrow 0$ (i.e. $\text{Im } \Pi \rightarrow 0$), we have $\bar{\rho}(q^2; \bar{\epsilon}) \rightarrow \delta(q^2 - m^2) = \rho(q^2)$ which is the probability that a stable particle of momentum q^μ gives a physically measurable contribution. At finite $\bar{\epsilon}$, $\bar{\rho}(q^2; \bar{\epsilon})$ extends this behaviour to resonant off-shell particles, meaning we can interpret Eq. (3.31) as the probability that an off-shell particle gives a measurable contribution.

So far, this chapter has only considered zero-temperature behaviour. By assuming the construction of $\bar{\rho}$ extends to finite temperatures,¹² we get that Γ_{BW} at $T > 0$ is the quantity which through Eq. (3.31) gives the probability for an off-shell particle to exist in a plasma. In other words, at $T > 0$, Γ_{BW} is a measure of the contribution from off-shell particles in a plasma – an interpretation in agreement with the one presented by Weldon in ref. [31]. This is a fairly reasonable result, and shows how the BW scheme accounts for resonant intermediate particles in a plasma. This thermal interpretation is, however, rather disconnected from the behaviour of Γ_{BW} as a *rate* – what does Eq. (3.31) have to do with the pace at which some process occurs? Up to this point, we have intentionally refrained from discussing the interpretation of Γ_{BW} at $T > 0$ as a rate, because thermal rates turn out to be inherently different from their zero-temperature counterparts.

3.4 Rates at Finite Temperatures

The discussion of how to treat and interpret decay and production rates at finite temperatures is not a new one [29, 31, 45, 56]. In a finite temperature plasma, the nature of rates varies drastically from that at zero temperature. At first glance, there are two key differences to notice:

- (i) In collider experiments of non-thermal processes, we have intimate control over initial and final states in experiments – we pride ourselves in being able to identify exactly *which* processes have occurred in a scattering experiment. At finite temperatures, however, this ability is lost since an idle plasma is able to induce conditions for a multitude of processes by itself. For example, in Section 2.2 we witnessed the ambiguity in identifying whether the process $\chi\chi \rightarrow \phi \rightarrow \psi\psi$ or $\phi \rightarrow \psi\psi$ occurred during resonance.

¹²We will justify this claim in Section 4.3.

(ii) In QFT at $T = 0$, the “background” upon which experiments are performed is the vacuum which has no real (on-shell) particles present. At finite temperatures, the interactions we wish to study are indistinguishable from the background (the plasma); the background itself consists of physical interactions. We can therefore not view a thermal process as one happening on top of an empty background in the same manner as at zero temperature.

If we wish to account for these differences, we must stop speaking in terms probabilities and rates of individual processes and instead speak in terms of the accumulative effect of *all* relevant scattering processes. In a plasma, the interpretation of the “rate of $A \rightarrow B$ ” becomes meaningless, as there is no way to distinguish the A involved in this process from the one that is involved in the process of, say, $C \rightarrow A$ in the surrounding plasma. This aligns with the principles of a statistical model wherein the relevance of the individual is negligible. By accumulating all individual processes we can instead study the full system.¹³

In order to address the differences between rates at zero and finite temperatures,¹⁴ let us start by considering a simple thermalized plasma where only two scalars, say ϕ and ξ , exist. The ϕ decay $\phi \rightarrow \xi\xi$ will happen at a rate Γ_d whose phase space is Bose enhanced by $(1 + \tilde{f}_\xi)(1 + \tilde{f}_\xi)$. Since real ξ are also part of the plasma, ϕ will also be produced by the inverse decay $\xi\xi \rightarrow \phi$ at a rate Γ_p with phase space enhanced by $f_\xi f_\xi$. It then follows that the phase space distribution of ϕ changes like [31]

$$\frac{\partial f_\phi}{\partial t} = -f_\phi \Gamma_d + (1 + \tilde{f}_\phi) \Gamma_p, \quad (3.32)$$

which is a fairly reasonable result to anyone familiar with thermal phase spaces and their Bose enhancement/Fermi blocking. However, a highly non-trivial result of Weldon’s is that the imaginary part of the ϕ self-energy $\Pi(\omega)$ satisfies¹⁵

$$\text{Im } \Pi(\omega) = \omega[\Gamma_d - \Gamma_p], \quad (3.33)$$

where ω is the energy of ϕ measured in the plasma rest frame.

Clearly, if we define the finite-temperature BW decay rate to be $\Gamma_{\text{BW}} \equiv \Gamma_d - \Gamma_p$, then Eq. (3.33) bears a strong resemblance to Eq. (2.20). We will therefore take the BW decay rate at finite temperature to be the imaginary component of the self-energy, just like at $T = 0$. This means that the finite-temperature BW decay rate amounts to subtracting a production rate from a decay rate – a rather reasonable result.

Unfortunately, this is where the similarities between Γ_{BW} at $T = 0$ and $T \neq 0$ begin to fade as additional oddities in the finite temperature case become apparent [31]:

¹³Note that there does exist cases where one *is* interested in studying individual processes in a plasma, for example when probing a plasma in a particle accelerator. This is however very different from the case at hand, where we are interested in studying the behaviour of the plasma that filled the early universe which was very much not subject to collider experiments (hopefully).

¹⁴This procedure mainly follows that of the seminal 1983 work by H. Weldon in ref. [31].

¹⁵Due to Weldon’s choice of convention, his original expression features an additional minus sign in front of ω , cf. Eq. (1.1) of ref. [31].

- (iii) If ϕ is a fermion, the imaginary self-energy comes out to be $\text{Im } \Pi(\omega) = \omega[\Gamma_d + \Gamma_p]$, meaning the total rate is $\Gamma_{\text{BW}} = \Gamma_d - \varepsilon_\phi \Gamma_p$ for arbitrary spin. The “natural definition” of subtracting decay from production is therefore lost. We will discover the origin behind this awkward sign difference in Section 6.2.
- (iv) The plasma provides a specific frame relative to which the energy of ϕ , ω , is defined. It is in this frame that ϕ follows the distribution $f_\phi(\omega)$. We are therefore not free to pick the frame of ϕ at leisure without at least Lorentz transforming f_ϕ out of the plasma frame. This is in contrast to Eq. (2.20) where the m_ϕ can always be seen as the energy in the ϕ rest frame. The ω -dependence of $\Gamma_{\text{BW}}(\omega)$ is therefore non-trivial at finite temperatures – a quality which ref. [23] claims is expressed through $I_{\psi_1\psi_2}(\gamma, s)$ in Eq. (2.32).
- (v) If $\Gamma_{\text{BW}} \neq 0$ truly behaved like a decay rate, we would expect the number of ϕ particles to diminish or increase over time. This is clearly not the case, as there will always be a constant population of ϕ present in the thermalized plasma.

This last point is especially important in understanding the difference between rates at zero and finite temperature: At $T = 0$, we think of particle decays as processes which reduce the number of initial-state particles. In a thermalized plasma, the rate at which the number of ϕ particles decreases must be identical to the rate at which it increases – otherwise there would not be an equilibrium. A thermal rate is therefore not something which describes the change in a particle population over time.

The question of “what is the rate of the specific process $\phi \rightarrow \xi\xi$ ” is not physically meaningful in a plasma. Although nothing is preventing us from sitting down and mathematically calculating the “rate” of this process using thermal theory, there is no way to measure it in a plasma experiment. We can only observe the accumulative effect of all relevant processes. Compare this to at $T = 0$ where we can calculate the rate of $\phi \rightarrow \xi\xi$ and prepare an experiment to measure it in.

Mathematically, Γ_{BW} at $T \geq 0$ is therefore nothing but the imaginary part/discontinuity of the ϕ self-energy. At $T = 0$, this quantity exactly matches the decay rate of ϕ , but at finite temperatures not so much. In Weldon’s own words [31]: “The purpose [...] is to compute $\text{Im } \Pi$ for $T \neq 0$ and organize it into a recognizable form as the square of an amplitude, integrated over phase space but weighed with certain statistical factors appropriate to a thermal distribution.” Γ_{BW} is thus a quantity which reproduces the decay rate in the limit $T \rightarrow 0$, and is structurally identical to how one would *expect* a decay rate to look at finite temperatures. However, due to the statistical nature of a thermalized plasma, the notion of “a rate” can not be carried over from zero to finite temperatures.

This is an interesting yet slightly distressing result – what on earth is Γ_{BW} at $T > 0$ if is not a rate of decay? It certainly has the dimensions of a rate and is structurally identical to how one would *expect* a rate to look at finite temperatures, so what gives? This dilemma can be traced back to the fact that a rate describes a temporal change in a system, while equilibrium systems are notoriously unchanging with time; two seemingly incompatible notions. Luckily, all hope is not yet lost because through our statistical analysis in Chapter 1

we know that the Boltzmann equation lets us describe the temporal behaviour of thermal systems. We established that whenever the thermal distribution of a particle population is knocked out of equilibrium, it is quickly attracted back towards the equilibrium distribution. It turns out that this behaviour is also expressed in the dynamics of Eq. (3.32): For small deviations from thermal equilibrium, the solutions to Eq. (3.32) are¹⁶ [31]

$$f_\phi(\omega, t) = \frac{1}{e^{\omega\beta} - \varepsilon_\phi} + c(\omega)e^{-t\Gamma_{\text{BW}}}, \quad (3.34)$$

where $c(\omega)$ is some arbitrary function. It follows that any thermal distribution function which is knocked slightly out of equilibrium is quickly pulled back in – the speed of which depends on the size of Γ_{BW} . We can therefore think of Γ_{BW} as an *equilibration rate* which tells us how quickly a system is pulled into equilibrium.

This interpretation actually emphasizes a crucial notion about thermal systems. Although statements like “an equilibrium system is unchanging” are true on a statistical scale, they undermine the fundamental idea that a plasma is continually undergoing processes which slightly edge it away from equilibrium. The plasma is not static (and does not want to stay static), yet it wants to stay in an (on average) unchanging state. In order to satisfy both of these desires, some temporal process must constantly make sure that (1) reactions happen and (2) reactions always favour a push towards equilibrium. The object which quantifies this behaviour is Γ_{BW} . This can, for example, be seen through Eq. (3.34), which tells us how quickly a perturbed equilibrium system returns to equilibrium, but also through Eq. (3.32), which shows that it becomes harder to push f_ϕ further away from equilibrium. In Section 6.2, we will discuss how the interpretation of Γ_{BW} as an equilibration rate can be unified with its role in accounting for off-shell resonance.

As this chapter comes to a conclusion, we summarize our main results. Starting with ideas from the Poincaré group, we showed how to introduce the concept of instability into the two-point correlator of a field. The natural way of going about this was by making the mass of a stable particle “less sharp” by widening the infinitely sharp spectral function, ρ . This led us to the revelation that $\text{Im } \Pi(m^2)$ was the width of a new (less sharp) spectral function $\bar{\rho}$, through which we reproduced the known BW propagator, Eq. (3.24). We then discovered that at $T = 0$, $m\Gamma_{\text{BW}} = \text{Im } \Pi(m^2)$ must be the total decay rate of a particle while at $T > 0$, $\text{Im } \Pi(\omega)$ is related to the probability that an off-shell particle exists in a plasma through Eq. (3.31). After an analysis of the behaviour of rates at finite temperatures, we found that Γ_{BW} does *not* behave like a decay rate in the traditional sense, which we reconciled by introducing the concept of an equilibration rate.

In all, the primary takeaway from this chapter is that the quantity which we now set out to calculate at finite temperature is $\text{Im } \Pi(\omega)$. To do so, we require the formalism of *thermal quantum field theory*.

¹⁶This solution only applies if the temperature is constant with time. Weldon also shows that $\Gamma_{\text{BW}} \geq 0$, cf. Eq. (2.34) in ref. [31].

Chapter 4

Thermal Field Theory

In the previous chapter, we established that in order to account for resonant s -channel particles in a plasma, we need “only” calculate $\text{Im } \Pi(\omega)$ at finite temperature. The goal of this chapter is to formulate a method that allows for this calculation. Meanwhile, we will end up deriving an alternative approach to the formalism of real-time thermal field theory and associated principles.

Just like in Chapter 3, our approach is based on exploring the consequences which the on-shell requirement, $p^2 = m^2$, has for physical particles. We will start with a study at $T = 0$ in order to lay the fundamental groundwork before extending our ideas to $T \geq 0$.

4.1 Superselection Rules

For $m > 0$, there are two disconnected hyperboloids in Minkowski space which satisfy $p^2 = m^2$, as illustrated in Figure 4.1. Let us assume for the moment that states with $p_0 < 0$ exist in full analogy to the usual states with $p_0 > 0$ and that they share the same properties as the latter (except for relations that involve the sign of p_0). We label the set of states with $p_0 > 0$ as the \mathcal{B}^+ branch, and states with $p_0 < 0$ as the \mathcal{B}^- branch. According to the Feynman-Stueckelberg interpretation of antiparticles [57], we can define the physical energy of a state on \mathcal{B}^- as $E \equiv -p_0 > 0$, and consider it as a state of the corresponding anti-particle [58].

If $p^2 \geq 0$, the sign of p_0 is invariant under the proper orthochronous Lorentz group $\text{SO}^+(1, 3)$.¹⁷ Hence, any future(past) directed timelike or null 4-vector will remain future(past) directed under $\text{SO}^+(1, 3)$ (this is *not* the case for $p^2 < 0$). In other words, no operation in $\text{SO}^+(1, 3)$ may take a four-vector with $p_0 > 0$ to one with $p_0 < 0$ and vice versa. The kinematics of a theory is therefore restricted to a single branch at a time, and we will assume that this notion extends to the dynamics as well.

In other words, a system on \mathcal{B}^+ can not evolve to a system on \mathcal{B}^- and vice versa. For this reason, the \mathcal{B}^- branch is often discarded or forgotten until it is needed. It turns out that, in our endeavour to model a thermal plasma, it will be advantageous to actually include both

¹⁷A great discussion on this can be found in ref. [58].

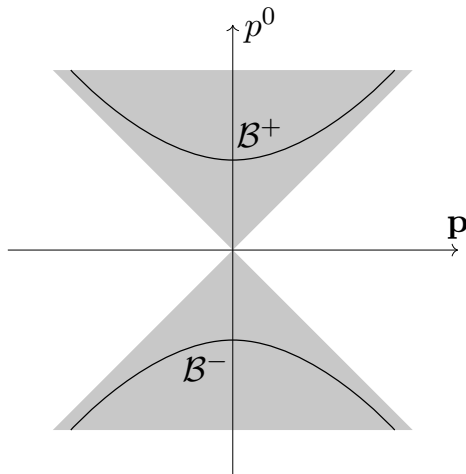


Figure 4.1: Light-cone in momentum space illustrating the two branches satisfying $p^2 = m^2$ for $m \neq 0$. The branches of positive- and negative p_0 are labelled \mathcal{B}^+ and \mathcal{B}^- , respectively.

branches in our model from the very beginning. In this section, we will therefore construct a formalism which allows for the inclusion of \mathcal{B}^- *without* affecting the known, well-established physics on \mathcal{B}^+ and while avoiding headaches like “negative energy” and mixing between branches.

Since the Hamiltonian, H , is the generator of time evolution, the fact that states on \mathcal{B}^+ may not evolve to states on \mathcal{B}^- means that the inner product $\langle \pm | H | \mp \rangle$ vanishes for all $|\pm\rangle \in \mathcal{B}^\pm$ on different branches. Mathematically speaking, this is known as a *selection rule* [59]. Crucially, this selection rule implies that S -matrix elements for scattering between the two branches vanish: $\langle \pm | S | \mp \rangle = 0$, meaning a system with $p_0 > 0$ may never scatter to a system with $p_0 < 0$, and vice versa. This amounts to requiring that a particle can not scatter into its corresponding anti-particle.

What about states which do not lay purely in \mathcal{B}^+ or \mathcal{B}^- ? That is, states which are a linear combination of states on different branches. A state like $\alpha |\text{electron}\rangle + \beta |\text{positron}\rangle$ is unphysical unless $\alpha = 0$ or $\beta = 0$, as any other values would allow for violation of conservation of internal quantum numbers. We will therefore assume that no physical state may take the form $|+\rangle + |-\rangle$, where $|\pm\rangle \in \mathcal{B}^\pm$. This is known as a *superselection rule* (SSR) [60, 61] and has several implications: Firstly, $\langle \pm | \mathcal{O} | \mp \rangle = 0$ for all physical observables \mathcal{O} , which implies the above-mentioned selection rule $\langle \pm | H | \mp \rangle = 0$. This effectively says that no measurement may make a physical system switch branches. Secondly, \mathcal{B}^+ and \mathcal{B}^- must be orthogonal spaces and the Hilbert space of all physical states that satisfy $p^2 = m^2$ decomposes as

$$\mathcal{H} = \mathcal{H}^+ \oplus \mathcal{H}^-, \quad (4.1)$$

where $\mathcal{H}^\pm \equiv \mathcal{B}^\pm$ are known as the two superselection *sectors*.

However, *why* do we want to introduce a SSR? At $T = 0$, contributions from different branches necessarily never mix, so our efforts seem rather redundant. At $T > 0$, this will turn

out to no longer be the case. When we extend the SSR to finite temperatures in Section 4.2, we show that the two branches end up interacting non-trivially.

Nevertheless, the way we formally introduce the SSR into QFT is by constructing a countable set of self-adjoint projection operators P_i on \mathcal{H} , which satisfy

$$P_i P_j = 0 \quad \text{for } i \neq j, \quad \sum_i P_i = \mathbb{1} \quad \text{and} \quad P_i P_i = P_i, \quad (4.2)$$

such that all observables commute with P_i [60]. In order to find such projection operators, we take inspiration in our assumption that $\mathcal{H}^+ = \mathcal{B}^+$ and $\mathcal{H}^- = \mathcal{B}^-$ are orthogonal spaces, and in the completeness relations for on-shell one-particle states that satisfy $\pm p_0 > 0$:

$$\mathbb{1}_{1\text{-particle}}^\pm = \int \frac{d^4 p}{(2\pi)^4} (2\pi) \delta(p^2 - m^2) \theta(\pm p_0) |\mathbf{p}\rangle\langle\mathbf{p}|. \quad (4.3)$$

The completeness relation on the Hilbert space of all on-shell one-particle states is then $\mathbb{1}_{1\text{-particle}}^+ + \mathbb{1}_{1\text{-particle}}^- = \mathbb{1}_{1\text{-particle}}$. A similar procedure can be performed for the Hilbert space of n -particle states. This lets us extend the completeness relation to the full Hilbert space of all on-shell states $|X\rangle \equiv |\mathbf{p}_1 \mathbf{p}_2 \dots \mathbf{p}_n\rangle$ as

$$\mathbb{1}^\pm \equiv \sum_X \int d\Pi_X^\pm |X\rangle\langle X|, \quad (4.4)$$

where the sum is over single- and multi-particle states X ,¹⁸ and we define the phase space measure¹⁹ of the state X on \mathcal{H}^\pm as

$$d\Pi_X^\pm \equiv \prod_{j \in X} \frac{d^4 p_j}{(2\pi)^4} (2\pi) \delta(p_j^2 - m^2) \theta(\pm p_j^0). \quad (4.5)$$

We can explicitly check that $\mathbb{1}^+$ and $\mathbb{1}^-$ satisfy the requirements in Eq. (4.2): Firstly, the orthogonality of \mathcal{B}^\pm implies that $\mathbb{1}^\pm \mathbb{1}^\mp = 0$. Secondly, using $\theta(x) + \theta(-x) = 1$, we have

$$\mathbb{1}^+ + \mathbb{1}^- = \sum_X \int \left[\prod_{j \in X} \frac{d^4 p_j}{(2\pi)^4} (2\pi) \delta(p_j^2 - m^2) \right] |X\rangle\langle X| = \mathbb{1}, \quad (4.6)$$

which follows from the completeness relation on \mathcal{H} as the space of all states satisfying $p^2 = m^2$. Lastly, for single-particle states (the extension to multi-particle states can be

¹⁸Technically, the sum in Eq. (4.4) is over all *inequivalent* phase space configurations. This will become important later when we consider identical final state particles which amounts to multiplying the phase space by the appropriate symmetry factor.

¹⁹The terms “phase space”, “phase space measure” and “volume element” are often used interchangeably. We will primarily be calling it a measure, as the term “phase space” already refers to $\mathbb{R}(1, 3)$ and the term “volume element” can be rather imprecise.

shown from this)

$$\mathbb{1}_{1\text{-particle}}^\pm \mathbb{1}_{1\text{-particle}}^\pm = \int d\Pi_X^\pm d\Pi_Y^\pm \langle X|Y\rangle |X\rangle\langle Y| \quad (4.7)$$

$$= \int \frac{d^3\mathbf{p}_X}{(2\pi)^3 2E_X} \frac{d^3\mathbf{p}_Y}{(2\pi)^3 2E_Y} 2E_Y (2\pi)^3 \delta^{(3)}(\mathbf{p}_X - \mathbf{p}_Y) |X\rangle\langle Y| \quad (4.8)$$

$$= \int \frac{d^3\mathbf{p}_X}{(2\pi)^3 2E_X} |X\rangle\langle X| \quad (4.9)$$

$$= \mathbb{1}_{1\text{-particle}}^\pm. \quad (4.10)$$

Therefore, $\mathbb{1}^+$ and $\mathbb{1}^-$ are projection operators which introduce the SSR that separates the two sectors \mathcal{H}^+ and \mathcal{H}^- . For a practical illustration on how to use $\mathbb{1}^+$ and $\mathbb{1}^-$ in calculations, see the derivation of the generalized optical theorem in Appendix A.1.

4.1.1 SSR and CPT

It turns out that the behaviour of the two sectors, \mathcal{H}^+ and \mathcal{H}^- , is closely linked to the inherent CPT symmetry of QFT. Here, CPT is the combination of a simultaneous charge conjugation, C, parity transformation, P, and time reversal, T. Though other combinations of C, P and T need not be exact symmetries [62–64], the CPT theorem says that any Lorentz invariant local QFT with Hermitian Hamiltonian must be exactly symmetric under CPT [42, 65]. The antiunitarity of CPT means that it relates the S -matrix of some process to the S -matrix of the reverse process where particles are replaced by their anti-particles and all spatial spin components reversed [42]. By the Feynman-Stueckelberg interpretation, we may therefore take the effect of a CPT transformation on the S -matrix to be

$$\langle A^+ | S | B^+ \rangle \xrightarrow{\text{CPT}} \langle B^- | S^\dagger | A^- \rangle \quad \text{for all } |A^\pm\rangle, |B^\pm\rangle \in \mathcal{H}^\pm. \quad (4.11)$$

We can therefore interpret a CPT transformation as a *change of sectors*. The inherent CPT invariance of QFT then tells us that the two sectors have identical physics. In terms of matrix elements, the CPT transformations becomes (up to a phase)

$$\mathcal{M}_{A \rightarrow B} \xrightarrow{\text{CPT}} \mathcal{M}_{\text{CP}B \rightarrow \text{CP}A}, \quad (4.12)$$

where the subscript CP X indicates that we reverse all spin z -components and replace particles by their anti-particles in a state X [42]. The time-reversal part of CPT is indicated through the switching of the initial- and final states in the matrix element subscript.

Before we proceed to working at finite temperatures, it becomes important to re-clarify the difference between *branches* and *sectors*. The former are always \mathcal{B}^\pm (the set of all on-shell states satisfying $\pm p_0 > 0$) while the latter are \mathcal{H}^\pm (the orthogonal spaces into which the Hilbert space of all states satisfying $p^2 = m^2$ decomposes under the SSR). At $T = 0$ these two turn out to be equivalent, but (as we shall soon see) this will no longer be the case as $T > 0$.

4.2 Finite Temperature

We will now extend the ideas of the previous section to finite temperatures. The procedure shown in this section is by no means perfectly formal, but it nevertheless succeeds as a proof of concept while defining the most important ideas. To the best of our knowledge, an extension of the SSR of the previous section to $T > 0$ has not been done in the literature before.

At $T = 0$, the SSR was implemented through the operators $\mathbb{1}^\pm$, which were defined via the phase space measure in Eq. (4.5). Our extension of the SSR to $T \geq 0$ will therefore be done by defining $\mathbb{1}_{T \geq 0}^\pm$ through a thermal phase space measure. This thermal measure will be constructed by modifying the $T = 0$ measure to be valid at finite temperatures. Importantly, the $T = 0$ measure in Eq. (4.5) is the same for both bosons and fermions. Since the spin-statistics theorem [66, 67] says that bosons and fermions behave differently in a statistical (e.g. thermal) setting, we expect that the extended $T \geq 0$ measure should differ not only in a T -dependence, but also in a spin-dependence. The extension to $T \geq 0$ can be found by noting three important qualities of a finite-temperature system:

1. Particles and anti-particles behave identically under the spin-statistics theorem. It is therefore expected that any thermal effects we add to our phase space should be independent of whether the phase space describes a particle or an anti-particle. Since the only possible difference between these two cases can be the sign of p_0 , we will take the additional thermal structure to be introduced through $n_A(p_0) \equiv f_A(|p_0|)$,²⁰ where $f_A(p_0)$ is the thermalized phase space distribution of a particle A , like in Eq. (2.9).
2. We want only on-shell particles to be measurable within the plasma, and can therefore expect the extension to feature a factor of $\delta(p^2 - m^2)$, just like in Eq. (4.5). If we want to include the effects of unstable particles without a sharp mass, we can do this later through a BW propagator, like we discovered in Chapter 3.
3. The thermal measure should reproduce Eq. (4.5) in the limit $T \rightarrow 0$. Since $n_A(p_0) \rightarrow 0$ as $T \rightarrow 0$, this means that the thermal correction should be *added* to Eq. (4.5) (the alternative would have been multiplication). Effectively, we are creating a linear combination of all different constraints which we want our phase space volume element to be subject to.

Together, this motivates the thermal phase space measure

$$d\Pi_{X, T \geq 0}^\pm \equiv \prod_{j \in X} \frac{d^4 p_j}{(2\pi)^4} (2\pi) \delta(p_j^2 - m_j^2) [\theta(\pm p_j^0) + \tilde{n}_j(p_j^0)], \quad (4.13)$$

as this expression satisfies the three points above, except in the appearance of

$$\tilde{n}_j(\omega) \equiv \tilde{f}_j(|\omega|) = \frac{\varepsilon_j}{e^{|\omega|\beta} - \varepsilon_j}, \quad (4.14)$$

²⁰ $n_A(p_0)$ must not be confused with the number density of Eq. (2.2) which shares an unfortunately similar labelling.

instead of the promised $n_j(\omega)$. This is only a sign-change in the fermionic case, and is as hard to motivate as the definition $\Gamma_{\text{BW}} = \Gamma_d - \varepsilon_\phi \Gamma_p$, which we encountered in Section 3.4. The factor of $[\theta(\pm p_j^0) + \tilde{n}_j(p_j^0)]$ is ubiquitous in thermal theory – more commonly known when expressed as

$$\theta(+p_0) + \tilde{n}_j(p_0) = \epsilon(p_0)(1 + \tilde{f}_j(p_0)), \quad (4.15)$$

$$\theta(-p_0) + \tilde{n}_j(p_0) = \epsilon(p_0)\tilde{f}_j(p_0). \quad (4.16)$$

These are the factors used in the suppression of the phase space due to Pauli blocking/Bose enhancement, so it is only natural that they appear in the volume element of our thermal phase space. Had we used $n_j(\omega)$ instead of $\tilde{n}_j(\omega)$ in Eq. (4.13), these blocking/enhancement terms would be different and not match those required by the spin-statistics theorem, but we shall see the true reason behind its appearance in Chapter 6. In the case of fermionic states, a sum over spin should be included in Eq. (4.13), cf. Eq. (4.17) in ref. [26]. For a broader discussion on the structure of the thermal phase space, see ref. [56].

At $T = 0$, we used that the superposition $|+\rangle + |-\rangle$ for $|\pm\rangle \in \mathcal{H}^\pm = \mathcal{B}^\pm$ is non-physical in order to argue for the orthogonality of the two Hilbert spaces with phase space measures $d\Pi^\pm$. Since $d\Pi_{T \geq 0}^\pm$ seems to be the appropriate extension of these measures to finite temperatures, we will assume that the exact same procedure is possible at $T \geq 0$. In other words, the finite-temperature Hilbert spaces $\mathcal{H}_{T \geq 0}^\pm$ are orthogonal spaces with phase space measures $d\Pi_{T \geq 0}^\pm$. In order to fully implement a SSR at $T \geq 0$, we may therefore at first be tempted to proceed as we did at $T = 0$ by defining a set of self-adjoint operators as

$$\mathbb{1}_{T \geq 0}^\pm \stackrel{?}{\equiv} \sum_X \int d\Pi_{X, T \geq 0}^\pm |X\rangle\langle X|. \quad (4.17)$$

While this definition would indeed satisfy $\mathbb{1}_{T \geq 0}^\pm \mathbb{1}_{T \geq 0}^\mp = 0$, it unfortunately does not satisfy the other requirements of Eq. (4.2). It turns out that this is a manifestation of the conventional inner product normalization²¹

$$\langle \mathbf{p} | \mathbf{k} \rangle = 2E_{\mathbf{p}} (2\pi)^3 \delta^{(3)}(\mathbf{p} - \mathbf{k}), \quad (4.18)$$

where $E_{\mathbf{p}} \equiv \sqrt{|\mathbf{p}|^2 + m^2}$. Under this inner product, it is straightforward to confirm that

$$(\mathbb{1}_{T \geq 0}^+ + \mathbb{1}_{T \geq 0}^-) |\mathbf{p}\rangle = (1 + 2\tilde{n}(E_{\mathbf{p}})) |\mathbf{p}\rangle, \quad (4.19)$$

meaning $\mathbb{1}_{T \geq 0}^+ + \mathbb{1}_{T \geq 0}^-$ is *not* the identity operator. Instead, we should use the *thermal* normalization

$$\langle \mathbf{p} | \mathbf{k} \rangle = \frac{2E_{\mathbf{p}}}{1 + 2\tilde{n}(E_{\mathbf{p}})} (2\pi)^3 \delta^{(3)}(\mathbf{p} - \mathbf{k}), \quad (4.20)$$

²¹Here, we take $|\mathbf{k}\rangle$ to be an excited vacuum state – analogous to at $T = 0$. As a result, we view the plasma as a statistical collection of many excited vacuum states.

which produces Eq. (4.18) in the limit $T \rightarrow 0$. If we adapt this normalization, we indeed recover $\mathbb{1}_{T \geq 0}^+ + \mathbb{1}_{T \geq 0}^- = \mathbb{1}_{T \geq 0}$, where $\mathbb{1}_{T \geq 0}$ is the identity operator on the space of all physical plasma states. However, in order to keep the behaviour of our $T > 0$ theory as similar to the known behaviour at $T = 0$, it is not advantageous to alter a concept as fundamental as normalization. We will therefore instead scale the identity operators themselves according to²²

$$\mathbb{1}_{T \geq 0}^\pm \equiv \sum_X \int \frac{d\Pi_{X, T \geq 0}^\pm}{1 + 2\tilde{n}_X(\omega_X)} |X\rangle\langle X|, \quad (4.21)$$

where $\omega_X \equiv \sum_{j \in X} k_j^0$. This is equivalent to choosing the normalization in Eq. (4.20) because we are literally scaling the size of the unit quantity. Meanwhile, it will allow us to continue using the $T = 0$ inner product in Eq. (4.18) while still having $\mathbb{1}_{T \geq 0}^+ + \mathbb{1}_{T \geq 0}^- = \mathbb{1}_{T \geq 0}$. Lastly, a similar procedure as in the previous section yields $\mathbb{1}_{T \geq 0}^\pm \mathbb{1}_{T \geq 0}^\pm = \mathbb{1}_{T \geq 0}^\pm$. In all, the operators in Eq. (4.21) satisfy the requirements of Eq. (4.2), meaning they are projection operators which implement a SSR at finite temperatures. The full Hilbert space of states that satisfy $p^2 = m^2$ and are part of a thermal plasma is therefore $\mathcal{H}_{T \geq 0} \equiv \mathcal{H}_{T \geq 0}^+ \oplus \mathcal{H}_{T \geq 0}^-$.

At $T = 0$, we implemented the SSR by first constructing the space of all on-shell states \mathcal{H} and then splitting it into \mathcal{H}^+ and \mathcal{H}^- . At $T > 0$, we did the reverse by first defining $\mathcal{H}_{T \geq 0}^\pm$ and then piecing them together to form the full Hilbert space of physical plasma states, $\mathcal{H}_{T \geq 0}$. But what exactly is this ‘‘plasma state space’’? Since $\mathbb{1}_{T \geq 0}^+ + \mathbb{1}_{T \geq 0}^- = \mathbb{1}_{T \geq 0}$ is the identity operator on $\mathcal{H}_{T \geq 0}$, we can uncover what $\mathcal{H}_{T \geq 0}$ is by observing

$$\mathbb{1}_{T \geq 0} = \mathbb{1}_{T \geq 0}^+ + \mathbb{1}_{T \geq 0}^- \quad (4.22)$$

$$= \sum_X \int \left[\prod_{j \in X} \frac{d^4 p_j}{(2\pi)^4} (2\pi) \delta(p_j^2 - m_j^2) \right] |X\rangle\langle X|. \quad (4.23)$$

All thermal factors cancel, and we are left with the same identity operator as at $T = 0$ (cf. Eq. (4.6)). In other words, the Hilbert space of all physical on-shell states is temperature independent: $\mathcal{H}_{T \geq 0} = \mathcal{H}$. When we go from studying systems at $T = 0$ to systems in a plasma with $T > 0$, the only thing that changes is the way \mathcal{H} decomposes into its SSR sectors.

This marks one of the most important differences between the SSR at $T = 0$ and at $T > 0$: At finite temperatures we have²³ $\mathcal{H}^\pm \neq \mathcal{B}^\pm$. This can explicitly be seen from Eq. (4.13), where the presence of $\tilde{n}_j(p_0)$ implies that the phase space measure $d\Pi_X^+$ now gets contributions from $p_0 < 0$, and $d\Pi_X^-$ from $p_0 > 0$. A finite-temperature system with

²²One may ask why we do not simply absorb the awkward factor of $1/(1 + 2\tilde{n}_X(\omega_X))$ into the definition of $d\Pi_{T \geq 0}^\pm$ and recover the simple structure of Eq. (4.17). While viable, this would negate the arguments we used to construct the phase space measure in the first place. It is rather comforting that the Pauli blocking/Bose enhancement structure emerges naturally within the phase space measure itself. One is free to choose where to put this awkward factor, but we found Eq. (4.21) to be the most convenient choice.

²³Henceforth, we will drop the subscript ‘‘ $T \geq 0$ ’’ and instead let the temperature dependence be implicit.

$p_0 > 0$ will therefore not consist exclusively of states within a single sector. Aware of this insight, we can formalize the relationship which the phase space measure in Eq. (4.13) has with the Pauli blocking/Bose enhancement structure by making the following observations:

$$\begin{aligned} d\Pi_X^+ \stackrel{p_0 > 0}{=} \prod_{j \in X} \frac{d^3 \mathbf{p}_j}{(2\pi)^3 2E_j} [1 + \tilde{f}_j(E_j)], & \quad d\Pi_X^- \stackrel{p_0 \leq 0}{=} \prod_{j \in X} \frac{d^3 \mathbf{p}_j}{(2\pi)^3 2E_j} [1 + \tilde{f}_j(E_j)], \\ d\Pi_X^+ \stackrel{p_0 \leq 0}{=} \prod_{j \in X} \frac{d^3 \mathbf{p}_j}{(2\pi)^3 2E_j} \tilde{f}_j(E_j), & \quad d\Pi_X^- \stackrel{p_0 > 0}{=} \prod_{j \in X} \frac{d^3 \mathbf{p}_j}{(2\pi)^3 2E_j} \tilde{f}_j(E_j), \end{aligned} \tag{4.24}$$

where we defined the energies as $E_j \equiv |p_j^0|$. If we for a minute forget the additional factor of ε_j in \tilde{f}_j compared to the expected f_j (in Appendix F we will argue that \tilde{f}_j actually *is* the correct choice for our thermal measure), we observe that the appropriate blocking/enhancement terms arise naturally in the phase space measures when individually evaluated at $p_0 > 0$ and $p_0 < 0$. This tells us that states on \mathcal{H}^\pm carry the thermal blocking/enhancement structure of initial states when $\pm p_0 < 0$. Similarly, states on \mathcal{H}^\pm carry the thermal structure of final states when $\pm p_0 > 0$. We will use this insight later in Section 6.4 when constructing a new collision operator with appropriate thermal blocking/enhancement factors.

How then are we to interpret particles and anti-particles at finite temperatures? Through Eq. (4.24), we observe that if the sign of p_0 makes \mathcal{H}^+ follow an initial(final)-state suppression, it will make states on \mathcal{H}^- follow a final(initial)-state suppression. Therefore, if we take \mathcal{H}^+ to contain particles and \mathcal{H}^- to contain anti-particles, we recover the idea of particles and anti-particles have opposite notions of the direction of time in a process (we formally prove this in Section 4.3). This extends the Feynman-Stueckelberg interpretation to finite temperatures, where we take states on \mathcal{H}^- to be anti-particles of states on \mathcal{H}^+ , and the energies are always positive $E \equiv |p_0|$. In the limit $T \rightarrow 0$, this recovers the existing Feynman-Stueckelberg interpretation since $\lim_{T \rightarrow 0} \mathcal{H}^\pm = \mathcal{B}^\pm$.

At $T = 0$, we arrived at the interpretation that a CPT transformation amounted to “switching SSR sectors”, and that the inherent CPT symmetry implied physically indistinguishable sectors. At $T \geq 0$, we will assume that a CPT transformation still switches between states in the sectors \mathcal{H}^\pm .²⁴ We therefore expect our thermal theory to express a CPT-invariance in the same manner as at $T = 0$, meaning results like Eq. (4.11) will be taken to hold at all temperatures. The CPT interpretation was more straightforward at $T = 0$ where we just happened to have $\mathcal{H}^\pm = \mathcal{B}^\pm$. We must therefore be careful, as this may impose a bias towards concluding a relationship between CPT and \mathcal{B}^\pm . Instead, we claim that this relationship in reality is between CPT and \mathcal{H}^\pm .

4.2.1 The Thermal BW Decay Rate

With the SSR at finite temperature in place, we can derive the optical theorem through a similar procedure as at $T = 0$; see Appendix A.2. Eq. (A.13) lets us calculate the imaginary

²⁴It might be possible to prove this statement through a more rigorous treatment of the CPT operator with respect to superselection rules. Unfortunately, that is outside the scope of this project.

component of forward scattering amplitudes, $\mathcal{M}_{A \rightarrow A}$. However, in order to calculate Γ_{BW} , we are interested in (the imaginary part of) $\Pi(\omega)$ – not $\mathcal{M}_{A \rightarrow A}$. Luckily, in Section 3.3, we concluded that the former is the amputated diagram of the latter. This means that if we substitute the matrix elements $\mathcal{M}_{A \rightarrow X}$ in Eq. (A.13) for ones where the external A -line is amputated, we should get the imaginary component of the self-energy instead of the forward scattering. We denote matrix elements where the external A is amputated by $\mathcal{M}_{\underline{A} \rightarrow X}$, giving

$$\Gamma_{\text{BW}}(p) = \frac{1}{2\omega_A} \frac{1}{1 + \tilde{f}_A(\omega_A)} \sum_X \int d\Pi_X^+ (2\pi)^4 \delta^{(4)}(p_A - p_X) |\mathcal{M}_{\underline{A} \rightarrow X}|^2. \quad (4.25)$$

This expression will finally let us calculate the BW decay rate at finite temperatures. Since Wick's theorem is well-defined at finite temperature [29, 68, 69], the matrix elements $\mathcal{M}_{\underline{A} \rightarrow X}$ in Eq. (4.25) are still constructed from contractions between field operators. In order to calculate these matrix elements, we therefore have to establish what contractions like $\overline{A_x A_y}$, i.e. the propagators, are at finite temperature.

4.3 Thermal Propagators

Usually, the thermal propagators are derived from an analytical continuation of imaginary-time thermal QFT and the Keldysh contour [26, 29, 30, 46], but we will show that they can also appear as an artefact of the SSR and choice of phase space.

Our approach to deriving the thermal propagator will be to first find an expression for the two-point correlator using the Källén-Lehmann spectral representation and then pick the free-field spectral function. We will be considering the case of A being a scalar field, and the extension to fermions and vectors will be stated at the end.

The primary difference between QFT at $T = 0$ and our approach at $T \geq 0$, is that we have taken the phase space measure to be as in Eq. (4.13) instead of as in Eq. (4.5). As long as we keep the SSR in mind, the approach to deriving the $T \geq 0$ correlator should be the same as at $T = 0$ but with the phase space volume element substituted by Eq. (4.13). Much of the derivation is therefore identical to the one done at $T = 0$ by Schwartz in Chapter 24 of ref. [40].

We define the time-ordered correlator as

$$iD(x - y) \equiv \langle \Omega | T \{ A(x) A(y) \} | \Omega \rangle \quad (4.26)$$

$$= \theta(x_0 - y_0) \langle \Omega | A(x) A(y) | \Omega \rangle + \theta(y_0 - x_0) \langle \Omega | A(y) A(x) | \Omega \rangle, \quad (4.27)$$

where $|\Omega\rangle$ is the vacuum state²⁵ and $T\{\dots\}$ indicates the conventional time-ordering. The finite-temperature vacuum expectation value of $A(x)A(y)$ can be expressed as

$$\langle \Omega | A(x) A(y) | \Omega \rangle = \langle \Omega | A(x) (\mathbb{1}^+ + \mathbb{1}^-) A(y) | \Omega \rangle = \langle A(x) A(y) \rangle_0^+ + \langle A(x) A(y) \rangle_0^-, \quad (4.28)$$

²⁵The reason why we are considering propagation on top of vacuum and not on top on, say, a plasma-background, is that we are viewing the full plasma as a statistical collection of excited vacuum states, cf. footnote 21.

where $\langle A(x)A(y) \rangle_0^\pm \equiv \langle \Omega | A(x) \mathbb{1}^\pm A(y) | \Omega \rangle$. Inserting into Eq. (4.27), the time-ordered correlator is then

$$iD(x-y) = \theta(x_0 - y_0) [\langle A(x)A(y) \rangle_0^+ + \langle A(x)A(y) \rangle_0^-] + \theta(y_0 - x_0) [\langle A(y)A(x) \rangle_0^+ + \langle A(y)A(x) \rangle_0^-]. \quad (4.29)$$

Now, since $\mathcal{H} = \mathcal{H}^+ \oplus \mathcal{H}^-$ is subject to a SSR, we know that a state on \mathcal{H}^+ may not evolve to one on \mathcal{H}^- , and vice versa. In other words, A propagates independently on each sector. Eq. (4.29) therefore describes two types of propagation – one on \mathcal{H}^+ and one on \mathcal{H}^- . We can formalize this by defining the sector-unique correlators

$$iD^\pm(x-y) \equiv \theta(x_0 - y_0) \langle A(x)A(y) \rangle_0^\pm + \theta(y_0 - x_0) \langle A(y)A(x) \rangle_0^\pm. \quad (4.30)$$

Using the same arguments as Schwartz in Chapter 24 of ref. [40], we have

$$\langle A(x)A(y) \rangle_0^\pm = \sum_X \int d\Pi_X^\pm e^{-ip_X \cdot (x-y)} |\langle \Omega | A(0) | X \rangle|^2, \quad (4.31)$$

$$\langle A(y)A(x) \rangle_0^\pm = \sum_X \int d\Pi_X^\pm e^{-ip_X \cdot (y-x)} |\langle \Omega | A(0) | X \rangle|^2. \quad (4.32)$$

By adding these two together under Eq. (4.30), we get

$$iD^\pm(x-y) = \int \frac{d^4q}{(2\pi)^4} e^{-iq(x-y)} \sum_X \int \frac{d^4p_X}{(2\pi)^4} (2\pi) |\langle \Omega | A(0) | X \rangle|^2 (2\pi)^4 \delta^{(4)}(q - p_X) \times \left[\frac{\pm i}{q^2 - m_X^2 \pm i\epsilon} + 2\pi \tilde{n}_A(q_0) \delta(q^2 - m_X^2) \right] \quad (4.33)$$

$$= \int_0^\infty d\mu^2 (2\pi) iG^\pm(x-y; A; \mu^2) \rho(\mu^2), \quad (4.34)$$

where

$$iG^\pm(x-y; \mu^2) \equiv \int \frac{d^4q}{(2\pi)^4} e^{-iq(x-y)} \left[\frac{\pm i}{q^2 - \mu^2 \pm i\epsilon} + 2\pi \tilde{n}_A(q_0) \delta(q^2 - \mu^2) \right] \quad (4.35)$$

is the thermal propagator for a scalar A with “mass” μ and spectral density²⁶

$$\rho(\mu^2) \equiv \sum_X \int \frac{d^4p_X}{(2\pi)^4} \delta(\mu^2 - m_X^2) (2\pi)^4 \delta^{(4)}(q - p_X) |\langle \Omega | A(0) | X \rangle|^2 \quad (4.36)$$

$$= \sum_X \delta(\mu^2 - m_X^2) |\langle \Omega | A(0) | X \rangle|^2. \quad (4.37)$$

²⁶This is technically abuse of notation, because $\rho(\mu^2)$ depends on q^μ which is an integral-parameter in the definition of $iG^\pm(x-y; \mu^2)$. These equalities are therefore only true when $\rho(\mu^2)$ is part of the d^4q -integral contained in the definition of $iG^\pm(x-y; \mu^2)$.

Note that the spectral density is temperature- and sector independent. This suffices as a justification for the claim made in Section 3.3 that the extension of $\bar{\rho}$ to finite temperature holds, because this extension can be done identically to at $T = 0$. Nevertheless, inserting the free thermal spectral function, $\rho_0(\mu^2) = \delta(\mu^2 - m^2)$, into Eq. (4.34) finally gives the momentum-space thermal propagator of a scalar, A :

$$iG^\pm(p) = \frac{\pm i}{p^2 - m_A^2 \pm i\epsilon} + 2\pi\tilde{n}_A(p_0)\delta(p^2 - m_A^2). \quad (4.38)$$

We observe that $iG^-(p) = (iG^+(p))^*$,²⁷ making iG^- the reverse time-ordered propagator. In other words, time-ordering is opposite on \mathcal{H}^- compared to on \mathcal{H}^+ , proving that our extension of the Feynman-Stueckelberg interpretation to $T > 0$ indeed features particles and anti-particles with different directions of time. Since CPT switches SSR sectors and includes a time reversal, it is only natural that time-ordering on \mathcal{H}^+ and \mathcal{H}^- differ.

The form of Eq. (4.38) is that of a $T = 0$ propagator with a thermal correction term. This correction only “activates” when the particle goes on-shell, which we take to mean that only on-shell particles may be part of a plasma.²⁸ Using the Sochocki-Plemelj theorem, Eq. (3.8), we have

$$iG^+(p) = \mathcal{P}\frac{i}{p^2 - m^2} + \pi(1 + 2\tilde{n}(p_0))\delta(p^2 - m^2) \quad (4.39)$$

$$= \mathcal{P}\frac{i}{p^2 - m^2} + \pi\left([\theta(p_0) + \tilde{n}(p_0)] + [\theta(-p_0) + \tilde{n}(-p_0)]\right)\delta(p^2 - m^2), \quad (4.40)$$

which, when compared to the phase space measure in Eq. (4.13), explicitly illustrates that propagation of on-shell particles on \mathcal{H}^+ is a mix of propagation on both \mathcal{B}^+ and \mathcal{B}^- .

In the fermionic or vector boson case, the procedure is principally identical. Any additional tensor structure will enter our expressions through the inner products in Eq. (4.31) and Eq. (4.32), meaning the thermal corrections appear in an identical manner to how they did for scalars. For a fermionic field A , we therefore have [29, 71]

$$iG^+(p) = (\not{p} + m_A) \left[\frac{i}{p^2 - m_A^2 + i\epsilon} + 2\pi\tilde{n}_A(p_0)\delta(p^2 - m_A^2) \right], \quad (4.41)$$

while for a vector boson, we have

$$iG_{\mu\nu}^+(p) = \left(-g_{\mu\nu} + (1 - \xi) \frac{p_\mu p_\nu}{p^2} \right) \left[\frac{i}{p^2 - m_A^2 + i\epsilon} + 2\pi\tilde{n}_A(p_0)\delta(p^2 - m_A^2) \right]. \quad (4.42)$$

Using these propagators, we can calculate the (amputated) matrix elements $\mathcal{M}_{\underline{A} \rightarrow X}$ required to determine the BW decay rate in Eq. (4.25).

²⁷In the case of propagators of arbitrary spin, the complex conjugation refers only to the $\pm i$ in the numerator and $\pm i\epsilon$ and not to group- or Dirac indices [26, 70].

²⁸As previously stated, resonant off-shell contributions are accounted for via the BW scheme.

4.3.1 The Thermal BW Propagator

We have not yet established what the BW *propagator* looks like at finite temperatures. Naïvely, one would expect that since the time-ordered scalar propagator at $T \geq 0$ takes the form Eq. (4.38), the scalar BW propagator at finite temperature should be

$$iG_{\text{BW}}(p) \stackrel{?}{=} \frac{i}{p^2 - m^2 + im\Gamma_{\text{BW}}} + 2\pi\tilde{n}(p_0)\delta(p^2 - m^2), \quad (4.43)$$

as this is the most trivial extension of the $T = 0$ BW propagator. However, due to the $\delta(p^2 - m^2)$ in Eq. (4.43), this form violates the ideas we thoroughly explored in Chapter 3 regarding an unstable particle having a “less sharp” mass than a stable particle. The δ in Eq. (4.43) would imply that only particles of sharp masses may contribute to the plasma, but as discussed at the end of Chapter 3, the idea behind the thermal BW propagator is to account for thermal effects of unstable resonant particles with non-sharp mass. In order to get to the appropriate BW propagator, we must instead “widen” the infinitely sharp $\delta(p^2 - m^2)$ appearing in Eq. (4.39). To do this, note that, when compared to the $T = 0$ time-ordered propagator

$$iG_F(p) = \mathcal{P} \frac{i}{p^2 - m^2} + \pi\delta(p^2 - m^2), \quad (4.44)$$

Eq. (4.39) simply corresponds to a re-scaling $\delta(p^2 - m^2) \rightarrow (1 + 2\tilde{n}(p_0))\delta(p^2 - m^2)$ in $G_F(p)$. This means that if we simply re-scale our distribution space by the appropriate factor, the finite temperature BW propagator will end up in the familiar form

$$\bar{G}(p^2; \bar{\epsilon}) = \frac{1}{p^2 - m^2 + i\bar{\epsilon}}, \quad (4.45)$$

which would be in accordance with the “widening of a resonance curve”-approach of Chapter 3. Luckily, we have already implemented this re-scaling when we chose the identity operators in Eq. (4.21) instead of Eq. (4.17). At finite temperature, we therefore still have

$$G_{\text{BW}}(p^2) = \bar{G}(p^2; \text{Im } \Pi(\omega)). \quad (4.46)$$

Lastly, since $\Pi(\omega)$ becomes temperature dependent, it follows that the location of the real pole mass, Eq. (3.22), is different from at $T = 0$. From this we can adopt the concept of a “thermal mass”, $m(T)$, into our propagators. Though this is an interesting in concept in its own regard, we will not discuss thermal masses at any length in this thesis.

4.4 Cutting Rules at Finite Temperature

Having established how the finite-temperature propagators behave, we can start calculating the matrix elements in Eq. (4.25) required for Γ_{BW} . In this section, we show how the concept of *finite temperature cutting rules* (first derived by Kobes and Semenoff in ref. [26])

emerges from the thermal theory which we have been constructing. The idea behind this cutting scheme is that it allows us to view the product of matrix elements $\mathcal{M}_{A \rightarrow X} \mathcal{M}_{A \rightarrow X}^\dagger$ in Eq. (4.25) as a single higher-order diagram. At zero temperature, these reduce to the celebrated *Cutkosky cutting rules* [72] which state that there is a one-to-one correspondence between the way that we can cut a loop diagram and the ways in which intermediate particles can go on-shell in the same diagram. At finite temperature, it will turn out that this one-to-one correspondence vanishes, and we will have to adapt the cutting rules accordingly.

The theory in which we will be illustrating these cutting rules in is the one relevant to the freeze-in process, i.e. the scalar singlet model in Eq. eq. (2.15), where we take ψ to be a scalar state the fermionic/vector behaviour later. The extension to arbitrary theories should be apparent. At LO, the only process to consider is $\phi \rightarrow \psi\psi$, which means that the BW rate is

$$\Gamma_{\text{BW}}(p) = \frac{1}{2\omega} \frac{1}{1 + f_\phi(\omega)} \int d\Pi_{\psi_1}^+ d\Pi_{\psi_2}^+ \mathcal{M}_{\phi \rightarrow \psi\psi} \mathcal{M}_{\phi \rightarrow \psi\psi}^\dagger (2\pi)^4 \delta^{(4)}(p - k - q) \quad (4.47)$$

where p^μ is the 4-momentum of ϕ , and k^μ and q^μ are the 4-momenta of the two final state ψ . The lowest order contribution to this expression comes from the diagram

$$\mathcal{M}_{\phi \rightarrow \psi\psi} = \text{---} \left\langle \begin{array}{l} \diagup \\ \diagdown \end{array} \right. + \mathcal{O}(\lambda^2) = -i\lambda + \mathcal{O}(\lambda^2), \quad (4.48)$$

where dashed lines indicate ϕ and solid lines indicate ψ . To $\mathcal{O}(\lambda^2)$, the integral required to calculate Γ_{BW} is therefore

$$\begin{aligned} & \int \frac{d^4k}{(2\pi)^4} \frac{d^4q}{(2\pi)^4} (-i\lambda) [\theta(k_0) + \tilde{n}_\psi(k_0)] 2\pi\delta(k^2 - m_\psi^2) \\ & \quad \times (+i\lambda) [\theta(q_0) + \tilde{n}_\psi(q_0)] 2\pi\delta(q^2 - m_\psi^2) \\ & \quad \times (2\pi)^4 \delta^{(4)}(p - k - q), \end{aligned} \quad (4.49)$$

where the thermal factors come from the phase space measures $d\Pi_{\psi_1}^+$ and $d\Pi_{\psi_2}^+$. We notice that if we define

$$Q_A(k) \equiv [\theta(k_0) + \tilde{n}_A(k_0)] 2\pi\delta(k^2 - m_A^2), \quad (4.50)$$

then we can write Eq. (4.49) as

$$\int \frac{d^4k}{(2\pi)^4} \frac{d^4q}{(2\pi)^4} (-i\lambda) Q_\psi(k) (+i\lambda) Q_\psi(q) \times (2\pi)^4 \delta^{(4)}(p - k - q). \quad (4.51)$$

If we simply pretend that $Q_A(k)$ is a propagator, this expression looks an awful lot like that

of a one-loop diagram:²⁹

$$\begin{array}{c} k \\ \circlearrowleft \\ q \end{array} \text{---} = \int \frac{d^4k}{(2\pi)^4} \frac{d^4q}{(2\pi)^4} (-i\lambda) iG_F(k) (-i\lambda) iG_F(q) \times (2\pi)^4 \delta^{(4)}(p-k-q). \quad (4.52)$$

The main difference between this expression and Eq. (4.51) is the sign in front of one of the $i\lambda$. In order to view Eq. (4.51) as a loop-diagram, we can therefore pretend that there exists another type of vertex (which we will indicate with a circle around that vertex) which contributes $+i\lambda$ instead of the usual $-i\lambda$. This means that we can diagrammatically represent the integral in Eq. (4.51) as³⁰

$$\left(\text{---} \begin{array}{c} / \\ \backslash \end{array} \right) \times \left(\text{---} \begin{array}{c} / \\ \backslash \end{array} \right)^\dagger = \text{---} \begin{array}{c} k \\ \diamond \\ q \end{array} \circ \text{---} \quad (4.53)$$

On the RHS, propagation from a non-circled to a circled vertex is given by $Q_\psi(p)$ (equivalently, propagation from a circled to a non-circled vertex is given by $Q_\psi(-p)$), the non-circled vertex contributes a $-i\lambda$ and the circled contributes a $+i\lambda$. In other words, we can view the integral over the product of matrix elements in Eq. (4.25) as a single matrix element constructed from circled and non-circled vertices with propagation through $Q_A(k)$. To $\mathcal{O}(\lambda^2)$, the BW rate can then be written

$$\Gamma_{\text{BW}} = \frac{1}{2\omega} \frac{1}{1 + \tilde{f}_\phi(\omega)} \times \left(\text{---} \begin{array}{c} \diamond \\ \circ \end{array} \text{---} + \mathcal{O}(\lambda^4) \right). \quad (4.54)$$

To properly illustrate this idea, let us consider a higher-order contribution to the same process. Denoting by $\mathcal{M}^{(n)}$ the $\mathcal{O}(\lambda^n)$ order contribution to the full matrix element, i.e. $\mathcal{M} = \sum_n \mathcal{M}^{(n)}$, we take $\mathcal{M}_{\underline{\phi} \rightarrow \psi\psi}^{(1)}$ to be as in Eq. (4.48) and

$$\mathcal{M}_{\underline{\phi} \rightarrow \psi\psi}^{(3)} = \text{---} \begin{array}{c} k_1 \\ / \\ \backslash \\ k_2 \end{array} \begin{array}{c} \downarrow \\ k_3 \end{array} \quad (4.55)$$

$$\begin{aligned} &= (-i\lambda)^3 \int \frac{d^4k_1}{(2\pi)^4} \frac{d^4k_2}{(2\pi)^4} \frac{d^4k_3}{(2\pi)^4} iG_\psi^+(k_1) iG_\psi^+(k_2) iG_\phi^+(k_3) \\ &\quad \times (2\pi)^{12} \delta^{(4)}(p-k_1-k_2) \delta^{(4)}(k_1-k_3-q) \delta^{(4)}(k_2+k_3-k) \end{aligned} \quad (4.56)$$

²⁹Unless noted otherwise, all momentum flows from the left to the right in the following diagrams.

³⁰The sharp corners in this diagram are merely an artistic choice to emphasize that the diagram comes from a diagrammatic product. This notation for multiplying together finite-temperature diagrams was first developed by Kobes and Semenoff in ref. [26].

where $iG_A^+(k)$ is the thermal propagator of a field A (which we found in Section 4.3). Then, one of the $\mathcal{O}(\lambda^4)$ contributions to Γ_{BW} in Eq. (4.54) is

$$\begin{aligned} & \int d\Pi_{\psi_1}^+ d\Pi_{\psi_2}^+ \mathcal{M}_{\phi \rightarrow \psi\psi}^{(1)} \left(\mathcal{M}_{\rightarrow \psi\psi}^{(3)} \right)^\dagger (2\pi)^4 \delta^{(4)}(p - k - q) \\ &= \int \frac{d^4k}{(2\pi)^4} \frac{d^4q}{(2\pi)^4} \frac{d^4k_1}{(2\pi)^4} \frac{d^4k_2}{(2\pi)^4} \frac{d^4k_3}{(2\pi)^4} (-i\lambda)(i\lambda)^3 Q_\psi(k) Q_\psi(q) iG_\psi^-(k_1) iG_\psi^-(k_2) iG_\phi^-(k_3) \\ & \quad \times (2\pi)^{16} \delta^{(4)}(p - k_1 - k_2) \delta^{(4)}(k_1 - k_3 - q) \delta^{(4)}(k_2 + k_3 - k) \delta^{(4)}(p - k - q). \end{aligned} \quad (4.57)$$

This expression also resembles that of a loop-diagram with circled and non-circled vertices. Particularly, if we define the propagator between circled (non-circled) vertices to be iG_A^- (iG_A^+), we note that we can diagrammatically represent the above product as

$$\left(\text{---} \langle \text{---} \right) \times \left(\text{---} \langle \text{---} \right)^\dagger = \text{---} \langle \text{---} \text{---} \text{---} \text{---} \rangle \text{---} . \quad (4.58)$$

This means that we can include one of the NLO contributions to the BW rate as

$$\Gamma_{\text{BW}} = \frac{1}{2\omega} \frac{1}{1 + \tilde{f}_\phi(\omega)} \times \left(\text{---} \langle \text{---} \rangle \text{---} + \text{---} \langle \text{---} \text{---} \text{---} \rangle \text{---} + \mathcal{O}(\lambda^4) \right). \quad (4.59)$$

It turns out that this diagrammatic representation extends to all orders of λ , and that for every product $\mathcal{M}_{\phi \rightarrow \psi\psi}^{(n)} \left(\mathcal{M}_{\phi \rightarrow \psi\psi}^{(m)} \right)^\dagger$, a corresponding loop-diagram consisting of circled and non-circled vertices exist. Although it is not difficult to convince oneself that this is true, we refer to ref. [26] for a more formal treatment of this claim. Hence, rather than viewing the integral required to calculate Γ_{BW} as consisting of the product of two diagrams, we can instead consider a single diagram consisting of circled and non-circled vertices and propagators $G_A^+(k)$, $G_A^-(k)$, $Q_A(k)$, $Q_A(-k)$ – one for each of the 2^2 different ways of connecting circled and non-circled vertices. We will refer to the diagrams constructed from circled and non-circled vertices that can be viewed as diagrammatic products of two diagrams as *compound diagrams*.

The compound diagram in Eq. (4.58) is one example of a family of similar compound

diagrams which also appear at NLO:

$$\left(\begin{array}{c} \diagup \\ \text{---} \triangleleft \\ \diagdown \end{array} \right) \times \left(\begin{array}{c} \diagup \\ \text{---} \triangleleft \\ \diagdown \end{array} \right)^\dagger = \begin{array}{c} \diagup \\ \text{---} \triangleleft \bigcirc \text{---} \\ \diagdown \end{array}, \quad (4.60)$$

$$\left(\begin{array}{c} \diagup \\ \text{---} \triangleleft \text{---} \\ \diagdown \end{array} \right) \times \left(\begin{array}{c} \diagup \\ \text{---} \triangleleft \text{---} \\ \diagdown \end{array} \right)^\dagger = \begin{array}{c} \diagup \\ \text{---} \triangleleft \bigcirc \text{---} \\ \bigcirc \end{array}, \quad (4.61)$$

$$\left(\begin{array}{c} \diagup \\ \text{---} \triangleleft \text{---} \\ \diagdown \end{array} \right) \times \left(\begin{array}{c} \diagup \\ \text{---} \triangleleft \text{---} \\ \diagdown \end{array} \right)^\dagger = \begin{array}{c} \bigcirc \\ \diagup \\ \text{---} \triangleleft \bigcirc \text{---} \\ \diagdown \end{array}. \quad (4.62)$$

In general, we observe that the effect of conjugating a diagram is to flip it along the vertical axis and circle all internal vertices. When this conjugate is multiplied by a non-conjugated diagram, the two are “glued” together in the most intuitive manner – forming a compound diagram. By our above definitions, these compound diagrams can then be calculated through the following set of rules (known as the finite temperature *cutting rules*):

- Non-circled vertices contribute a factor $-i\lambda$, circled vertices contribute a factor $+i\lambda$.
- Propagation from a non-circled to a circled vertex is given by $Q_A(k)$,
- Propagation from a circled to a non-circled vertex is given by $Q_A(-k)$,
- Propagation between two non-circled vertices is given by $iG_A^+(k)$,
- Propagation between two circled vertices is given by $iG_A^-(k)$,

In the case of arbitrary spin, $Q_A(k)$ becomes³¹

$$Q_A(k) \equiv [\theta(k_0) + \tilde{n}_A(k_0)] 2\pi\delta(k^2 - m_A^2) \times \begin{cases} 1 & A \text{ is a scalar,} \\ (\not{k} + m_A) & A \text{ is a fermion,} \\ \left(-g_{\mu\nu} + (1 - \xi) \frac{k_\mu k_\nu}{k^2}\right) & A \text{ is a vector boson.} \end{cases} \quad (4.63)$$

Although derived through a phase space subject to a SSR, these cutting rules align with those found in the literature [26–29, 73]. The question then becomes, can we construct a QFT which reproduces these compound diagrams? That is, can we create a field theory with Feynman rules that allows for 4 types of propagation and 2 types of vertices? If so, we can just simply consider the diagrams permitted by this theory rather than painstakingly “gluing” together different matrix elements, like we have been doing so far.

³¹The representation-specific structures, like Dirac matrices and the spacetime metric, appear due to contractions with final states.

4.5 Thermal Quantum Field Theory

If we want to describe four types of propagation between two different types of vertices, a natural suggestion is to collect them into a 2×2 propagator with components iG_{ab} for $a, b \in \{1, 2\}$, which describes the propagation from a vertex of type a to a vertex of type b . By diagrammatically representing a vertex of type 1 (2) as non-circled (circled), the 4 types of propagation outlined in the cutting rules of the previous section can be expressed through the 2×2 propagator as

$$iG_{ab}(k) \equiv \begin{pmatrix} iG_A^+(k) & Q_A(-k) \\ Q_A(k) & iG_A^-(k) \end{pmatrix}_{ab}. \quad (4.64)$$

By the results of Section 4.3, we know that a field A decomposes into a component A_+ which acts on states in \mathcal{H}^+ and propagates with iG_A^+ , and into A_- acting on \mathcal{H}^- and propagating with iG_A^- . This behaviour is expressed by the diagonal components iG_{11} and iG_{22} , respectively, and we will be addressing the interpretation of the off-diagonal elements iG_{12} and iG_{21} shortly.

In order to reproduce the cutting rules of the previous section, we will therefore consider the free generating functional

$$\mathcal{Z}_0[j_1, j_2] \propto \exp \left\{ -\frac{i}{2} \int d^4x d^4y j_a(x) G_{ab}(x-y) j_b(y) \right\}, \quad (4.65)$$

where j_1 and j_2 are source currents which couple to A_+ and A_- , respectively. In order to extend this to an interacting theory, we must determine how the interaction terms of the Lagrangian, $\mathcal{L}_I[A_+, A_-]$, look. This is not a trivial task, because even though we may know how the full field A couples, we have not defined how its components, A_+ and A_- , couple. Firstly, the SSR forbids scattering from one sector to another, meaning A_+ and A_- do not couple to each other. This means that \mathcal{L}_I must take the form $\mathcal{L}_I[A_+, A_-] = \mathcal{L}_I^+[A_+] + \mathcal{L}_I^-[A_-]$, for some functionals \mathcal{L}_I^+ and \mathcal{L}_I^- . Secondly, we want circled vertices to be identical to non-circled vertices up to a factor of -1 , meaning we must have $\mathcal{L}_I^+ = -\mathcal{L}_I^- \equiv \mathcal{V}$ as functionals.³² Thus, the full generating functional at finite temperature is

$$\mathcal{Z}[j_1, j_2] \propto \exp \left\{ -i \int d^4x \left[\mathcal{V} \left(\frac{\delta}{i\delta j_1(x)} \right) - \mathcal{V} \left(\frac{\delta}{i\delta j_2(x)} \right) \right] \right\} \mathcal{Z}_0[j_1, j_2], \quad (4.66)$$

which is the generating functional in real-time thermal QFT [29, 30, 46, 74–76]. It can be explicitly checked that the Feynman rules of this theory exactly match those of the cutting rules in the previous section.

In contrast to a usual derivation of real-time thermal QFT, we have not really claimed that Eq. (4.66) is the correct description of a general field in a thermal plasma. Instead, we merely observed a pattern in the product of matrix elements in Eq. (4.25) and formalized

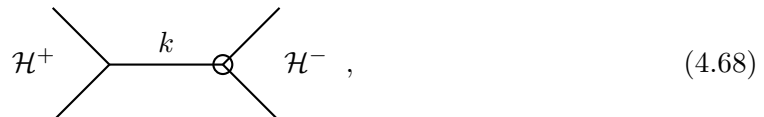
³²This is, of course, assuming real coupling constants. Although any CP-invariant theory has real coupling constants, an appropriate conjugation is required in the case of complex couplings.

them in a diagrammatic manner through cutting rules. The theory described in Eq. (4.66) is simply artificially constructed in order to produce Feynman rules akin to the cutting rules. Despite this, the results of our approach matches those of the conventional methods which aim to be a general field theoretic description of a thermalized system. Using analytic continuation one can even prove that Eq. (4.66) reproduces the generating functional of imaginary-time thermal QFT, and by extension, the partition function of a thermal system [29, 46, 75] (cf. Appendix E). There is a lot to be said about how our approach to deriving real-time thermal QFT compares to a conventional approach, which we explore in Section 6.1.

Before proceeding, we must discuss the elephant in the room; the off-diagonal elements of the 2×2 propagator iG_{ab} seem to imply that fields may propagate from one sector to another even though the SSR is implemented to directly prevent this. To address this, it helps to look at the behaviour of iG_{ab} in the $T \rightarrow 0$ limit (here in the case of A being a scalar):

$$\lim_{T \rightarrow 0} iG_{ab}(k) = \begin{pmatrix} iG_F(k) & \theta(-k_0)2\pi\delta(k^2 - m_A^2) \\ \theta(+k_0)2\pi\delta(k^2 - m_A^2) & (iG_F(k))^* \end{pmatrix}_{ab}. \quad (4.67)$$

In this limit, the off-diagonal elements carry step functions which fix the sign of p_0 , e.g. the propagation of $A_+ \rightarrow A_-$ carries $\theta(+k_0)$. Thus, if we attempt an inter-sector scattering like



where the initial states lie on \mathcal{H}^+ and the final states on \mathcal{H}^- , the integrand will contain the product $\theta(+k_0)\theta(-k_0) = 0$. Such scattering processes therefore do not contribute.

At $T > 0$, the presence of $\tilde{n}_A(k_0)$ in the off-diagonals invalidates the argument used for $T = 0$. Luckily, the SSR makes sure that any S -matrix for inter-sector scattering vanishes, meaning the process in Eq. (4.68) *does* vanish. What does *not* vanish, however, is internal inter-sector propagation, e.g. a particle may propagate from \mathcal{H}^+ to \mathcal{H}^- and back to \mathcal{H}^+ via internal propagation. Since the SSR only claims to disallow certain *measurable* processes, we must reach the conclusion that internal particles are indeed allowed to switch sectors. This is only natural because internal particles have no on-shell requirement, meaning they do not submit to any single sector. At $T = 0$ this effect vanishes due to conservation of momentum, but at $T > 0$ the effect becomes quite prevalent.

This may seem rather paradoxical; we claim that only internal (off-shell) particles are subject to inter-sector propagation, but this propagation features a factor $\delta(p^2 - m^2)$, putting them on-shell. The resolution is that such internal processes are *not measurable*. Although our theory technically predicts inter-sector scattering, the SSR will always make sure that no such process is measured. This is comparable to how gauge invariant theories technically predict the production of ghost particles, but the spin-statistics theorem prevent such processes from ever being measured.

While on this topic, we should scrutinize how literally we can interpret all 4 components iG_{ab} as propagators. This 2×2 “propagator” was constructed solely in order to reproduce

the cutting rules of the previous section, and even through the results of Section 4.3 tell us that $iG_{11} = iG_A^+$ and $iG_{22} = iG_A^-$ indeed *are* propagators, we are still “pretending” as if $iG_{12}(k) = Q_A(-k)$ and $iG_{21}(k) = Q_A(k)$ are propagators. However, if we look at Eq. (4.31) for a free spectral function, $\rho_0(q^2; A) = \delta(q^2 - m_A^2)$, we see that

$$\langle A(x)A(y) \rangle_0^\pm = \int \frac{d^4k}{(2\pi)^4} e^{-ik(x-y)} Q_A(\pm k). \quad (4.69)$$

In position-space this means that the time-ordered propagators can be written as

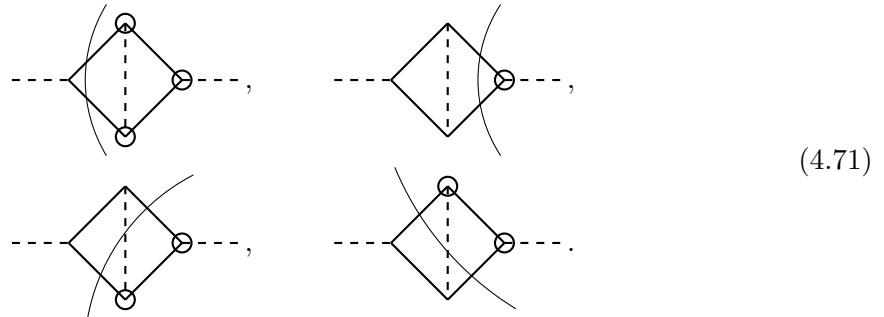
$$iG_A^\pm(x-y) = \theta(\pm(x_0 - y_0))Q_A(x-y) + \theta(\pm(y_0 - x_0))Q_A(y-x), \quad (4.70)$$

meaning $Q_A(k)$ and $Q_A(-k)$ were actually propagators all along! It is therefore appropriate to claim that all components iG_{ab} indeed are propagators. Furthermore, from Eq. (A.8), we get the Kubo-Martin-Schwinger relation [24, 25, 29, 30]: $Q_A(k) = \varepsilon_A e^{ik_0\beta} Q_A(-k)$.

4.6 What is Cutting?

So far, we have not really justified why we call the rules which we based our thermal QFT on for “cutting” rules. In this section, we will rationalize this naming and outline the ideas behind the concept of cutting, both at zero- and finite temperature.

By looking at the compound diagrams on the RHS of Eq. (4.58), Eq. (4.60), Eq. (4.61) and Eq. (4.62), we observe that the circled vertices form a connected set in the sense that we can draw a connected line vertically through all the lines propagated by Q_A (and through these lines only!) such that all circled vertices will be to the right of this line, and all non-circled to the left:



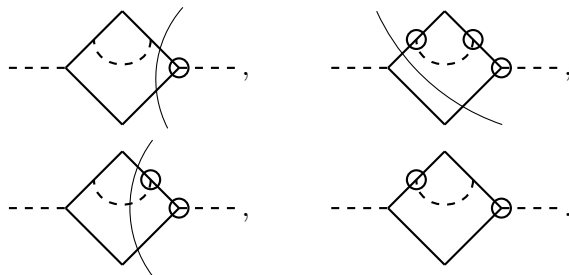
Since a compound diagram (by definition) is a product of a diagram and a conjugated diagram, its leftmost vertex (the one connected to the external initial state) must always be non-circled and its rightmost vertex (the one connected to the external final state) must always be circled. From this and Eq. (4.71), it appears that there is a one-to-one correspondence between the ways that we can cut a loop diagram and the ways we can construct compound diagrams. In other words, for the above example, there are only 4

topologically different ways of vertically cutting through the diagram


(4.72)

and there are only 4 ways of circling its vertices while creating the above-mentioned connected sets. We therefore propose that, instead of thinking in terms of “ways to circle a diagram”, we can think in terms of “ways to cut a diagram” – hence the naming of *cutting* rules.

How can we be sure that this notion extends to arbitrary compound diagrams? As a matter of fact, we can *not*! Although all compound diagrams must have its rightmost vertex circled and leftmost non-circled, we cannot generalize the notion of cutting to all compound diagrams. Take for example the 4 additional compound diagram which our theory, Eq. (2.15), produces at $\mathcal{O}(\lambda^4)$:


(4.73)

Of these, only the three first are cuttable. In the last diagram, there is no way to draw a vertical line through the Q_A lines while keeping circled vertices to the right and non-circled to the left. The notion of “cutting” therefore breaks down in this case. The above proposal is therefore *wrong*. We *must* think in terms of ways to circle compound diagrams.

At zero temperature, one can show that this uncuttable diagram vanishes: As $T \rightarrow 0$ we have $Q_A(k) \rightarrow \theta(k_0)2\pi\delta(k^2 - m_A^2)$, meaning cut particles must have $k_0 > 0$ when flowing from the left to the right side of the cutting line. The specific arrangement of circled and non-circled vertices in the last diagram of Eq. (4.73) therefore violates conservation of momentum in at least one vertex, meaning the diagram vanishes. At $T = 0$, this ends up being the case for all compound diagrams where the circled and non-circled vertices do not form connected sets [77]. In other words, at $T = 0$, every non-zero compound diagram can be viewed as one that has been physically “cut” through its Q_A lines. These are the well-established cutting rules at zero temperature [72, 77].

At finite temperature, however, this is no longer the case, as the appearance of $\tilde{n}_A(k_0)$ in $Q_A(k)$ means that k_0 is no longer restricted to be purely positive when flowing from the left to the right side of the cutting line. As such, the last diagram in Eq. (4.73) is non-zero at finite temperatures, meaning we cannot view all possible non-zero compound diagrams as ones that can be “cut” the way we can at $T = 0$. Nevertheless, it is convention to stick with the naming of “cutting rules” at finite temperatures even though the concept of “cutting” breaks down.

The awkward behaviour of this “uncuttable” compound diagram can be traced back to the diagrammatic product which it originates from:³³

$$\left(\text{---} \langle \text{---} \right) \times \left(\text{---} \circ \text{---} \right)^\dagger = \text{---} \diamond \text{---} . \quad (4.74)$$

Noticeably, this is the only compound diagram we have studied so far that comes from a product of diagrams which do not contain only non-circled vertices – none of the other diagrams in Eq. (4.71) nor Eq. (4.73) feature circled vertices in their diagrammatic product representation. The reason is that the diagram

$$\text{---} \circ \text{---} \quad (4.75)$$

is simply not one which can be calculated as $\mathcal{M}_{A \rightarrow X}$ in the QFT used for the matrix elements in Eq. (4.25). The fact that this diagram appears is a direct consequence of our formulation of a thermal QFT (cf. Eq. (4.66)) whose Feynman rules are designed to match the cutting rules. In other words, by switching to the 2×2 propagator and real-time thermal QFT, we end up producing *more* diagrams than we intended to.

The question then becomes, should we include such uncuttable compound diagrams when they were not part of our original plan? This problem was first encountered by Kobes and Semenoff in 1985 when they derived the thermal cutting rules for the very first time [26]. They discovered that, at $T > 0$, the sum of all *cuttable* compound diagrams feature ill-defined distributions, like products of identical δ -functions. If, however, one also includes the non-cuttable compound diagrams, like Eq. (4.75), into this sum, all such ill-defined distributions cancel, giving a well-behaved expression. At zero temperature, such a cancellation also happens between the three cuttable diagrams in Eq. (4.73), but at finite temperature, additional ambiguous terms arise in these three diagrams that do not cancel among themselves. For a more in-depth discussion that extends to higher orders, see ref. [26].

In order to maintain well-defined expressions, we will therefore include uncuttable compound diagrams in our calculations. Accumulatively, these diagrams make up the $A_+ \rightarrow A_-$ self-energy

$$\Pi_{21}^A(p) \equiv \text{---} \overset{p}{\langle} \text{---} \circ \text{---} \text{---} , \quad (4.76)$$

meaning the BW decay rate in Eq. (4.25) can be written on the compact form

$$\Gamma_{\text{BW}} = \frac{1}{2\omega} \frac{1}{1 + \tilde{f}_A(\omega)} \Pi_{21}^A(p), \quad (4.77)$$

where ω is the A energy in the plasma frame. This equation constitutes one of our central results, as we can finally start calculating Γ_{BW} at finite temperatures.

³³This is under the interpretation that conjugating a circled vertex turns it into a non-circled vertex.

Chapter 5

Calculating Decay Rates at $T \geq 0$

In this chapter, we will calculate Γ_{BW} for the theory in Eq. (2.15) to both one- and two-loop order, where the majority of the maths required for the latter has been moved to Appendix B. By calculating the BW rate we can compare it to the one derived by ref. [23] in Eq. (2.32).

In the following expressions, we will allow for ψ to be either a scalar or a fermion. In order to avoid having to write one explicit expression for each case, the following expressions will be written in a manner that easily allows one to extract both the fermionic and the bosonic expressions. Any expression which contains red symbols is a fermionic one, and to recover the bosonic one, simply remove the red symbols in the most intuitive manner. For example, the fermionic expression $f(x)g(x)h(x)$ becomes the bosonic expression $f(x)h(x)$. The Feynman diagrams will be drawn with scalar lines as the extension to fermionic lines is trivial.

It should also be mentioned that if ψ is a scalar (fermion), then the coupling λ has mass dimension 1 (0). In the scalar case, this makes the interpretation of the coupling constant dependent on the relevant energy scale.

5.1 One-Loop Order

It is in our interest to first consider the case where ϕ couples to two different particles, ψ_1 and ψ_2 through $\mathcal{L}_I \supset -\lambda\phi\psi_1\psi_2$, because the existing BW decay rate in Eq. (2.32) claims to hold for different final state particles. Later, we will focus on $\psi_1 = \psi_2$.

5.1.1 Different Final States: $\psi_1 \neq \psi_2$

In the following, ψ_1 and ψ_2 are taken to be of the same particle type (boson or fermion) with $m_{\psi_2} > m_{\psi_1}$. At LO, the only contribution to Π_{21}^ϕ is

$$\Pi_{21}^\phi = \text{---} \begin{array}{c} \psi_1 \\ \diagup \quad \diagdown \\ \psi_2 \end{array} \text{---} + \mathcal{O}(\lambda^4), \quad (5.1)$$

where one of the solid lines indicates ψ_1 with internal momentum k^μ and the other indicates ψ_2 with internal momentum q^μ . Using Eq. (4.77), we get

$$\begin{aligned} \Gamma_{\text{BW}}(p) = \frac{\lambda^2}{2\omega} \frac{1}{1 + f_\phi(\omega)} \sum_{\psi_1 \psi_2} \int \frac{d^4 k}{(2\pi)^3} \frac{d^4 q}{(2\pi)^3} (2\pi)^4 \delta^{(4)}(p - k - q) \delta(k^2 - m_{\psi_1}^2) \delta(q^2 - m_{\psi_2}^2) \\ \times \epsilon(k^\mu u_\mu) \epsilon(q^\mu u_\mu) (1 + \tilde{f}_{\psi_1}(k^\mu u_\mu)) (1 + \tilde{f}_{\psi_2}(q^\mu u_\mu)) \quad (5.2) \\ \times (-4)(k_\mu q^\mu + m_{\psi_1} m_{\psi_2}) \end{aligned}$$

where we used the identity in Eq. (4.15) and $\varepsilon_{\psi_1} \varepsilon_{\psi_2} = +1$. To continue, let us focus on the interplay between the two on-shell δ 's; we have

$$\begin{aligned} \delta(k^2 - m_{\psi_1}^2) \delta(q^2 - m_{\psi_2}^2) = \\ \frac{1}{4E_{\psi_1} E_{\psi_2}} [\delta(k_0 - E_{\psi_1}) + \delta(k_0 + E_{\psi_1})] [\delta(q_0 - E_{\psi_2}) + \delta(q_0 + E_{\psi_2})], \quad (5.3) \end{aligned}$$

where E_{ψ_1} and E_{ψ_2} are the ψ_1 and ψ_2 energies, respectively, in the frame where the plasma moves with a relative 4-velocity u^μ . The cross term $\delta(k_0 + E_{\psi_1}) \delta(q_0 + E_{\psi_2})$ in Eq. (5.3) vanishes due to the $\delta^{(4)}(p - k - q)$ in Γ_{BW} . The two cross terms $\delta(k_0 \pm E_{\psi_1}) \delta(q_0 \mp E_{\psi_2})$ imply that $p_0 = \mp(E_{\psi_1} - E_{\psi_2})$. Since ϕ is on \mathcal{B}^+ , we have $p_0 > 0$, meaning one of these cross terms must vanish while the other survives. Since $m_{\psi_2} > m_{\psi_1}$, it follows that the cross term $\delta(k_0 - E_{\psi_1}) \delta(q_0 + E_{\psi_2})$ vanishes because it would imply $p_0 < 0$. Thus, the only surviving δ cross terms are $\delta(k_0 - E_{\psi_1}) \delta(q_0 - E_{\psi_2})$ and $\delta(k_0 + E_{\psi_1}) \delta(q_0 - E_{\psi_2})$, giving

$$\begin{aligned} \Gamma_{\text{BW}}(p) = \frac{\lambda^2}{2\omega} \frac{1}{1 + f_\phi(\omega)} \sum_{\psi_1 \psi_2} \int \frac{d^3 \mathbf{k}}{(2\pi)^3 2E_{\psi_1}} \frac{d^3 \mathbf{q}}{(2\pi)^3 2E_{\psi_2}} (2\pi)^4 \delta^{(3)}(\mathbf{p} - \mathbf{k} - \mathbf{q}) \\ \times \left[\delta(p_0 - E_{\psi_1} - E_{\psi_2}) \left(1 + \tilde{f}_{\psi_1}(k^\mu u_\mu) \right)_{k_0=E_{\psi_1}} \left(1 + \tilde{f}_{\psi_2}(q^\mu u_\mu) \right)_{q_0=E_{\psi_2}} \quad (5.4) \right. \\ \times (-4)(E_{\psi_1} E_{\psi_2} - \mathbf{k} \cdot \mathbf{q} - m_{\psi_1} m_{\psi_2}) \\ \left. + \delta(p_0 + E_{\psi_1} - E_{\psi_2}) \tilde{f}_{\psi_1}(-k^\mu u_\mu)_{k_0=-E_{\psi_1}} \left(1 + \tilde{f}_{\psi_2}(q^\mu u_\mu) \right)_{q_0=E_{\psi_2}} \right. \\ \left. \times (-4)(-E_{\psi_1} E_{\psi_2} - \mathbf{k} \cdot \mathbf{q} - m_{\psi_1} m_{\psi_2}) \right]. \end{aligned}$$

Here, we used the identity $1 + \tilde{f}_A(\omega) + \tilde{f}_A(-\omega) = 0$ in order to rewrite the thermal suppressions inside the square brackets. Looking at the structure of these phase space suppressions, we see that the factor $(1 + \tilde{f}_{\psi_1}(k^\mu u_\mu))(1 + \tilde{f}_{\psi_2}(q^\mu u_\mu))$ corresponds to a phase space where both ψ_1 and ψ_2 are final states: $\phi \rightarrow \psi_1 \psi_2$. The factor $\tilde{f}_{\psi_1}(-k^\mu u_\mu)(1 + \tilde{f}_{\psi_2}(q^\mu u_\mu))$ is equivalent to ψ_1 being an initial state and ψ_2 a final state: $\phi \psi_1 \rightarrow \psi_2$. For example, the Lorentz transformed energy

$$(k^\mu u_\mu)_{k_0=E_{\psi_1}} = E_{\psi_1} u_0 - k^i u_i$$

indicates a ψ_1 *leaving* the vertex with 3-momentum \mathbf{k} , while

$$-(k^\mu u_\mu)_{k_0=-E_{\psi_1}} = E_{\psi_1} u_0 - (-k^i) u_i$$

can be thought of as an initial ψ_1 *entering* the vertex with momentum $-\mathbf{k}$. We can associate one such process to each of the 4 possible δ cross terms in Eq. (5.3):

$$\delta(k_0 - E_{\psi_1})\delta(q_0 - E_{\psi_2}) \longrightarrow \phi \rightarrow \psi_1\psi_2, \quad (5.5)$$

$$\delta(k_0 - E_{\psi_1})\delta(q_0 + E_{\psi_2}) \longrightarrow \phi\psi_2 \rightarrow \psi_1, \quad (5.6)$$

$$\delta(k_0 + E_{\psi_1})\delta(q_0 - E_{\psi_2}) \longrightarrow \phi\psi_1 \rightarrow \psi_2, \quad (5.7)$$

$$\delta(k_0 + E_{\psi_1})\delta(q_0 + E_{\psi_2}) \longrightarrow \phi\psi_1\psi_2 \rightarrow |\Omega\rangle, \quad (5.8)$$

where $|\Omega\rangle$ represents a vacuum state. Due to conservation of momentum, the processes in Eq. (5.6) and in Eq. (5.8) are forbidden (the former is not allowed because $m_\phi + m_{\psi_2} > m_{\psi_1}$). This means that, out of all the possible processes involving ψ_1 , ψ_2 and an initial ϕ , the expression in Eq. (5.4) accounts for all kinematically allowed processes: $\phi \rightarrow \psi_1\psi_2$ and $\phi\psi_1 \rightarrow \psi_2$. Usually, we do not have to account for additional processes in our calculations, but luckily all contributions from the latter process vanishes as $T \rightarrow 0$. This can be seen by going to the plasma frame where $\tilde{f}_{\psi_1}(-k^\mu u_\mu)_{k_0=-E_{\psi_1}} = \tilde{f}_{\psi_1}(E_{\psi_1})$ which vanishes as $T \rightarrow 0$.

Why must we suddenly account for additional processes at $T > 0$? The reason for this was already argued for in Section 3.4 where we concluded that if we want Γ_{BW} to actually behave like a rate at finite temperatures, we must consider the accumulative effect of *all* relevant processes. Supposedly then, these processes are $\phi \rightarrow \psi_1\psi_2$ and $\phi\psi_1 \rightarrow \psi_2$. In a plasma, the background is indistinguishable from the foreground, and there is a population of ψ_1 present for ϕ to interact with, meaning the process $\phi\psi_1 \rightarrow \psi_2$ necessarily occurs. At zero temperature, the background upon which a lone ϕ propagates does not contain any ψ_1 to couple with – hence the exclusion of such a process when calculating Γ_{BW} at $T = 0$.

It is important to mention that the identification of the terms of Eq. (5.4) with different ϕ processes through their phase space suppression is merely an interpretation and should be applied with caution. According to Eq. (4.25), all matrix elements used to calculate Γ_{BW} are of the form $\phi \rightarrow X$, which excludes $\phi\psi_1 \rightarrow \psi_2$. A more faithful interpretation of the appearance of new non-zero δ cross-terms at $T > 0$ is that, since \mathcal{B}^+ contains states from both \mathcal{H}^+ and \mathcal{H}^- , we must account for the four different ways that ψ_1 and ψ_2 can be put in these sectors. The four possible ways of putting ψ_1 and ψ_2 in \mathcal{H}^+ and \mathcal{H}^- correspond to the four processes in Eq. (5.5) to Eq. (5.8). Out of these four, only two satisfy conservation of 4-momentum for a time-like mediator ϕ . This is further supported by the above-mentioned interpretation that the 3-momentum of the incoming ψ_1 in the process $\phi\psi_1 \rightarrow \psi_2$ is $-\mathbf{k}$, which indicates a backwards trajectory when ψ_1 is on \mathcal{H}^- – in agreement with the Feynman-Stueckelberg interpretation of anti-particle-processes happening in reverse compared to particle processes.

The necessity of including additional processes was first mentioned by Weldon in ref. [31]. Here, he assigns the reason behind the appearance of this extra process as due to an additional cut in the ϕ self-energy that is not present at $T = 0$. The discontinuity across this cut is purely

imaginary and behaves like any other thermal rate. We can therefore associate $\mathcal{B}^\pm \neq \mathcal{H}^\pm$ at $T > 0$ with the appearance of an additional cut along the self-energy. What is more, Eq. (5.4) is organized exactly in the manner which Weldon desired (cf. Section 3.4); Γ_{BW} is structurally identical to how one would *expect* a decay rate to look at finite temperatures.

The BW decay rate derived by ref. [23] in Eq. (2.32) does not account for the process $\phi\psi_1 \rightarrow \psi_2$. In their derivation, they instead operate under the notion that since the specific decay process is $\phi \rightarrow \psi_1\psi_2$, then the rate at which the ϕ population decreases is given by that process alone. At zero temperature this is a correct notion because there Γ_{BW} truly is a decay rate, but at finite temperatures we have established that this is no longer the case. If we remember to include the process $\phi\psi_1 \rightarrow \psi_2$ while deriving Eq. (2.32), we get

$$\Gamma_{\text{BW}} = \frac{1}{1 + f_\phi(\omega)} \sum_{\psi_1 \neq \psi_2} \left[\Gamma_{\phi \rightarrow \psi_1\psi_2} I_{\psi_1\psi_2}(\gamma, s) + \Gamma_{\phi\psi_1 \rightarrow \psi_2} I_{\psi_2}^{\psi_1}(\gamma, s) \right], \quad (5.9)$$

where $\Gamma_{A \rightarrow B}$ is the $T = 0$ rate for the process $A \rightarrow B$ and

$$I_{\psi_2}^{\psi_1}(\gamma, s) \equiv \frac{1}{2} \int_{-1}^1 d\cos\theta \tilde{f}_{\psi_1}(k^\mu u_\mu) (1 + \tilde{f}_{\psi_2}(q^\mu u_\mu)). \quad (5.10)$$

This expression agrees with the one we derived in Eq. (5.4). Given slight modifications, the BW decay rate derived in ref. [23] therefore agrees with ours to the lowest order.

Actually, the ideas behind the derivation in ref. [23] must be tweaked a slight bit more than just including the process $\phi\psi_1 \rightarrow \psi_2$. If we naïvely include this process with the traditional phase space suppressions, then $I_{\psi_2}^{\psi_1}$ would be defined through f_{ψ_1} instead of through \tilde{f}_{ψ_1} – leading to a sign-difference in the fermionic case. It is exactly this difference between working in terms of f_A instead of in terms of \tilde{f}_A which leads to the awkward sign-differences between scalar and fermion processes, like the one we struggled to motivate in the definition of Γ_{BW} back in Section 3.4. Working in terms of \tilde{f}_A avoids having to motivate the pesky sign-differences which otherwise would appear depending on spin. We shall see another example of this in Section 6.2.

5.1.2 Identical Final States: $\psi_1 = \psi_2$

Here, we consider the case of identical final state particles: $\psi_1 = \psi_2 \equiv \psi$. In the ϕ rest-frame, we have $\mathbf{p} = 0 \Rightarrow \mathbf{k} = -\mathbf{q} \Rightarrow E_{\psi_1} = E_{\psi_2} \equiv E_\psi$. The $\delta(p_0 + E_{\psi_1} - E_{\psi_2})$ appearing in the term corresponding to the process $\phi\psi_1 \rightarrow \psi_2$ in Eq. (5.4) thus becomes $\delta(p_0)$. For any non-zero p_0 , we therefore do not get any contribution from this term. This is rather reasonable, because the process $\phi\psi \rightarrow \psi$ is not kinematically viable for a time-like massive ϕ . If ψ is a scalar, we multiply the phase space by a symmetry factor of 1/2, but not if ψ is a fermion, giving

$$\begin{aligned} \Gamma_{\text{BW}}(p) = & 2 \frac{1}{2} \frac{\lambda^2}{2\omega} \frac{1}{1 + f_\phi(\omega)} \sum_{\psi} \int \frac{d^4k}{(2\pi)^3 2E_\psi} \frac{d^4q}{(2\pi)^3 2E_\psi} (2\pi)^4 \delta^{(4)}(p - k - q) \\ & \times \delta(k_0 - E_\psi) \delta(q_0 - E_\psi) (1 + \tilde{f}_\psi(k^\mu u_\mu)) (1 + \tilde{f}_\psi(q^\mu u_\mu)) \\ & \times (-4) (E_\psi^2 - \mathbf{k} \cdot \mathbf{q} - m_\psi^2) \end{aligned} \quad (5.11)$$

This BW decay rate matches the one derived in ref. [23] to LO.

5.2 Two-Loop Order

Here, we will construct Γ_{BW} to $\mathcal{O}(\lambda^4)$ in the case of identical final states. Up to $\mathcal{O}(\lambda^4)$, the possible compound diagrams are

$$\begin{aligned}
\Pi_{21}^\phi = & \text{---} \langle \text{diamond} \rangle \text{---} \\
& + \text{---} \langle \text{diamond with vertical dashed line} \rangle \text{---} + \text{---} \langle \text{diamond with vertical dashed line and top vertex correction} \rangle \text{---} + \text{---} \langle \text{diamond with vertical dashed line and bottom vertex correction} \rangle \text{---} + \text{---} \langle \text{diamond with vertical dashed line and both vertex corrections} \rangle \text{---} \\
& + \text{---} \langle \text{diamond with horizontal dashed line} \rangle \text{---} + \text{---} \langle \text{diamond with horizontal dashed line and top vertex correction} \rangle \text{---} + \text{---} \langle \text{diamond with horizontal dashed line and bottom vertex correction} \rangle \text{---} + \text{---} \langle \text{diamond with horizontal dashed line and both vertex corrections} \rangle \text{---} \\
& + \mathcal{O}(\lambda^6)
\end{aligned} \tag{5.12}$$

We identify two classes of compound diagrams; ones corresponding to vertex corrections (second line of Eq. (5.12)) and ones corresponding to ψ self-energy corrections (third line of Eq. (5.12)). We will consider one class at a time.

5.2.1 Vertex Corrections

The four diagrams to calculate here are

$$\begin{aligned}
\mathcal{M}_1 = & \text{---} \langle \text{diamond with vertical dashed line} \rangle \text{---}, & \mathcal{M}_2 = & \text{---} \langle \text{diamond with vertical dashed line and top vertex correction} \rangle \text{---}, \\
\mathcal{M}_3 = & \text{---} \langle \text{diamond with vertical dashed line and bottom vertex correction} \rangle \text{---}, & \mathcal{M}_4 = & \text{---} \langle \text{diamond with vertical dashed line and both vertex corrections} \rangle \text{---}.
\end{aligned} \tag{5.13}$$

Their sum can be written as

$$\mathcal{M}_{\text{vertex}} = \mathcal{M}_1 + \mathcal{M}_2 + \mathcal{M}_3 + \mathcal{M}_4 \tag{5.14}$$

$$= -\lambda^4 \int \frac{d^4 k}{(2\pi)^4} \frac{d^4 l}{(2\pi)^4} (-\text{tr}\{Z\}) [\mathcal{N}_1 + \mathcal{N}_2 - \mathcal{N}_3 - \mathcal{N}_4], \tag{5.15}$$

where

$$\text{tr}\{Z\} \equiv \text{tr}\{(k + m_\psi)(l + m_\psi)(l - p + m_\psi)(k - p + m_\psi)\} \tag{5.16}$$

$$\begin{aligned}
& = 4[k \cdot l(4m_\psi^2 + p^2) - l \cdot p(k^2 + 3m_\psi^2) - k \cdot p(l^2 + 3m_\psi^2) \\
& \quad + m_\psi^2(k^2 + l^2 + p^2) + k^2 l^2 + m_\psi^4]
\end{aligned} \tag{5.17}$$

and

$$\begin{aligned}
\mathcal{N}_1(k, l) &\equiv W_\psi(k)W_\psi^+(l)W_\psi^-(l-p)W_\psi(k-p)W_\phi(k-l), \\
\mathcal{N}_2(k, l) &\equiv W_\psi^+(k)W_\psi^*(l)W_\psi^*(l-p)W_\psi^-(k-p)W_\phi^*(k-l), \\
\mathcal{N}_3(k, l) &\equiv W_\psi^+(k)W_\psi^*(l)W_\psi^-(l-p)W_\psi(k-p)W_\phi^-(k-l), \\
\mathcal{N}_4(k, l) &\equiv W_\psi(k)W_\psi^+(l)W_\psi^*(l-p)W_\psi^-(k-p)W_\phi^+(k-l),
\end{aligned} \tag{5.18}$$

for

$$W_A(k) \equiv \frac{i}{k^2 - m_A^2 + i\epsilon} + 2\pi\tilde{n}_A(k_0)\delta(k^2 - m_A^2), \tag{5.19}$$

$$W_A^\pm(k) \equiv [\theta(\pm k_0) + \tilde{n}_A(k_0)]2\pi\delta(k^2 - m_A^2). \tag{5.20}$$

Note that $\text{tr}\{Z\}$ is symmetric under $k \leftrightarrow l$ and that $\mathcal{N}_1(k, l) = (\mathcal{N}_2(l, k))^*$ and $\mathcal{N}_3(k, l) = (\mathcal{N}_4(l, k))^*$. Hence,

$$\mathcal{M}_{\text{vertex}} = -\lambda^4 \int \frac{d^4k}{(2\pi)^4} \frac{d^4l}{(2\pi)^4} (-\text{tr}\{Z\})2[\text{Re}\{\mathcal{N}_1\} - \text{Re}\{\mathcal{N}_3\}]. \tag{5.21}$$

We have performed such two-loop vertex calculations in Appendix B.

5.2.2 Self-Energy Corrections

Here, we consider the contribution from the four *self-energy* diagrams:

$$\mathcal{M}_{\text{SE}} = \text{---} \langle \text{diag}_1 \rangle \text{---} + \text{---} \langle \text{diag}_2 \rangle \text{---} + \text{---} \langle \text{diag}_3 \rangle \text{---} + \text{---} \langle \text{diag}_4 \rangle \text{---} + \dots \tag{5.22}$$

$$= \text{---} \langle \text{blob} \rangle \text{---}, \tag{5.23}$$

where the upper line with a ‘‘blob’’ defines the $\psi_+ \rightarrow \psi_-$ correlator, $D_{21}(k)$:

$$iD_{21}(k) = \text{---} \langle \text{diag}_1 \rangle \text{---} + \text{---} \langle \text{diag}_2 \rangle \text{---} + \text{---} \langle \text{diag}_3 \rangle \text{---} + \text{---} \langle \text{diag}_4 \rangle \text{---} + \dots \tag{5.24}$$

By defining the correlator with n 1PI insertions as³⁴

$$iD_{21}^{(n)}(k) \equiv \text{---} \overbrace{\langle \text{diag}_1 \rangle \dots \langle \text{diag}_1 \rangle}^{n \text{ times}} \text{---} \tag{5.25}$$

³⁴ $D_{11}^{(n)}(k)$, $D_{12}^{(n)}(k)$ and $D_{22}^{(n)}(k)$ are defined similarly, but with different initial- and final vertex circlings.

where the 1PI insertion considers all possible circlings of vertices, we can write

$$iD_{21}(k) = \sum_{n=0}^{\infty} iD_{21}^{(n)}(k). \quad (5.26)$$

Note that $iD_{ab}^{(0)}(k) = iG_{ab}(k)$ is just the $b \rightarrow a$ thermal propagator. Using this construction, we can write the contribution to \mathcal{M}_{SE} , with n and m 1PI insertions on respectively the upper and lower lines in the loop of Eq. (5.23), as

$$\mathcal{M}_{\text{SE}}^{(nm)}(p) \equiv (-i\lambda)(+i\lambda) \int \frac{d^4k}{(2\pi)^4} (-1) \text{tr} \left\{ iD_{21}^{(n)}(k) iD_{12}^{(m)}(p-k) \right\}, \quad (5.27)$$

For example, the sum of all two-loop contributions in Eq. (5.22) corresponds to $\mathcal{M}_{\text{SE}}^{(10)}$.

Next, we establish a procedure which greatly simplifies the calculation of Eq. (5.27) for arbitrary n and m . The thermal 2×2 propagator iG_{ab} of a field A , can be diagonalized through a Bogoliubov transformation as [29, 46, 70]

$$iG_{ab}(k) = U_{ac}(k_0) \begin{pmatrix} iG_F(k) & 0 \\ 0 & (iG_F(k))^* \end{pmatrix}_{cd} U_{db}(k_0), \quad (5.28)$$

where $iG_F(k)$ is the $T = 0$ time-ordered propagator of A and

$$U(k_0) \equiv \begin{pmatrix} [\theta(k_0) + \varepsilon_A \theta(-k_0)] \sqrt{1 + \tilde{n}_A(k_0)} & \varepsilon_A e^{-\beta k_0/2} \sqrt{n_A(k_0)} \\ e^{\beta k_0/2} \sqrt{n_A(k_0)} & [\theta(k_0) + \varepsilon_A \theta(-k_0)] \sqrt{1 + \tilde{n}_A(k_0)} \end{pmatrix}. \quad (5.29)$$

Through the Dyson equation [53], Le Bellac [29] shows that by defining a quantity $\bar{\Pi}^A(k)$ which is related to the $A_+ \rightarrow A_+$ self-energy, Π_{11}^A , through

$$\text{Re} \{ \bar{\Pi}^A(k) \} \equiv \text{Re} \{ \Pi_{11}^A(k) \}, \quad \text{Im} \{ \bar{\Pi}^A(k) \} \equiv \frac{\epsilon(k_0)}{1 + 2\tilde{f}_A(k_0)} \text{Im} \{ \Pi_{11}^A(k) \}, \quad (5.30)$$

then we can perform the same diagonalization procedure to $D_{ab}^{(n)}$ as

$$iD_{ab}^{(n)}(k) = U_{ac}(k_0) \begin{pmatrix} i\tilde{D}^{(n)}(k) & 0 \\ 0 & (i\tilde{D}^{(n)}(k))^* \end{pmatrix}_{cd} U_{db}(k_0), \quad (5.31)$$

where

$$i\tilde{D}^{(n)}(k) = \left(\prod_{i=1}^n [iG_F(k) (-i\bar{\Pi}^A(k))] \right) iG_F(k). \quad (5.32)$$

Hence, we can write the two correlators in Eq. (5.27) as (for $n > 0$)³⁵

$$iD_{21}^{(n)}(k) = U_{21}(k_0) U_{11}(k_0) i\tilde{D}^{(n)}(k) + U_{22}(k_0) U_{21}(k_0) (i\tilde{D}^{(n)}(k))^* \quad (5.33)$$

$$= \epsilon(k_0) (1 + \tilde{f}_A(k_0)) 2\text{Re} \left\{ i\tilde{D}^{(n)}(k) \right\}, \quad (5.34)$$

$$iD_{12}^{(n)}(k) = \epsilon(k_0) \tilde{f}_A(k_0) 2\text{Re} \left\{ i\tilde{D}^{(n)}(k) \right\}. \quad (5.35)$$

³⁵Again, the conjugations do not apply to Dirac indices.

These may be inserted into Eq. (5.27), which through Eq. (5.32), allows us to express $\mathcal{M}_{\text{SE}}^{(nm)}(p)$ in terms of the $\psi_+ \rightarrow \psi_+$ self-energy Π_{11}^ψ . Therefore, $\mathcal{M}_{\text{SE}}^{(10)}$ becomes

$$\mathcal{M}_{\text{SE}}^{(10)} = \lambda^2 \int \frac{d^4k}{(2\pi)^4} \epsilon(k_0) (1 + \tilde{f}_\psi(k_0)) (-1) \text{tr} \left\{ 2\text{Re} \left\{ i\tilde{D}^{(1)}(k) \right\} Q_\psi(k-p) \right\}. \quad (5.36)$$

Why have we gone through all the trouble of rewriting \mathcal{M}_{SE} in terms of Π_{11}^ψ ? There are two main benefits:

1. Through the theory in Eq. (4.66), we can calculate $\Pi_{11}^\psi(k)$ and insert its value directly into Eq. (5.36). For example, ref. [46] has calculated this exact quantity to $\mathcal{O}(\lambda^2)$ for both scalar and fermion ψ , which we can insert into Eq. (5.36) to obtain the $\mathcal{O}(\lambda^4)$ expression. In the fermionic case, inserting $\Pi_{11}^\psi(k)$ is slightly more complicated than the scalar case due to non-trivial angular dependences, which we have shown how to account for in Appendix C. Depending on the situation, it might be beneficial to have the option of calculating $\Pi_{11}^\psi(k)$ separately from Γ_{BW} .
2. When looking at Eq. (5.22), one may be concerned that the diagrams feature ill-defined products of distributions, like $\delta(k^2 - m_A^2) \times \delta(k^2 - m_A^2)$ – so-called “pinching singularities”. From the above construction, we observe that the final expression for $iD_{ab}^{(n)}(k)$ (and hence, $\mathcal{M}_{\text{SE}}^{(nm)}$) contains no such products. Meanwhile, products of propagators, $iG_F(k)$ (which appear in Eq. (5.32)), are well-defined through the identity [29]

$$\lim_{\epsilon \rightarrow 0} \frac{1}{(x + i\epsilon)^{n+1}} = \mathcal{P} \frac{1}{x^{n+1}} - i\pi \frac{(-1)^n}{n!} \frac{d^n}{dx^n} \delta(x). \quad (5.37)$$

This proves the claim we made back in Section 4.6 that $\Pi_{21}^A(\omega)$ is only well-defined once the sum of all compound diagrams has been taken.

The identity in Eq. (5.37) will prove to be rather troublesome when we later perform numerical integrals, as the integral $\int dx \mathcal{P} \frac{1}{x^2}$ diverges. In order to fix this, we use a regularization procedure outlined in Appendix D.

A takeaway from this and the previous section is that the BW decay rate derived by ref. [23] only agrees with our result to LO (given a few modifications to their approach). At NLO and beyond, our expressions feature thermal dependencies not present in Eq. (2.32).

5.3 Numerical Calculations

Although the Γ_{BW} which we have derived may analytically disagree with the one derived in ref. [23], we can not yet claim any physical relevance of our expression before we observe how it behaves physically. As such, we turn to calculating and evaluating the two-loop corrections to Γ_{BW} derived in the previous section.

It is no secret that thermal loop calculations become very complicated, very quickly. For example, the first time the fermion self-energy Π_{11}^ψ was fully analytically calculated

to *one*-loop order was as recently as in 2021 [46]. As such, we can not expect to be able to fully analytically solve the two-loop integrals required to calculate Γ_{BW} to $\mathcal{O}(\lambda^4)$. The few analytical integrals that we can hope to perform are further complicated by the fact that the thermal distribution functions are defined in the plasma frame, while analytical calculations are the easiest to perform in the c.o.m frame. This introduces an awkward angular dependence through Eq. (2.26). In all, it turns out that in order to calculate Γ_{BW} to $\mathcal{O}(\lambda^4)$, we will have to perform several *numerical* triple integrals over highly irregular and oscillatory integrands.

Unfortunately, I made a mistake in the analytical two-loop calculations. I forgot that the expression in Eq. (5.21) and Eq. (5.36) are given in the *plasma frame*, and simply assumed that one could pass to the c.o.m frame where $p^\mu = (p_0, 0, 0, 0)$ without having to Lorentz transform the thermal distribution functions, like we have done in Eq. (5.11).³⁶ Effectively, this mistake discards any physical effect induced by the fact that the c.o.m frame and the plasma frame are two very distinct frames. Analytically, this mistake actually ended up reducing the above-mentioned triple integrals to be only double integrals, which in turn made the numerical implementation way easier than if the mistake had not been made. By the time the mistake was discovered, there was not enough time left in the project to extend these double integral calculations to their correct triple integral counterparts. Since the focus of this thesis is on the analytical aspects of thermal physics and features rather theory-heavy work, it is likely that time simply would not have sufficed for a complete numerical triple integration anyway.

Therefore, instead of simply discarding the erroneous results, we decided to see if we could potentially extract *some* physical data from them – like the order to which Γ_{BW} scales with T or the relevance of the $\mathcal{O}(\lambda^4)$ terms compared to the $\mathcal{O}(\lambda^2)$ terms, and so on. The hope is that, somewhere in the parameter space, our erroneous result will carry attributes of the true physical behaviour. *A priori*, there is no reason why this should be the case, since our mistake is quite a severe one. It is therefore up to us to study our results and *a posteriori* determine whether they are worthy of physical interpretation or if they are consistently nonsensical. As such, the remainder of this section illustrates how a numerical analysis of the two-loop calculations *would* go, had they been implemented correctly.

We will take ψ to be a scalar with $m_\psi < m_\phi$ as this trivializes some angular dependences. The (erroneous) one-loop contributions to Γ_{BW} then becomes (cf. Eq. (5.11))

$$\Gamma_{\text{BW}}(p_0) = \frac{\lambda^2}{32\pi m_\phi} \frac{1}{1 + f_\phi(p_0)} \sum_\psi \theta(p_0 - 2m_\psi) \left[1 + \tilde{f}_\psi \left(\frac{p_0}{2} \right) \right]^2 \sqrt{1 - 4m_\psi^2/p_0^2}. \quad (5.38)$$

In Appendix B we show how to perform the calculations required at $\mathcal{O}(\lambda^4)$, resulting in the

³⁶This mistake only concerns the explicit two-loop calculations performed in Appendix B. All the other results presented in this thesis should be correct in their respective frames.

$\mathcal{O}(\lambda^4)$ -order corrections:

$$\begin{aligned}\Pi_{21}^\phi(p_0) &\stackrel{\mathcal{O}(\lambda^4)}{=} \mathcal{M}_{\text{vertex}}(p_0) + \mathcal{M}_{\text{SE}}(p_0) \\ &= \mathcal{M}_{\text{vertex}}^{\mathcal{N}_1}(p_0) + \mathcal{M}_{\text{vertex}}^{\mathcal{N}_2}(p_0) + \mathcal{M}_{\text{SE}}^{(10)}(p_0),\end{aligned}\tag{5.39}$$

where $\mathcal{M}_{\text{vertex}}^{\mathcal{N}_1}(p_0)$ and $\mathcal{M}_{\text{vertex}}^{\mathcal{N}_2}(p_0)$ are given in Eq. (B.10) and Eq. (B.18), respectively, and

$$\begin{aligned}\mathcal{M}_{\text{SE}}^{(10)}(p_0) &= \frac{\lambda^4}{(2\pi)^3} \frac{1}{16p_0^2} \int_{\mathbb{R} \setminus [-m_\psi, m_\psi]} dy \int_{\mathbb{R} \setminus [-m_\phi, m_\phi]} dx \theta(j(x, y)) \mathcal{P} \frac{1}{(y + p_0/2)^2} \\ &\quad \times \epsilon(x)\epsilon(y)\epsilon(x + y + p_0)\tilde{f}_\phi(x)\tilde{f}_\psi(y)(1 + \tilde{f}_\psi(x + y + p_0)),\end{aligned}\tag{5.40}$$

where $j(x, y) \equiv 2\sqrt{x^2 - m_\phi^2}\sqrt{y^2 - m_\psi^2} - |(x + y + p_0)^2 - x^2 - y^2 + m_\phi^2|$.

Matters are complicated by the appearance of a UV divergence in the integrand of $\mathcal{M}_{\text{SE}}^{(10)}$ at $y = -p_0/2$. In Appendix D we regularize and renormalize our expressions in order to make this UV divergence disappear. Note that, due to Eq. (5.37), a renormalization procedure would have been required even if we had not made the error mentioned above. The approach of Appendix D should therefore be considered valid in the correct approach as well.

In calculating $\mathcal{M}_{\text{SE}}^{(10)}$ we used a procedure mostly identical to the one used in Appendix B.2 by calculating each of the diagrams in Eq. (5.22). As stated at the end of Section 5.2.2, we *could* instead have used the existing expression for $\Pi_{11}^\psi(k)$, found in ref. [46], and simplified the calculations. However, we found that the above-mentioned renormalization procedure became much more painless if we simply did all the calculations manually. The process was alleviated by the result of Section 5.2.2 which told us that all pinching singularities *must* cancel – effectively letting us take $\delta(k^2 - m_A^2) \times \delta(k^2 - m_A^2) = 0$ in the calculations.

The (renormalized) physical BW decay rate (cf. Eq. (D.7)) can then be written as

$$\Gamma_{\text{BW}}^{\text{phys}}(p_0, T) = A(p_0, T)\tilde{\lambda}_R^2 + B(p_0, T)\tilde{\lambda}_R^4 + \mathcal{O}(\tilde{\lambda}_R^6),\tag{5.41}$$

where we have introduced the *dimensionless* renormalized coupling constant $\tilde{\lambda}_R \equiv \lambda_R/m_\phi$,³⁷ and defined

$$A(p_0, T) \equiv m_\phi^2 \Gamma_{\text{BW}}^{(2)}(p_0, T),\tag{5.42}$$

$$B(p_0, T) \equiv m_\phi^4 \left(\Gamma_{\text{BW}}^{(4)}(p_0, T) - \Gamma_{\text{BW}}^{(4)}(m_\phi, 0) \right),\tag{5.43}$$

for $\Gamma_{\text{BW}}^{(n)}$ being the $\tilde{\lambda}_R^n$ -order contribution to Γ_{BW} . That is, $\Gamma_{\text{BW}}^{(2)}$ is given by Eq. (5.38) and $\Gamma_{\text{BW}}^{(4)}$ is calculated through Eq. (5.39), where we have also included a symmetry factor of 1/2 into the latter due to the identical final state scalars. By splitting A and B into their $T = 0$ and $T > 0$ parts, $A^0(p_0)$, $B^0(p_0)$ and $A^\beta(p_0, T)$, $B^\beta(p_0, T)$, respectively, we get 4 different quantities of varying interest:

³⁷The reason behind this is that it is easier to work in terms of dimensionless couplings. The scaling was done with respect to m_ϕ as this is the relevant energy scale for p_0 in the domain of resonance. If ψ were a fermion, λ_R would already be dimensionless and would not require scaling.

- $A^0(p_0)$ is trivially (m_ϕ times) the known LO decay rate at $T = 0$,
- $A^\beta(p_0, T)$ has already been studied in the literature [23],³⁸
- $B^0(p_0)$ is cancelled by the renormalization conditions (cf. Eq. (D.7)),
- $B^\beta(p_0, T)$ is non-trivial.

When performing numerical computations we are therefore the most interested in studying $B^\beta(p_0, T)$. Since contributions from B^β are suppressed by a factor $\tilde{\lambda}_R^2$ relative to that of A , one would initially suspect that the effects from B^β are, at best, miniscule. However, due to the non-trivial temperature dependence of B^β , we can not immediately say whether $B(p_0, T)\tilde{\lambda}_R^4$ is larger or smaller than $A(p_0, T)\tilde{\lambda}_R^2$ at any given temperature.

An interesting question is then of when

$$\frac{|B(p_0, T)|\tilde{\lambda}_R^4}{|A(p_0, T)|\tilde{\lambda}_R^2} \gtrsim 1 \quad (5.44)$$

holds. To answer this, we will aim to find a temperature T_* such that, for some $\tilde{\lambda}_R$,

$$\left| \frac{B(p_0, T)}{A(p_0, T)} \right| \geq \tilde{\lambda}_R^{-2} \quad \forall T \geq T_*. \quad (5.45)$$

If T_* exists, then at temperatures above it, the $\mathcal{O}(\tilde{\lambda}_R^4)$ terms of $\Gamma_{\text{BW}}^{\text{phys}}$ actually dominate over the $\mathcal{O}(\tilde{\lambda}_R^2)$ terms.

5.3.1 Results

The numerics are computed using `Mathematica 13.0`, and we will be working in units of the Higgs boson mass $m_\phi = 125.25 \pm 0.17$ GeV [78]. By plotting T_* as a function of p_0 for different $\tilde{\lambda}_R$, we can understand how the higher-order thermal corrections behave. We start by studying how our expressions depend on $\tau \equiv \log_{10}(T/m_\phi)$ through

$$Y(\tau) \equiv \log_{10} \left| \frac{B(p_0, 10^\tau m_\phi)}{A(p_0, 10^\tau m_\phi)} \right|. \quad (5.46)$$

We plot $Y(\tau)$ for several p_0 in the domain of resonance in Figure 5.1. We observe that at around $T \approx 5m_\phi$, $Y(\tau)$ has a drastic drop, but as τ increases past this, it appears to behave rather linearly. We can utilize this behaviour and try to approximate

$$Y(\tau) \approx a\tau + b \quad (5.47)$$

for $\tau \gtrsim 2$. The coefficients a and b are listed in Table 5.1 for several p_0 in the domain of resonance and $m_\psi = 0.1m_\phi$. We observe that $a \approx 1$ and $b \approx -1.2$ – except in the case of

³⁸Due to the mistake we made, our $A^\beta(p_0, T)$ will not really be the same as the one in ref. [23], but any physical quantities which we are hoping remain intact should be the same.

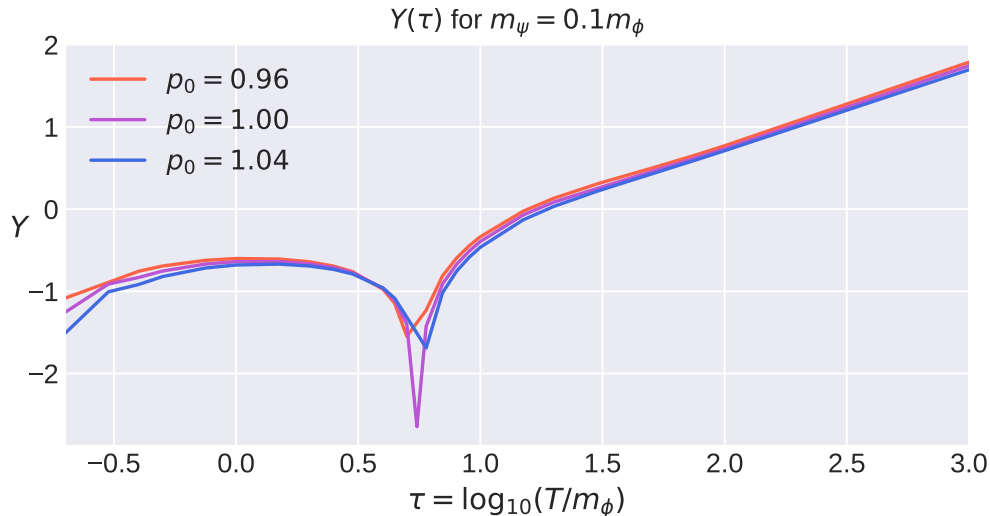


Figure 5.1: Plot of $Y(\tau)$ for $m_\psi = 0.1m_\phi$, illustrating that the linear behaviour of Eq. (5.47) only appears as T becomes large.

$p_0 = 0.92$. We see no reason as to why the point of $p_0 = 0.92$ should merit any physical significance or odd behaviour. Simulations with other parameters yielded no such behaviour, which is why we regard the data point at $p_0 = 0.92$ as a numerical anomaly, and we lend no physical reason to its behaviour. Unfortunately, due to our implementation of the double integral in *Mathematica 13.0*, we were unable to get any specific uncertainties for the coefficients themselves, which inhibited us from performing a typical χ^2 test on our linear fit. The R^2 -value³⁹ of all these linear fits was $R^2 = 0.999$, except in the case of $p_0 = 0.92$ which yielded $R^2 = 0.840$. Disregarding the numerical anomaly, this tells us that as T grows very large, $Y(\tau)$ behaves almost indistinguishably from a linear function.

Using the fit $Y(\tau) = a\tau + b$ for $\tau \geq 2$, we can find T_* as a function of p_0 and $\tilde{\lambda}_R$:

$$T_*(p_0, \tilde{\lambda}_R) = 10^{-\frac{b(p_0)}{a(p_0)}} \times \tilde{\lambda}_R^{-\frac{2}{a(p_0)}} \quad (5.48)$$

Since $a(p_0)$ and $b(p_0)$ are rather constant in p_0 , (cf. Table 5.1) it follows that, for a fixed $\tilde{\lambda}_R$, $T_*(p_0, \tilde{\lambda}_R)$ will likely be of constant order of magnitude as a function of p_0 . This behaviour is illustrated in Figure 5.2 for $\tilde{\lambda}_R = 10^{-6}, 10^{-7}, 10^{-8}, 10^{-9}$, again for $m_\psi = 0.1m_\phi$.

From Table 5.1 we observe that $a \approx 1$. Curiously, all a -values are slightly less than 1. *A priori* one would expect an $a \approx 1$ to take values both slightly above and below 1. The reason behind this behaviour is that only in the limit $T \rightarrow \infty$ is $a = 1$. At any finite (yet large) T , contributions from lower order T -terms will still contribute somewhat. This can be seen through the plot in Figure 5.1 where the non-linear contributions to $Y(\tau)$ are relevant

³⁹The R^2 value (also known as the *coefficient of determination*) quantifies the amount of variability between a data set and a proposed fit. Here, a value of $R^2 = 1$ corresponds to 0% variation and a perfect fit.

p_0	a	b	p_0	a	b
0.90	0.992	-1.17	1.00	0.999	-1.25
0.91	0.997	-1.22	1.01	0.988	-1.20
0.92	0.987	-0.536	1.02	0.990	-1.21
0.93	0.992	-1.19	1.03	0.994	-1.23
0.94	0.994	-1.20	1.04	0.990	-1.25
0.95	0.992	-1.20	1.05	0.989	-1.22
0.96	0.991	-1.16	1.06	0.992	-1.23
0.97	0.993	-1.21	1.07	0.988	-1.20
0.98	0.992	-1.21	1.08	0.994	-1.23
0.99	0.989	-1.20	1.09	0.988	-1.21
			1.10	0.987	-1.21

Table 5.1: Linear fit of Eq. (5.47) for $m_\psi = 0.1m_\phi$. The temperatures used in the fit are $\tau = 2, 3, 4, 5, 6, 7, 8, 9, 10, 11$. For the Hadamard regularization, we used $\xi = 10^{-4}$ and $\xi = 8 \times 10^{-5}$.

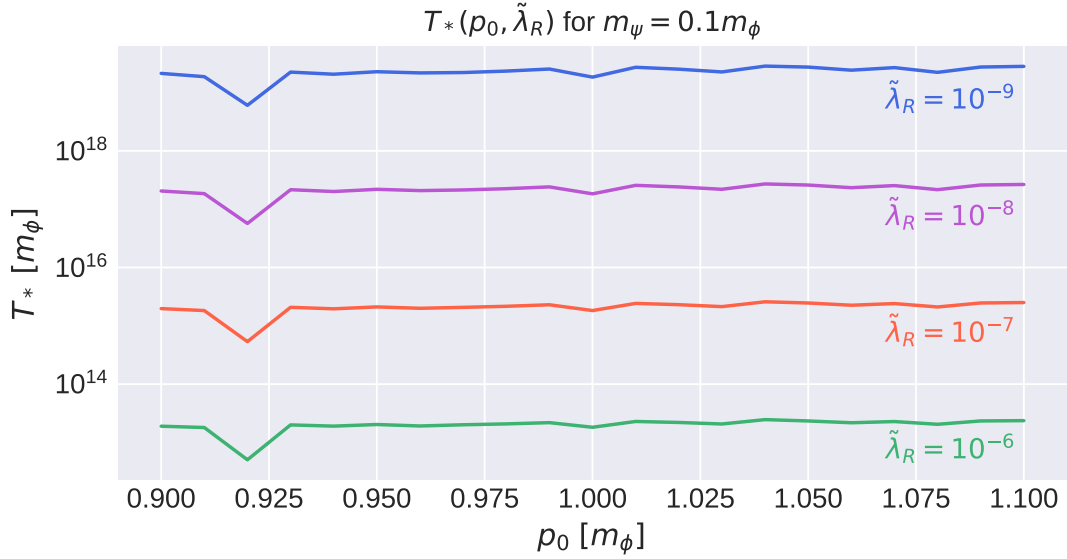


Figure 5.2: Plot of $T_*(p_0, \tilde{\lambda}_R)$ for $\tilde{\lambda}_R = 10^{-6}, 10^{-7}, 10^{-8}, 10^{-9}$. We observe that the magnitude of T_* is rather constant in p_0 , except for at the numerical anomaly at $p_0 = 0.92$.

at smaller T . Therefore, a will always approach 1 from below. Had we performed the same study for the size of the three-loop contributions compared to $B(p_0, T)$, we would also expect any linear coefficient to converge from below.

Nevertheless, $a \approx 1$ implies that

$$\left| \frac{B(p_0, T)}{A(p_0, T)} \right| \sim T^1, \quad (5.49)$$

which means that $B(p_0, T)$ increases faster with temperature than $A(p_0, T)$.

This is certainly a weird and unexpected behaviour – it seems to imply that we can always make the NLO term relevant by simply increasing the temperature. By extending a similar analysis to a generic loop order, it follows that we should be able to make *any* term of arbitrary order dominate over the preceding ones by simply turning up the temperature. The absurdity of this result can most likely be linked back to the mistake we made regarding the thermal distribution functions in the c.o.m frame. As mentioned, a crucial consequence of this mistake is that it discards any physical effect induced by the fact that the c.o.m- and the plasma frame are two very distinct frames. These effects become especially relevant in the high- T regime which Eq. (5.49) claims to describe. In a plasma, each c.o.m energy (p_0 in the c.o.m frame) has a probability of occurring, which depends on the thermal distribution and T . For example, in a plasma following a Bose-Einstein distribution, the average c.o.m energy is proportional to the temperature, $\langle p_0 \rangle \approx 2.71 T$ [79].⁴⁰ By dimensional analysis, the RHS of Eq. (5.49) should be scaled by a factor of $1/p_0$. Since our error removed any dependence of the c.o.m frame relative to the plasma, it is only reasonable to expect that in order to account for our mistake we should substitute $1/p_0$ for $1/\langle p_0 \rangle$, giving a temperature-independent ratio between $B(p_0, T)$ and $A(p_0, T)$, which is far more reasonable. Another consequence of our mistake is that Eq. (5.49) does not account for the fact that the further away that a p_0 is from the average $\langle p_0 \rangle$, the less likely it is to occur in the statistical plasma. Since $\langle p_0 \rangle$ scales with the temperature, the contributions from the domain of resonance $p_0 \sim m_\phi$ in a high-temperature plasma should be even further suppressed than Eq. (5.49) implies.

We must therefore conclude that our mistake makes our numerical results useless in the high-temperature regime. It might turn out that the mistake is more forgiving in the case of low temperatures. However, even if this turned out to be the case, it is highly likely that no new insight would have been gained from such a study, since the low- T case just approaches the known Γ_{BW} at $T = 0$. It is therefore very probable that the mistake we made earlier greatly affects the extent to which we can interpret our results as physical.

Therefore, we are unfortunately unable to present any physically interpretable numerical two-loop results. While regrettable, this does not mean that our numerical study was a complete failure, as we established several useful notions, for example how to account for two-loop UV-divergences through the renormalization scheme outlined in Appendix D. Concepts like Hadamard regularization and the physical BW rate of Eq. (D.7) can be used in a

⁴⁰This result follows from a numerical calculation of the average energy in a plasma following the Bose-Einstein distribution: $\langle E \rangle = \int d\Pi_{\text{phys}} E / (\exp(E\beta) - 1)$ in the relativistic regime, $T \gg m$.

physically accurate two-loop computation in the future. Hopefully, the trials and tribulation we have gone through may lay the foundation for such a calculation.

It should not go unmentioned that several months was spent on this numerically fruitless endeavour, during which we had to overcome hurdles like highly oscillatory integrands, fragile principal values, singular poles, numerical inaccuracies, stubborn ξ -values, code parallelization and slowly converging double-integrals. We can safely say that the numerical results of this section are very accurate and represent exactly what we set out to calculate at the end of Section 5.3. Luckily, we were able to detect the mistake we made, and we tried to extract *some* physical results from the erroneous data. When this proved infeasible, we identified exactly *why* our results were wrong and how this was a direct manifestation of our mistake.

Chapter 6

Discussion

While it is regrettable that we did not get to present or discuss any numerical results, there is still plenty to be said about the analytical results of this thesis, which will be the aim of this chapter. We will start by discussing the differences between our approach to thermal QFT (cf. Chapter 4) and the conventional approaches to real- and imaginary-time thermal QFT. Thereafter, we will continue the discussion regarding rates at finite temperature and relate the numerous interpretations we have had of Γ_{BW} throughout this thesis. From this, we turn to an exploration of how the differences between \mathcal{B}^\pm and \mathcal{H}^\pm manifest themselves at finite temperatures. Finally, we aim to contextualize the work that we have done – how does one use our results in a freeze-in calculation? We also address why our BW decay rate disagrees with the one in ref. [23].

6.1 The Many Formalisms of Thermal Quantum Field Theory

To the best of our knowledge, the extension of the $T = 0$ SSR to $T > 0$ and the derivation of real-time thermal QFT in Chapter 4 has not been done before in the literature. This raises the question of how the approach to real-time thermal QFT in Chapter 4 (which we will call the *SSR approach*), differs from the conventional approaches to thermal QFT.

Conventionally, real-time thermal QFT starts by first deriving the imaginary-time formalism of thermal QFT (which we have briefly outlined in Appendix E) and then performing an analytical continuation of its generating functional to real times. This is clearly a fundamentally different approach to real-time thermal QFT than the SSR approach, but since they both result in the same generating functional, Eq. (4.66), they must produce the same observables. There are therefore three different formalisms/approaches to thermal QFT to consider – the existing, conventional approaches of real- and imaginary-time thermal QFT, and the SSR approach to real-time thermal QFT. In this section we scrutinize the SSR approach and uncover both its disadvantages and advantages as a formalism of thermal QFT.

A downside to the SSR approach is that uncuttable compound diagrams (like the last one in Eq. (4.73)) do not appear naturally through the optical theorem at finite temperatures.

They merely appear as a consequence of defining a QFT with Feynman rules matching the $T \geq 0$ cutting rules. We decided upon their inclusion by arguing that their exclusion would lead to ill-defined expressions.⁴¹ In the conventional approach, there is no such ambiguity, as the full theory of Eq. (4.66) naturally appears during the analytic continuation from imaginary- to real-time. In fact, this analytical continuation actually yields a *larger* set of viable propagators than the SSR approach:

$$iG_{ab}(k) = \begin{pmatrix} iG_A^+(k) & e^{\sigma k_0} Q_A(-k) \\ e^{-\sigma k_0} Q_A(k) & iG_A^-(k) \end{pmatrix}, \quad (6.1)$$

where $\sigma \in [0, \beta]$ [28, 29, 68, 74]. This σ appears due to an ambiguity in the contour along which one takes the analytical continuation of the imaginary-time generating functional. It turns out that the formal requirements (set by the mathematical rules of analytic continuation and the Osterwalder-Schrader theorem [54]) which this contour, \mathcal{C} , must obey are:

- (i) \mathcal{C} starts from a large, negative real value, $-t_0 \rightarrow -\infty$, and follows the real axis to t_0 ,
- (ii) \mathcal{C} then goes from t_0 down to some $t_0 - i\sigma$, where $0 \leq \sigma \leq \beta$,
- (iii) \mathcal{C} then goes back, parallel to the real axis, to $-t_0 - i\sigma$,
- (iv) \mathcal{C} lastly goes vertically down to $-t_0 - i\beta$.

For a more in-depth discussion of this analytical continuation and the origin of these rules, see refs. [29, 74, 75]. This type of contour is called a *Keldysh contour* [74, 80], and is illustrated in Figure 6.1. In order to arrive at the generating functional in Eq. (4.66), one has to argue that the contributions from the vertical segments in the Keldysh contour (points (ii) and (iv) above) can be factored out of the analytical continuation of the generating functional. There exist “proofs” for why this is sometimes allowed [74, 75], but in general it is difficult to argue for and motivate. Since we make no such assumption/argument in the SSR approach, it comes as no surprise that the theory derived in Chapter 4 does not explicitly feature a σ . This is not really a loss for the SSR approach, because it turns out that all Green’s functions (and hence, observables) are independent of σ [29]. Although we could technically introduce a σ into the SSR approach by taking the propagator to be as in Eq. (6.1), it becomes highly unclear exactly *what* σ is supposed to represent when it is not related to a Keldysh contour. The only σ -values that see any use in the literature are $\sigma = 0$, which corresponds to the SSR formalism, and $\sigma = \beta/2$, which yields a symmetric propagator and can be used as a quick argument for why $T = 0$ counterterms renormalize the $T > 0$ theory (see Section 3.5 of ref. [29]). It is therefore not really crucial that a real-time thermal QFT features a non-zero σ .

⁴¹There is a potential analogy here to how soft collinear IR divergences at $T = 0$ are cancelled only once a sum of experimentally indistinguishable processes has been taken. The fact that a similar cancellation also appears in thermal processes might be a manifestation of our experimental inability to tell individual thermal processes apart, which we discussed thoroughly in Section 3.4.

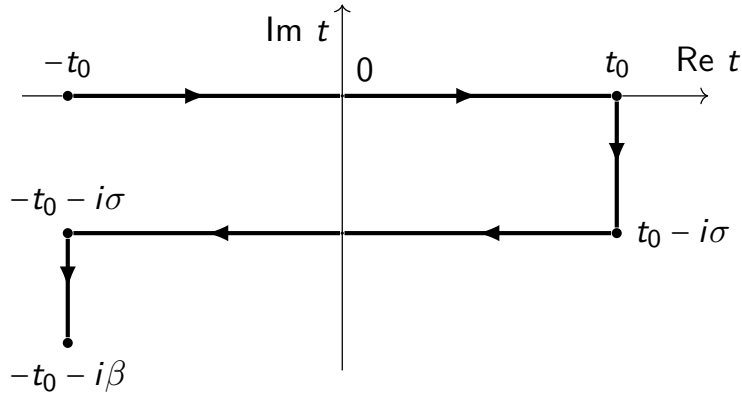


Figure 6.1: The Keldysh contour, along which the analytical continuation of the imaginary-time generating functional is taken in order to create a real-time thermal QFT. This contour illustrates the origin of the contour parameter σ in the conventional real-time formalism. Here, $t_0 \rightarrow \infty$.

When compared to the imaginary-time formalism, the SSR approach fares as well as the conventional real-time approach. The main downside of both real-time formalisms is the presence of a 2×2 propagator which greatly increases the number of diagrams and processes to consider. In imaginary-time, there is only a single propagator, but the presence of a discrete energy spectrum (see Appendix E) means that perturbative calculations are done through sums over energies instead of through integrals.⁴² Nevertheless, a clear benefit of the imaginary-time formalism is that its core principles are more directly based in statistical concepts – it is defined directly through a partition function, which we illustrate in Appendix E. As such, in the imaginary-time formalism, all statistical quantities have their corresponding QFT quantity, like the free energy is the statistical counterpart of the field-theoretical self-energy. The imaginary-time formalism therefore stays much more true to its statistical foundations, while the main statistical aspect of the SSR approach is that of the thermal phase space distributions in Eq. (4.13).

There are also a multitude of benefits to the SSR approach. In a conventional derivation of real-time thermal QFT, the appearance of the 2×2 propagator is often regarded as a surprising result and a mathematical quirk. It feels somewhat arbitrary that at some point into the derivation, one has to “double the degrees of freedom” in order to make the analytical continuation from imaginary- to real-time work. In the SSR approach, however, the doubling is a result of the careful inclusion of both SSR sectors since the very beginning. As a matter of fact, since the finite-temperature SSR is an extension of the $T = 0$ SSR, the doubling can be linked all the way back to the fact that the on-shell requirement $p^2 = m^2$ has two hyperboloid solutions in Minkowski space – \mathcal{B}^+ for $p_0 > 0$ and \mathcal{B}^- for $p_0 < 0$, cf. Figure 4.1. Since the BW scheme (per Chapter 3) is also based on the on-shell requirement $p^2 = m^2$, the

⁴²Actually, there exists analytical tricks which lets one convert these sums into integrals [29, 30, 75], but the resulting expressions are still very different from the ones we are used to for a continuous energy spectrum.

SSR approach is therefore more intimately related to the BW rate and its role in accounting for off-shell resonance. Had we simply derived $\text{Im } \Pi(\omega)$ at $T > 0$ using the conventional real-time formalism, we would technically have ended up with the same result as Eq. (4.77). However, the relationship which Γ_{BW} shares with the off-shell behaviour of unstable particles would not be as apparent, which is critical to our understanding of the BW rate at finite temperatures.

6.2 Understanding Rates

In our endeavour to understand what Γ_{BW} is, we have encountered several interpretations. On the one hand, the derivation of the BW scheme in Chapter 3 uncovered that Γ_{BW} is related to the probability that an off-shell resonant particle exists in a heat bath through Eq. (3.31); in agreement with Weldon [31]. On the other hand, we also established that Γ_{BW} may be seen as the equilibration rate which tells us how quickly a perturbed equilibrium system returns to equilibrium; also in agreement with Weldon [31]. The only thing that is lacking is the link between these two interpretations – how can Γ_{BW} be both of these, seemingly unrelated, things at the same time?

At the foundation of the equilibration-interpretation of Γ_{BW} are the quantities of Γ_d and Γ_p , which are related to the evolution of the phase space distributions through Eq. (3.32). We are therefore interested in addressing how Γ_d and Γ_p are related to the SSR approach. To explore this, consider a thermalized plasma with two particle populations, A and B . In Section 3.4 we stated a result of Weldon’s which says that the thermal BW decay rate of A is [31]

$$\Gamma_{\text{BW}} = \Gamma_d - \varepsilon_A \Gamma_p, \quad (6.2)$$

and we motivated this by the bosonic case reducing to “decay minus production”. Clearly, this motivation fails in the fermionic case, and that is because this motivation is not a valid one at all: If we were actually subtracting production from decay in a thermalized system, we *should* get 0. There simply can not be any net production/decrease in either A or B in a thermalized system.

To illustrate what is actually going on, we will take both A and B to lie on \mathcal{B}^+ , meaning they decompose into two sets of populations $A_+, B_+ \in \mathcal{H}^+$ and $A_-, B_- \in \mathcal{H}^-$. Since we have two sets of populations that cannot mix (by the SSR), it is only reasonable that we must have *two* rates as well. We therefore claim that Γ_d is the rate of $A_+ \rightarrow B_+$, while Γ_p is that of $A_- \rightarrow B_-$. To prove this, we start by using Weldon’s definitions of Γ_d and Γ_p for

B being a state of n particles $|B\rangle = |B_1\rangle \otimes |B_2\rangle \cdots \otimes |B_n\rangle$ [31].⁴³

$$\Gamma_d(\omega) = \frac{1}{2\omega} \int \prod_{i=1}^n \left(\frac{d^3 \mathbf{p}_{B_i}}{(2\pi)^3 2E_{B_i}} (1 + \varepsilon_{B_i} f_{B_i}(E_{B_i})) \right) |\mathcal{M}_{\underline{A} \rightarrow B}|^2, \quad (6.3)$$

$$\Gamma_p(\omega) = \frac{1}{2\omega} \int \prod_{i=1}^n \left(\frac{d^3 \mathbf{p}_{B_i}}{(2\pi)^3 2E_{B_i}} f_{B_i}(E_{B_i}) \right) |\mathcal{M}_{B \rightarrow \underline{A}}|^2, \quad (6.4)$$

where ω is the energy of the A population in the plasma frame. Compare this to the BW rate, Eq. (4.25), which the SSR approach predicts:

$$\Gamma_{\text{BW}}(\omega) = \frac{1}{2\omega} \frac{1}{1 + \tilde{f}_B(\omega)} \int d\Pi_B^+ |\mathcal{M}_{\underline{A} \rightarrow B}|^2 \quad (6.5)$$

$$= \frac{1}{2\omega} (1 - \varepsilon_B e^{-\omega\beta}) \int d\Pi_B^+ |\mathcal{M}_{\underline{A} \rightarrow B}|^2 \quad (6.6)$$

$$\stackrel{\text{(A.8)}}{=} \frac{1}{2\omega} \int d\Pi_B^+ |\mathcal{M}_{\underline{A} \rightarrow B}|^2 - \frac{1}{2\omega} \int d\Pi_B^- |\mathcal{M}_{B \rightarrow \underline{A}}|^2. \quad (6.7)$$

If we demand that all the n states which make up B satisfy $p_0 > 0$, i.e. $|B\rangle \in (\mathcal{B}^+)^{\otimes n}$, we have

$$d\Pi_B^+ = \prod_{i=1}^n \left(\frac{d^3 \mathbf{p}_{B_i}}{(2\pi)^3 2E_{B_i}} (1 + \varepsilon_{B_i} f_{B_i}(E_{B_i})) \right), \quad (6.8)$$

$$d\Pi_B^- = \varepsilon_B \times \prod_{i=1}^n \left(\frac{d^3 \mathbf{p}_{B_i}}{(2\pi)^3 2E_{B_i}} f_{B_i}(E_{B_i}) \right), \quad (6.9)$$

meaning Eq. (6.7) gives

$$\Gamma_{\text{BW}}(\omega) = \Gamma_d - \varepsilon_B \Gamma_p, \quad (6.10)$$

reproducing Weldon's result in Eq. (6.2). The awkward summing/subtracting of Γ_d and Γ_p therefore has nothing to do with accumulation of decay- and production rates, but is instead a decomposition of Γ_{BW} into the rates on two different SSR sectors. The labelling as “production” and “decay” is therefore rather misleading. It follows that the quantities Γ_d and Γ_p correspond to the rates of the two distinct processes $A_+ \rightarrow B_+$ and $A_- \rightarrow B_-$, respectively. Since these are *different* processes concerning *different* populations, there is no reason why their sum should vanish, hence why the argument used to motivate Eq. (6.2) is invalid. Since Γ_d and Γ_p determine the evolution of the phase space distribution through Eq. (3.32), we have successfully illustrated how the interpretation of Γ_{BW} as an equilibration rate also fits into the SSR approach.

Furthermore, Eq. (6.10) illustrates a point we made at the end of Section 5.1.1, where we claimed that if we chose to work in terms of the “thermal” distribution functions \tilde{f}_A

⁴³Henceforth, for the sake of brevity, we have chosen to absorb a factor of $(2\pi)^4 \delta^{(4)}(p_A - p_{B_1} \cdots - p_{B_n})$ into the square matrix element $|\mathcal{M}_{\underline{A} \rightarrow B}|^2$.

instead of f_A (and likewise \tilde{n}_A instead of n_A), then awkward sign-differences (like the one in Eq. (6.10)) are always absorbed into our expressions. Consider, for example, Γ_d in Eq. (6.3) and Γ_p in Eq. (6.4): The former is already expressed in terms of $\varepsilon_{B_i} f_{B_i} = \tilde{f}_{B_i}$, but the latter is not. If we multiply a factor of ε_B into the definition of Γ_p , we instead get the neat expression $\Gamma_{\text{BW}} = \Gamma_d - \Gamma_p$. Although this can be interpreted (somewhat misleadingly) as decay minus production, the minus-difference is really a result of the Feynman-Stueckelberg interpretation, where we take states on \mathcal{H}^- to propagate backwards in time relative to \mathcal{H}^+ . Since these rates are odd in their temporal components, it follows that the sign of Γ_p is opposite to that of Γ_d . In other words, we are technically *adding* the rates from two sectors but the Feynman-Stueckelberg interpretation introduces a sign-difference between them.

Another example of the usefulness of working in terms of \tilde{f} instead of f can be seen in the evolution of the phase space distribution, Eq. (3.32), which may be written in terms of \tilde{f} as (again multiplying a factor of ε_B into the definition Γ_p):

$$\frac{\partial \tilde{f}_A}{\partial t} = -\tilde{f}_A \Gamma_d + (1 + \tilde{f}_A) \Gamma_p. \quad (6.11)$$

As a bonus, this too illustrates the fact that the signs of Γ_p and Γ_d differ under addition – here with the temporal component explicitly visible on the LHS.

6.3 Branch versus Sector

In this section, we discuss the differences between working in terms of particles on the two *branches* \mathcal{B}^\pm (the set of all on-shell states satisfying $\pm p_0 < 0$) and particles on the two *sectors* \mathcal{H}^\pm (the orthogonal spaces into which the full Hilbert space decomposes under the SSR). In deriving Eq. (6.10) we had to assume that all single-particle states which make up B lie on \mathcal{B}^+ . Since any other assumption would yield a different result than Eq. (6.10), it follows that Weldon must have (inadvertently) made the same assumption when deriving the same result. In the context of particle physics, this is an extremely reasonable (and often trivialized) assumption – “of course” do we want our particles to be on the \mathcal{B}^+ branch! But in the context of finite-temperature SSR, this is a distinct and explicit choice that we have just made which must be justified. We have actually made this assumption once before without justifying it or even discussing other options: When deriving the optical theorem at finite temperatures in Appendix A.2, we also took the final states to be on \mathcal{B}^+ , and it is about time we scrutinize this choice.

In other words, when calculating Γ_{BW} for $A \rightarrow B$, we actually have two choices: One where A, B are on \mathcal{H}^+ , which we will call $\Gamma_{\text{BW}}^{\mathcal{H}^+}$, and the one which we derived in Appendix A.2 where A, B are on \mathcal{B}^+ , which we will call $\Gamma_{\text{BW}}^{\mathcal{B}^+}$. It then follows that

$$\frac{\Gamma_{\text{BW}}^{\mathcal{B}^+}}{\Gamma_{\text{BW}}^{\mathcal{H}^+}} = 1 + \varepsilon_A e^{-\beta\omega}, \quad (6.12)$$

which is a non-perturbative result. We observe that the two rates agree in the limit $T \rightarrow 0$, and that for $T > 0$, the discrepancies vanish as ω grows. This is very reasonable since both

of these cases imply a system with negligible thermal effects, i.e. approaching the case of $\mathcal{H}^+ = \mathcal{B}^+$. Since both $\Gamma_{\text{BW}}^{\mathcal{B}^+}$ and $\Gamma_{\text{BW}}^{\mathcal{H}^+}$ are valid choices for the BW decay rate, it begs the question of which one we should use in the BW propagator when we want to account for off-shell resonant particles?

The answer depends on the type of system we are studying. One example is that of accelerator experiments with quark-gluon plasmas, where individual cold particles are radiated from the $T > 0$ plasma.⁴⁴ Since the radiated particles are non-thermal upon measurement, the SSR which they are subject to is the one at $T = 0$ with $\mathcal{H}^\pm = \mathcal{B}^\pm$. Therefore, the final (measured) state of such a process must lie in \mathcal{B}^+ (or \mathcal{B}^- depending on your convention). Conservation of momentum implies that the initial state too lies in \mathcal{B}^+ . In this case, it may therefore be more appropriate to work in terms of states on \mathcal{B}^+ and use $\Gamma_{\text{BW}}^{\mathcal{B}^+}$ as the BW decay rate.

Then when do we use $\Gamma_{\text{BW}}^{\mathcal{H}^+}$? In this case, both the initial and final states are in \mathcal{H}^+ , making it the appropriate rate to use when the entire process is contained within the plasma. For example, $\Gamma_{\text{BW}}^{\mathcal{H}^+}$ is the most appropriate choice for the annihilation DM \rightarrow SM in a freeze-out process, since the decay starts and ends within the same plasma. In freeze-in, however, the visible and dark sectors are not thermalized. For a freeze-in DM production $\psi\psi \rightarrow \chi\chi$, it might therefore be the most appropriate to actually work in terms of \mathcal{B}^+ . However, in Section 2.1.3 we saw that we can view the scalar singlet DM freeze-in process through the lens of DM annihilation $\chi\chi \rightarrow \phi \rightarrow \psi\psi$ (cf. Eq. (2.12)). Here, the intermediate resonant Higgs decay $\phi \rightarrow \psi\psi$ is thermalized. Since this is the process whose decay rate we have been primarily concerned with in thesis, we propose that a more appropriate choice for the BW decay rate to use in such resonance calculations is $\Gamma_{\text{BW}}^{\mathcal{H}^+}$. Since freeze-in typically happens at much larger temperatures than freeze-out, the difference between $\Gamma_{\text{BW}}^{\mathcal{H}^+}$ and $\Gamma_{\text{BW}}^{\mathcal{B}^+}$ is much more noticeable in the freeze-in scheme. For an accurate freeze-in implementation it is therefore important to properly assert which BW decay rate one works with.

6.4 Contextualizing Applications

In the freeze-in scheme, the dark sector is *not* thermalized, while the visible sector is. When we decompose the DM annihilation $\chi\chi \rightarrow \phi \rightarrow \psi\psi$ into $\chi\chi \rightarrow \phi$ and $\phi \rightarrow \psi\psi$, like in Eq. (2.22), we create an awkward mixing of in- and out-of-equilibrium processes. Since most of our work so far has been on processes that are either fully thermalized or not thermalized at all, it becomes unclear how to interpret processes that are a combination of the two. When calculating Γ_{BW} , we have intentionally ignored the process $\chi\chi \rightarrow \phi$ as it is not perfectly clear how to combine this non-thermal process with the thermal process of $\phi \rightarrow \psi\psi$. For example, if we add the rates of these two together, will the result still be interpretable as an equilibration rate? Seeing as Γ_{BW} behaves so intrinsically differently at $T = 0$ and $T > 0$, it is not even clear if we *can* add these rates together and expect a physically consistent answer. Furthermore, according to our definition of the particle/anti-particle duality at

⁴⁴Ref. [76] discusses applications of thermal QFT to the study of quark gluon plasmas.

finite temperatures, it seems that the freeze-in dark- and visible sectors may operate under different notions of particles and anti-particles. In order to account this, one will have to explore how the SSR sectors of different statistical systems interact.

Luckily, in the context of freeze-in, the feebleness of the SM-DM coupling asserts that contributions from $\chi\chi \rightarrow \phi$ are very small, meaning the above concerns are likely negligible when calculating the BW rate of ϕ . It is nevertheless highly desirable that these problems be addressed, which is a possible avenue of future analysis.

6.4.1 Applying the BW Rate

Although we derived an expression for Γ_{BW} at $T \geq 0$, we have not really addressed how to *use* it to calculate the DM relic density. We have indirectly implied that our Γ_{BW} should simply be inserted into Eq. (2.22) instead of the one which ref. [23] uses. If this were the full story then it must mean that the BW rate in Eq. (2.32) (which we will call Γ'_{BW}) is the wrong rate to insert into the very expressions from which it was derived – a rather unintuitive statement.⁴⁵ We must therefore scrutinize the reasons why Γ_{BW} and Γ'_{BW} differ beyond LO.

From the collision operator in Eq. (2.7), we see that the Bose enhancement/Pauli blocking-terms are responsible for all thermal aspects of the entire collision operator, while $|\mathcal{M}|^2$ is responsible for all QFT aspects. Since Bose enhancement and Pauli blocking are inherently quantum mechanical (QM) effects⁴⁶ and $|\mathcal{M}|^2$ is calculated at $T = 0$, it should follow that ref. [23] implements a thermal behaviour that is not inherently field-theoretical. Since we derived Γ_{BW} with thermal QFT and since QFT generally reproduces the effects of QM at LO, it is no surprise that $\Gamma_{\text{BW}} = \Gamma'_{\text{BW}}$ holds at this order only.

We should therefore expect that the difference between Γ_{BW} and Γ'_{BW} only increases with temperature, as it is in the high-energy regime where the differences between QFT and QM become important. Accounting for these effects therefore becomes especially important for a UV-dominated freeze-in process. This, in addition to the above discussion of whether to use $\Gamma_{\text{BW}}^{\mathcal{H}^+}$ or $\Gamma_{\text{BW}}^{\mathcal{B}^+}$ in resonant decay calculations, are two new areas in which the freeze-in mechanism is sensitive to temperatures and in-medium effects.

To summarize, if we want a field-theoretic approach to the freeze-in/out mechanisms, we must substitute the collision operator in Eq. (2.7) for an object from thermal QFT – a theory that, by its very name, accounts for both thermal- and field-theoretic aspects at the same time. It is in this new collision operator that we should equip the BW propagator with our newly derived Γ_{BW} .

⁴⁵This does not mean that it is *wrong* to substitute Γ'_{BW} for Γ_{BW} in the expressions derived by ref. [23]. More than likely, this would still increase the accuracy of a DM relic calculation. It just means that there is a nuance to the situation.

⁴⁶To be specific, the thermal distribution functions $f_A(k_0)$ come from classical statistical physics, but the notion of final-states being suppressed/enhanced by $1 + f_A$ comes from QM.

6.4.2 The Collision Operator

In Appendix F we show how the idea behind the initial/final state thermal suppression⁴⁷ factors of f and $1 + \tilde{f}$ emerge as a result of the SSR and the thermal phase space measure – a rather important result. When describing thermal processes, one conventionally multiplies the $T = 0$ phase space by one of these factors depending on if it describes an initial- or final state. Under this conventional notion, it is not clear if the phase space of internal on-shell particles should be suppressed by f or by $1 + \tilde{f}$, as they have no notion of being “initial” or “final”. This is the reason why higher-order thermal QFT processes simply cannot have their thermal components factored out, like Eq. (2.7) suggests. In the SSR approach, on the other hand, all thermal aspects are introduced through the thermal measure in Eq. (4.13) which carries no notion of states being “initial” or “final”. The SSR approach therefore completely discards the notion of distinguishing between initial- and final state suppressions, and is instead only interested in which sector an on-shell particle belongs to.

Using this insight, we can propose a collision operator for the process $A \rightarrow B$ which respects thermal QFT:

$$C = \int d\Pi_{AB} |\mathcal{M}_{A \rightarrow B}|^2, \quad (6.13)$$

where $\mathcal{M}_{A \rightarrow B}$ is calculated with the Feynman rules of real-time thermal QFT and $d\Pi_{AB}$ is the measure of the thermal phase space consisting of on-shell A and B .⁴⁸ This collision operator takes the exact form one would expect – it is simply an integral over a plasma phase space times a scattering amplitude. In Section 4.2 we found that the Hilbert space of thermal on-shell states is the same as the Hilbert space of on-shell states at $T = 0$, i.e. $d\Pi_{AB}$ is simply the term in the square brackets in Eq. (4.23). In fact, by rewriting this term it can be shown that

$$d\Pi_{AB} = \frac{1}{1 + 2\tilde{n}_{AB}(\omega)} (d\Pi_{AB}^+ + d\Pi_{AB}^-) \quad (6.14)$$

$$= d\Pi_{AB}^+ - d\Pi_{AB}^-, \quad (6.15)$$

where $d\Pi_{AB}^\pm$ are the thermal phase space measures of A and B on \mathcal{H}^\pm , as given by Eq. (4.13). Assuming CP symmetry, the proposed collision operator can then be written as

$$C = \int d\Pi_{AB}^+ |\mathcal{M}_{A \rightarrow B}|^2 - \int d\Pi_{AB}^- |\mathcal{M}_{B \rightarrow A}|^2. \quad (6.16)$$

This collision operator is starting to look a lot like one wherein we subtract “production” from “decay”. In fact, we can produce this exact structure by simply letting (due to the same reasons that we struggled to motivate in Appendix F) $|A\rangle \in (\mathcal{B}^+)^{\otimes n}$ and $|B\rangle \in (\mathcal{B}^-)^{\otimes m}$ be n - and m -particle states on different branches. For example, the collision operator in

⁴⁷For the sake of brevity, we say “suppression” in place of “Bose enhancement/Pauli suppression”.

⁴⁸This measure also absorbs all symmetry factors and other relevant degrees of freedom.

Eq. (2.7) can then be recovered by letting $|A\rangle = |\psi\psi\rangle$ and $|B\rangle = |\chi\chi\rangle$, which gives:

$$C = \int d\Pi_{\psi\psi\chi\chi}^+ |\mathcal{M}_{\psi\psi\rightarrow\chi\chi}|^2 - \int d\Pi_{\psi\psi\chi\chi}^- |\mathcal{M}_{\chi\chi\rightarrow\psi\psi}|^2 \quad (6.17)$$

$$= \int d\Pi_{\text{tot}} (1 + \tilde{f}_\psi(E_{\mathbf{k}}))(1 + \tilde{f}_\psi(E'_{\mathbf{k}}))(1 + \tilde{f}_\chi(-E_{\mathbf{p}}))(1 + \tilde{f}_\chi(-E'_{\mathbf{p}})) |\mathcal{M}_{\psi\psi\rightarrow\chi\chi}|^2 \\ \times \varepsilon(E_{\mathbf{k}})\varepsilon(E'_{\mathbf{k}})\varepsilon(-E_{\mathbf{p}})\varepsilon(-E'_{\mathbf{p}}) \quad (6.18)$$

$$- \int d\Pi_{\text{tot}} \tilde{f}_\psi(E_{\mathbf{k}})\tilde{f}_\psi(E'_{\mathbf{k}})\tilde{f}_\chi(-E_{\mathbf{p}})\tilde{f}_\chi(-E'_{\mathbf{p}}) |\mathcal{M}_{\chi\chi\rightarrow\psi\psi}|^2 \\ \times \varepsilon(E_{\mathbf{k}})\varepsilon(E'_{\mathbf{k}})\varepsilon(-E_{\mathbf{p}})\varepsilon(-E'_{\mathbf{p}}) \\ = \int d\Pi_{\text{tot}} \left[|\mathcal{M}_{\psi\psi\rightarrow\chi\chi}|^2 f_\psi(E_{\mathbf{k}})f_\psi(E'_{\mathbf{k}}) \left(1 + \tilde{f}_\chi(E_{\mathbf{p}})\right) \left(1 + \tilde{f}_\chi(E'_{\mathbf{p}})\right) \right. \\ \left. - |\mathcal{M}_{\chi\chi\rightarrow\psi\psi}|^2 f_\chi(E_{\mathbf{p}})f_\chi(E'_{\mathbf{p}}) \left(1 + \tilde{f}_\psi(E_{\mathbf{k}})\right) \left(1 + \tilde{f}_\psi(E'_{\mathbf{k}})\right) \right], \quad (6.19)$$

where the energies $E_{\mathbf{q}} \equiv |q_0|$ are defined according to the finite-temperature Feynman-Stueckelberg interpretation and $d\Pi_{\text{tot}}$ is the same as in Eq. (2.8). Since thermal QFT produces the same results as non-thermal QFT to tree-level, this expression exactly matches the collision operator in Eq. (2.7) at LO.

The collision operator in Eq. (6.13) therefore reproduces the expected collision operator structure while still being a field-theoretic object. However, as previously discussed, when a process is contained entirely within a plasma, it is the most natural to work with states on \mathcal{H}^+ instead of \mathcal{B}^+ . In this case, the contribution from the \mathcal{H}^- sector vanishes, meaning the collision operator would reduce to

$$\int d\Pi_{AB}^+ |\mathcal{M}_{A\rightarrow B}|^2. \quad (6.20)$$

The notion of having to subtract “production” processes from “decay” processes is no longer needed, as there is only contribution from a single sector. The suppression factors of the initial and final states are inherently built into the physical phase space $d\Pi_{AB}^+$, as illustrated in Appendix F. The appropriate thermal suppressions of internal on-shell particles are accounted for via the propagators used in the thermal QFT Feynman rules.

This begs the question of why this seemingly simple collision operator has not been proposed before, as its matrix elements are calculable with the existing formalism of real-time thermal QFT. We believe that there are two main reasons:

1. Without the SSR, it is very hard to justify working in terms of states on \mathcal{H}^\pm instead of the well-established and conventional approach of using states on \mathcal{B}^\pm . Since iG^\pm (which appear in the real-time thermal QFT Feynman rules) are the propagators of particles on \mathcal{H}^\pm , it would be wrong to use the thermal QFT formalism for processes on \mathcal{B}^+ without at least considering a change of basis.

2. The notion of phase space suppressions that are specific to initial and final states is completely abandoned. Instead, we have a phase space measure which only cares about which sector a state is in. Since this behaviour follows from the newly derived finite temperature SSR, it is reasonable that this idea has not been implemented in a collision operator before.

Unfortunately, we have not had a time to explore the proposed collision operator beyond this point.

Chapter 7

Final Remarks

Here, we state the final remarks of this thesis. We summarize the work that we have done as well as concisely state our main results. Finally, we mention a couple avenues of future work and research.

7.1 Summary of Work

The work done in this thesis can largely be split into four categories:

Understanding Rates at Finite Temperature

In order to account for the resonant behaviour of intermediate Higgs bosons in a freeze-in scalar singlet model, we were quickly drawn towards the odd behaviour of rates in a thermalized system. A large focus was put on interpreting exactly *what* a rate is – both at zero- and at finite temperatures. To explore this, we derived the BW scheme by first studying how unstable particles differ from stable ones and then expressing their differing behaviour through the lens of an approximated propagator. We showed how the notion of a non-sharp mass emerged and that the BW propagator was the appropriate tool to implement this behaviour. This allowed us to build an intuition of the BW rate at finite temperature as an object directly related to the probability that an off-shell particle exists in a plasma.

We were also interested in the role which Γ_{BW} plays as an actual *rate*, for which we turned to its interpretation as an equilibration rate. How exactly this notion of “equilibration” fitted into the SSR scheme was not perfectly clear until Section 6.2, where we derived several of Weldon’s results (cf. ref. [31]) and showed how they all fit into the SSR scheme. Here, we discovered that the concepts of the rate of “decay” Γ_d and “production” Γ_p can be completely abandoned in the SSR approach.

Creating a Field-Theoretic Thermal BW Rate

Although an expression for Γ_{BW} already existed in the literature [23], we observed several oddities in its definitions. We therefore set out to derive the BW rate ourselves through thermal QFT. In doing so, we encountered the optical theorem at finite temperatures and

established the thermal cutting rules. At LO, we showed how to recreate the BW rate found in ref. [23] (given slight modifications to their approach). At NLO, we created expressions for the vertex- and self-energy corrections for both final-state fermions and scalars. For the self-energy corrections, we showed that all pinching singularities cancel and introduced a scheme which let you calculate n -loop expressions using $n-1$ -loop results. In Appendix C, we showed how to account for non-trivial angular behaviour when inserting these expressions for fermions.

We also discussed the reason for *why* our Γ_{BW} differed from the one derived in ref. [23], and concluded upon the latter featuring a thermal structure that was not inherently field-theoretical. In order to fix this, the collision operator itself must be altered, and we proposed the form of Eq. (6.13).

Studying Thermal QFT

We started the chapter on thermal QFT by studying a superselection rule at zero temperature. The ideas behind this SSR were then extended to finite temperatures, where we discovered that the sectors into which the SSR splits the Hilbert space of on-shell particles are different at $T = 0$ and $T > 0$. The fact that $\mathcal{B}^\pm \neq \mathcal{H}^\pm$ at $T > 0$ was then built upon for the remainder of the thesis to re-derive known concepts like the Kubo-Martin-Schwinger condition, thermal propagators, finite temperature cutting rules and the generating functional of real-time thermal QFT. We also quickly explored the consequences which the CPT invariance of QFT has for the SSR.

Although initially presented as a heuristic derivation of real-time thermal QFT, the SSR approach proved to be a reliable resource in understanding the behaviour of thermal systems in general. It let us reproduce and interpret the results of Weldon [31] in a manner which completely discards phase space suppression/enhancements that are unique to initial- and final states. Even though it produces the same observables as the conventional real-time thermal QFT, the SSR approach was derived without referring to the Keldysh contour while still providing a natural interpretation of the doubling of degrees of freedom.

Numerical Calculations

Since our Γ_{BW} differed fundamentally from the one existing in the literature, we wanted to compare how these differences were expressed quantitatively. We spent a lot of time on a numerical implementation of the two-loop order contributions to Γ_{BW} , but due to an unfortunate mistake made during analytical calculations, we were unable to produce any physically interpretable results. This numerical endeavour was however not a complete waste of time, because we established methods for numerical renormalization and regularization that would be useable in an accurate calculation.

7.2 Review of Key Results

There are three main results of this thesis:

Correcting the Existing BW Rate

Since the beginning of this project, a main focus has been to derive a field-theoretic expression for Γ_{BW} in order to support or refute the heuristically derived BW rate in ref. [23]. The Γ_{BW} in Eq. (4.77) therefore constitutes one of our main results. Although the imaginary component of forward scattering at finite temperatures has been considered before, we have been focusing on its role in accounting for resonant intermediate particles. From Eq. (4.77), we showed that the existing BW rate lacked the contribution from certain processes at LO, and that it outright disagreed with our expression past LO.

We argued that the LO discrepancies were due to the existing expression not accounting for all relevant processes possible in the plasmas. As such, we showed that by slightly adjusting the existing approach to include these additional processes, the two rates agree at LO. Beyond this order, the differences were due to our rate being calculated with thermal field theory, while the existing expression featured a temperature dependence that was not inherently field-theoretical.

The SSR Approach to Real-Time Thermal QFT

Another of our main results is that of the SSR approach to real-time thermal QFT. While its observables can be shown to be identical to those produced by a conventional approach, it succeeds in illustrating the origin of the (otherwise abstruse) doubling of degrees of freedom in real-time thermal QFT. By choosing to work with states exclusive to \mathcal{H}^+ instead of \mathcal{B}^+ , it shows how we can dispose of notions like “different phase space suppressions for initial and final states” and “accumulation of production and decay rates as $\Gamma_{\text{BW}} = \Gamma_d - \Gamma_p$ ”. The SSR also allowed for a natural extension of the optical theorem and the Feynman-Stueckelberg interpretation to finite temperatures.

A Field-Theoretic Collision Operator

Our third and final result is that of the proposed collision operator in Eq. (6.13). It builds upon the ideas of the SSR approach by considering how the full phase space measure can be split into contributions from the two sectors \mathcal{H}^+ and \mathcal{H}^- (cf. Eq. (6.16)). From this, we showed how the structure of the well-established collision operator in Eq. (2.7) emerges by choosing to work with states in \mathcal{B}^\pm . If we wish for an accurate freeze-out/in calculation, it is likely that this collision operator will appropriately account for field-theoretic thermal behaviour.

7.3 Further Work

Throughout this thesis we have several times hinted at potential avenues of further research:

Numerical Two-Loop Calculations.

An accurate two-loop study of our Γ_{BW} would shed some light on whether the shift to a field-theoretic collision operator is merited at all, since it might turn out that any corrections are negligible in the relevant part of the physical parameter space. This time, it would be highly

favourable if the calculations were done without making any mistakes. Since the two-loop expressions in Section 5.2 also hold for final state fermions, it would also be interesting to see a fermionic study and compare it to the scalar results. As mentioned, the renormalization and regularization ideas of Appendix D will still be applicable for such a study.

Formalizing the SSR Approach

It would be interesting to continue exploring the ideas underlining the SSR approach. For this type of work, there are two especially prominent avenues of work: (1) Making the “derivation” of the SSR approach in Chapter 4 more mathematically formal. Here, one could also attempt to formalize the relationship between the SSR and CPT, like hinted at in Section 4.1.1. (2) Continue exploring how the SSR approach may be used in interpretations of thermal systems. For example, it would be nice to see if the contour parameter σ has an interpretation faithful to the SSR approach, or a further study of the differences between working with states on \mathcal{H}^\pm instead of on \mathcal{B}^\pm . Additionally, we have primarily focused on in-equilibrium processes, but it would be beneficial to extend the ideas of the SSR to the out-of-equilibrium case, as this has been previously analysed in the conventional real-time approach [80, 81]. This would also make it easier to address the concerns outlined at the start of Section 6.4 regarding how to account for a mixing of in- and out-of-equilibrium processes.

Due to a lack of time, we were unable to justify in Appendix F why inter-branch scattering processes produce the known thermal phase space suppression of initial- and final states. Since the applicability of the proposed collision operator relies on this type of scattering, an explanation is sorely needed.

The Collision Operator

We ended Chapter 6 on a cliffhanger, as time did simply not suffice to continue exploring the consequences of the proposed field-theoretic collision operator in Eq. (6.13). Exploring such collision operators is the next clear step in the search for a more accurate freeze-in/out DM relic density prediction. What remains to be seen is if the field-theoretic collision operator for a freeze-in Higgs portal would still allow for the decomposition and factorization of the process $\psi\psi \rightarrow \phi \rightarrow \chi\chi$ into $\psi\psi \rightarrow \phi$ and $\phi \rightarrow \chi\chi$, like done in Eq. (2.22). Due to the non-trivial behaviour of higher-order real-time thermal QFT, such a factorization will likely not be possible, so one should explore how to adapt the notion of s -channel resonant behaviour to finite-temperature systems.

Appendices

Appendix A

The Optical Theorem

A.1 Zero Temperature

In this appendix, we will derive the $T = 0$ *optical theorem* for states on $\mathcal{H}^\pm = \mathcal{B}^\pm$.

Decomposing the S -matrix as $S \equiv \mathbb{1} + i\mathcal{T}$, unitarity implies $i(\mathcal{T}^\dagger - \mathcal{T}) = \mathcal{T}^\dagger\mathcal{T}$. Acting on $\mathcal{T}^\dagger\mathcal{T}$ with initial and final states, we get

$$\langle f | \mathcal{T}^\dagger \mathcal{T} | i \rangle = \langle f | \mathcal{T}^\dagger (\mathbb{1}^+ + \mathbb{1}^-) \mathcal{T} | i \rangle \quad (\text{A.1})$$

$$= \sum_X \int d\Pi_X^+ \langle f | \mathcal{T}^\dagger | X \rangle \langle X | \mathcal{T} | i \rangle + \sum_X \int d\Pi_X^- \langle f | \mathcal{T}^\dagger | X \rangle \langle X | \mathcal{T} | i \rangle. \quad (\text{A.2})$$

We will take our initial and final states to lie within the same sector, that is, $|f\rangle, |i\rangle \in \mathcal{H}^\pm$. From the SSR, it then follows that the inner product $\langle f | \mathcal{T}^\dagger | X \rangle$ (equivalently, $\langle X | \mathcal{T} | i \rangle$) vanishes for $|X\rangle \in \mathcal{H}^\mp$, meaning one of the sums in Eq. (A.2) must also vanish, giving the *generalized* optical theorem

$$i \langle f^\pm | (\mathcal{T}^\dagger - \mathcal{T}) | i^\pm \rangle = \sum_X \int d\Pi_X^\pm \mathcal{M}_{X \rightarrow f}^\dagger \mathcal{M}_{i \rightarrow X} \delta^{(4)}(p_f - p_X) \delta^{(4)}(p_i - p_X) (2\pi)^8, \quad (\text{A.3})$$

where $|A^\pm\rangle$ indicates a state in \mathcal{H}^\pm , and $\langle B | \mathcal{T} | A \rangle \equiv (2\pi)^4 \delta^{(4)}(p_A - p_B) \mathcal{M}_{A \rightarrow B}$. In our endeavour to calculate imaginary components of self-energies, we are especially interested in the case of forward scattering, $|f^\pm\rangle = |i^\pm\rangle \equiv |A^\pm\rangle$:

$$\text{Im} \mathcal{M}_{A^\pm \rightarrow A^\pm} = \frac{1}{2} \sum_X \int d\Pi_X^\pm (2\pi)^4 \delta^{(4)}(p_A - p_X) |\mathcal{M}_{A^\pm \rightarrow X}|^2. \quad (\text{A.4})$$

One of the key takeaways from this demonstration at $T = 0$ is that the effects from one of the branches always vanishes from physical quantities.

A.2 Finite Temperature

In this appendix, we show how to derive the optical theorem for $T \geq 0$ through the finite-temperature SSR outlined in Section 4.2.

Instead of deriving the *generalized* optical theorem (like we did at $T = 0$, cf. Eq. (A.3)), we will immediately proceed to consider the case of forward scattering, i.e. identical initial and final states $|i\rangle = |f\rangle \equiv |A\rangle$. Assuming $|A\rangle$ to have $p_0 > 0$, i.e. $|A\rangle \in \mathcal{B}^+$, $|A\rangle$ must have components on both \mathcal{H}^+ and \mathcal{H}^- (since $\mathcal{B}^\pm \neq \mathcal{H}^\pm$), labelled $|A^+\rangle$ and $|A^-\rangle$, respectively. Using that unitarity implies $i(\mathcal{T}^\dagger - \mathcal{T}) = \mathcal{T}^\dagger \mathcal{T}$, we sandwich $\mathcal{T}^\dagger \mathcal{T}$ between $\langle A|$ and $|A\rangle$, giving

$$\langle A| i(\mathcal{T}^\dagger - \mathcal{T}) |A\rangle = \langle A| \mathcal{T}^\dagger (\mathbb{1}^+ + \mathbb{1}^-) \mathcal{T} |A\rangle \quad (\text{A.5})$$

$$\begin{aligned} &= \sum_X \int \frac{d\Pi_X^+}{1 + 2\tilde{n}_X(\omega_X)} \langle A^+| \mathcal{T}^\dagger |X\rangle \langle X| \mathcal{T} |A^+\rangle \\ &\quad + \sum_X \int \frac{d\Pi_X^-}{1 + 2\tilde{n}_X(\omega_X)} \langle A^-| \mathcal{T}^\dagger |X\rangle \langle X| \mathcal{T} |A^-\rangle. \end{aligned} \quad (\text{A.6})$$

To proceed, the first thing to note is that, for a one-particle state, j , we have

$$d\Pi_j^- = d\Pi_j^+ \varepsilon_j e^{-\beta k_j^0}, \quad (\text{A.7})$$

which we will later see is equivalent to the Kubo-Martin-Schwinger condition [24, 25]. For multiparticle states, X , we therefore have

$$d\Pi_X^- = d\Pi_X^+ \prod_{j \in X} \varepsilon_j e^{-\beta k_j^0} = d\Pi_X^+ \varepsilon_X e^{-\beta \omega_X}, \quad (\text{A.8})$$

where $\varepsilon_X \equiv \prod_{j \in X} \varepsilon_j$. Due to the δ 's in Eq. (4.13), $\varepsilon_X e^{-\beta \omega_X}$ can be pulled out of the phase space integral. The second thing to note is the property of Eq. (4.11), which implies

$$\langle A^-| \mathcal{T}^\dagger |X^-\rangle \langle X^-| \mathcal{T} |A^-\rangle \xrightarrow{\text{CPT}} \langle A^+| \mathcal{T}^\dagger |X^+\rangle \langle X^+| \mathcal{T} |A^+\rangle. \quad (\text{A.9})$$

Where $|X^\pm\rangle$ is the component of $|X\rangle$ on \mathcal{H}^\pm . The SSR and the antiunitarity of CPT [42] then implies that

$$\langle A^-| \mathcal{T}^\dagger |X\rangle \langle X| \mathcal{T} |A^-\rangle = \langle A^+| \mathcal{T}^\dagger |X\rangle \langle X| \mathcal{T} |A^+\rangle. \quad (\text{A.10})$$

À propos, this is the reason why the total decay rate of a particle is exactly equal to that of its anti-particle. Combined, Eq. (A.8) and Eq. (A.10) imply the equality

$$\begin{aligned} &\int \frac{d\Pi_X^-}{1 + 2\tilde{n}_X(\omega_X)} \langle A^-| \mathcal{T}^\dagger |X\rangle \langle X| \mathcal{T} |A^-\rangle = \\ &\quad \int \frac{d\Pi_X^+}{1 + 2\tilde{n}_X(\omega_X)} \varepsilon_X e^{-\beta \omega_X} \langle A^+| \mathcal{T}^\dagger |X\rangle \langle X| \mathcal{T} |A^+\rangle \end{aligned} \quad (\text{A.11})$$

Thus, we get the finite temperature expression

$$\langle A | i(\mathcal{T}^\dagger - \mathcal{T}) | A \rangle = \sum_X \frac{1 + \varepsilon_X e^{-\beta\omega_X}}{1 + 2\tilde{n}_X(\omega_X)} \int d\Pi_X^+ \langle A^+ | \mathcal{T}^\dagger | X \rangle \langle X | \mathcal{T} | A^+ \rangle, \quad (\text{A.12})$$

where we pulled the terms dependent on ω_X out of the integral. This is the optical theorem at finite temperature. By the definition $\langle B | \mathcal{T} | A \rangle \equiv (2\pi)^4 \delta^{(4)}(p_A - p_B) \mathcal{M}_{A \rightarrow B}$, we can write Eq. (A.12) as

$$\text{Im } \mathcal{M}_{A \rightarrow A} = \frac{1}{2} \sum_X \frac{1 + \varepsilon_A e^{-\beta\omega_A}}{1 + 2\tilde{n}_A(\omega_A)} \int d\Pi_X^+ (2\pi)^4 \delta^{(4)}(p_A - p_X) |\mathcal{M}_{A \rightarrow X}|^2. \quad (\text{A.13})$$

Appendix B

Scalar Two-loop Vertex Calculations

In this appendix, we show how to tackle the integrals in the vertex corrections of Eq. (5.21) in the case of ψ being a scalar with $m_\psi < m_\phi$. Unfortunately, as mentioned at the start of Section 5.3, I made a mistake when performing the calculations in this appendix (all analytical expressions *outside* this appendix should be correct). I took the thermal distribution functions to be $f(k_0)$ in the c.o.m frame, when in reality they should have been $f(k^\mu u_\mu)$ where u^μ is the 4-velocity at which the plasma moves in the c.o.m frame. Due to the mistake, our final answer will only feature single- and double integrals, when in reality it should have also featured triple integrals. The calculations in this appendix are therefore technically wrong, but they do feature ideas and approaches which would be equally useful in a correct approach.

In the c.o.m frame, we have $p^\mu = (p_0, 0, 0, 0)$, meaning the only angular dependence of the integrand in $\mathcal{M}_{\text{vertex}}$ comes from the product $\mathbf{k} \cdot \mathbf{l} = rt \cos \alpha$, where $r \equiv |\mathbf{k}|$, $t \equiv |\mathbf{l}|$ and α is the angle between \mathbf{k} and \mathbf{l} in the plane they span. We can therefore write

$$\mathcal{M}_{\text{vertex}} = -\frac{4\lambda^4}{(2\pi)^6} \int dk_0 dr dl_0 dt d\cos \alpha r^2 t^2 [\text{Re} \{\mathcal{N}_1\} - \text{Re} \{\mathcal{N}_3\}], \quad (\text{B.1})$$

where we used $\int d\Omega_k d\Omega_l F(\mathbf{k} \cdot \mathbf{l}) = 4\pi \cdot 2\pi \int_{-1}^1 d\cos \alpha F(rt \cos \alpha)$ and \mathcal{N}_1 and \mathcal{N}_3 are defined in Eq. (5.18). We separate the above integral into contributions from the terms featuring \mathcal{N}_1 and \mathcal{N}_3 , respectively, as

$$\mathcal{M}_{\text{vertex}} = \mathcal{M}_{\text{vertex}}^{\mathcal{N}_1} + \mathcal{M}_{\text{vertex}}^{\mathcal{N}_3}, \quad (\text{B.2})$$

and solve each separately. In the following, define $\omega_r \equiv \sqrt{r^2 + m_\psi^2}$ and $\omega_t \equiv \sqrt{t^2 + m_\psi^2}$.

B.1 Contributions from $\text{Re}\{\mathcal{N}_1\}$

First, we note that we can factor out the δ 's appearing in the integrand of $\mathcal{M}_{\text{vertex}}^{\mathcal{N}_1}$ as

$$\begin{aligned} \mathcal{M}_{\text{vertex}}^{\mathcal{N}_1} = & -\frac{4\lambda^4}{(2\pi)^6} \int dk_0 dr dl_0 dt d\cos\alpha \delta(l^2 - m_\psi^2) \delta((l-p)^2 - m_\psi^2) \\ & \times \left[\delta(h) A_1 + \delta(k_0^2 - \omega_r^2) B_1 + \delta((k_0 - p_0)^2 - \omega_r^2) C_1 \right. \\ & \left. + \delta(h) \delta(k_0^2 - \omega_r^2) \delta((k_0 - p_0)^2 - \omega_r^2) D_1 \right], \end{aligned} \quad (\text{B.3})$$

where $h(k_0, l_0, r, t, \alpha) \equiv (k-l)^2 - m_\phi^2 = (k_0 - l_0)^2 - r^2 - t^2 + 2rt \cos\alpha - m_\phi^2$ and

$$\begin{aligned} A_1(k_0, l_0, r, t) \equiv & -4\pi^3 r^2 t^2 [\theta(l_0) + \tilde{n}_\psi(l_0)] [\theta(p_0 - l_0) + \tilde{n}_\psi(p_0 - l_0)] \\ & \times (1 + 2\tilde{n}_\phi(k_0 - l_0)) \mathcal{P} \frac{1}{k_0^2 - \omega_r^2} \mathcal{P} \frac{1}{(k_0 - p_0)^2 - \omega_r^2}, \end{aligned} \quad (\text{B.4})$$

$$\begin{aligned} B_1(k_0, l_0, r, t, \alpha) \equiv & -4\pi^3 r^2 t^2 [\theta(l_0) + \tilde{n}_\psi(l_0)] [\theta(p_0 - l_0) + \tilde{n}_\psi(p_0 - l_0)] \\ & \times (1 + 2\tilde{n}_\psi(k_0)) \mathcal{P} \frac{1}{h(k_0, l_0, r, t, \alpha)} \mathcal{P} \frac{1}{(k_0 - p_0)^2 - \omega_r^2}, \end{aligned} \quad (\text{B.5})$$

$$\begin{aligned} C_1(k_0, l_0, r, t, \alpha) \equiv & -4\pi^3 r^2 t^2 [\theta(l_0) + \tilde{n}_\psi(l_0)] [\theta(p_0 - l_0) + \tilde{n}_\psi(p_0 - l_0)] \\ & \times (1 + 2\tilde{n}_\psi(k_0 - p_0)) \mathcal{P} \frac{1}{h(k_0, l_0, r, t, \alpha)} \mathcal{P} \frac{1}{k_0^2 - \omega_r^2}, \end{aligned} \quad (\text{B.6})$$

$$\begin{aligned} D_1(k_0, l_0, r, t) \equiv & 4\pi^5 r^2 t^2 [\theta(l_0) + \tilde{n}_\psi(l_0)] [\theta(p_0 - l_0) + \tilde{n}_\psi(p_0 - l_0)] \\ & \times (1 + 2\tilde{n}_\phi(k_0 - l_0)) (1 + 2\tilde{n}_\psi(k_0)) (1 + 2\tilde{n}_\psi(k_0 - p_0)). \end{aligned} \quad (\text{B.7})$$

By extracting the δ 's in Eq. (B.3) this way, we can trivialize several integrals. Particularly, we can write the product of δ 's in the first line of Eq. (B.3) as

$$\delta(l^2 - m_\psi^2) \delta((l-p)^2 - m_\psi^2) = \frac{1}{4\omega_t^2} [\delta(l_0 - \omega_t) + \delta(l_0 + \omega_t)] [\delta(l_0 - p_0 - \omega_t) + \delta(l_0 - p_0 + \omega_t)].$$

Next, since all α -dependence lies in $h(k_0, l_0, r, t, \alpha)$, it follows that the $d\cos\alpha$ integrals can be performed by employing the two identities

$$\int_{-1}^1 d\cos\alpha \delta(h(k_0, l_0, r, t, \alpha)) = \theta(2rt - |(k_0 - l_0)^2 - r^2 - t^2 - m_\phi^2|) \mathcal{P} \frac{1}{2rt}, \quad (\text{B.8})$$

$$\int_{-1}^1 d\cos\alpha \mathcal{P} \frac{1}{h(k_0, l_0, r, t, \alpha)} = \mathcal{P} \ln \left| \frac{(k_0 - l_0)^2 - (r-t)^2 - m_\phi^2}{(k_0 - l_0)^2 - (r+t)^2 - m_\phi^2} \right| \mathcal{P} \frac{1}{2rt}, \quad (\text{B.9})$$

where, in the last expression, both the fraction and the logarithm are principal values. From this, it follows that the contributions from the term featuring D_1 vanishes, while the contributions from the B_1 and C_1 terms can be shown to be identical. The calculations required to show this are tedious although rather straightforward to perform and are not listed here.

In all, this gives

$$\begin{aligned}
\mathcal{M}_{\text{vertex}}^{\mathcal{N}_1} = & \frac{\lambda^4}{8p_0(2\pi)^3} \theta(p_0 - 2m_\psi) \left(1 + \tilde{f}_\psi\left(\frac{p_0}{2}\right)\right)^2 \left[\right. \\
& \int_{\mathbb{R} \setminus [\frac{p_0}{2} - m_\phi, \frac{p_0}{2} + m_\phi]} dk_0 \left(1 + 2\tilde{n}_\phi\left(k_0 - \frac{p_0}{2}\right)\right) \mathcal{P} \frac{1}{p_0(2k_0 - p_0)} \\
& \quad \times \mathcal{P} \ln \left| \frac{(r_-^2 - c_2(k_0))(r_+^2 - c_1(k_0))}{(r_-^2 - c_1(k_0))(r_+^2 - c_2(k_0))} \right| \\
& - 2 \int_{\mathbb{R} \setminus [-m_\psi, m_\psi]} dk_0 (1 + 2\tilde{n}_\psi(k_0)) \mathcal{P} \frac{1}{p_0(2k_0 - p_0)} \\
& \quad \times \mathcal{P} \ln \left| \frac{\left(k_0 - \frac{p_0}{2}\right)^2 - \left(\sqrt{k_0^2 - m_\psi^2} - \frac{1}{2}\sqrt{p_0^2 - 4m_\psi^2}\right)^2 - m_\phi^2}{\left(k_0 - \frac{p_0}{2}\right)^2 - \left(\sqrt{k_0^2 - m_\psi^2} + \frac{1}{2}\sqrt{p_0^2 - 4m_\psi^2}\right)^2 - m_\phi^2} \right| \left. \right]
\end{aligned} \tag{B.10}$$

where

$$r_\pm = \frac{1}{2} \sqrt{p_0^2 - 4m_\psi^2} \pm \sqrt{\left(k_0 - \frac{p_0}{2}\right)^2 - m_\phi^2}, \tag{B.11}$$

$$c_1(k_0) = k_0^2 - m_\psi^2, \tag{B.12}$$

$$c_2(k_0) = (k_0 - p_0)^2 - m_\psi^2. \tag{B.13}$$

B.2 Contributions from $\text{Re}\{\mathcal{N}_3\}$

We can write the integrand of (B.1) containing $\text{Re}\{\mathcal{N}_3\}$ as

$$\begin{aligned}
\mathcal{M}_{\text{vertex}}^{\mathcal{N}_3} = & -\frac{4\lambda^4}{(2\pi)^6} \int dk_0 dr dl_0 dt d\cos\alpha \delta(k^2 - m_\psi^2) \delta((l-p)^2 - m_\psi^2) \delta((k-l)^2 - m_\phi^2) \\
& \times [A_3 + \delta(l_0^2 - \omega_t^2) \delta((k_0 - p_0)^2 - \omega_r^2) D_3]
\end{aligned} \tag{B.14}$$

where

$$\begin{aligned}
A_3(k_0, l_0, r, t) \equiv & -r^2 t^2 (2\pi)^3 [\theta(k_0) + \tilde{n}_\chi(k_0)] [\theta(p_0 - l_0) + \tilde{n}_\chi(p_0 - l_0)] \\
& \cdot [\theta(l_0 - k_0) + \tilde{n}_\phi(l_0 - k_0)] \mathcal{P} \frac{1}{l_0^2 - \omega_t^2} \mathcal{P} \frac{1}{(k_0 - p_0)^2 - \omega_r^2},
\end{aligned} \tag{B.15}$$

$$\begin{aligned}
D_3(k_0, l_0, r, t) \equiv & -r^2 t^2 8\pi^5 [\theta(k_0) + \tilde{n}_\chi(k_0)] [\theta(p_0 - l_0) + \tilde{n}_\chi(p_0 - l_0)] \\
& \cdot [\theta(l_0 - k_0) + \tilde{n}_\phi(l_0 - k_0)] (1 + 2\tilde{n}_\chi(l_0)) (1 + 2\tilde{n}_\chi(k_0 - p_0)).
\end{aligned} \tag{B.16}$$

Here, all angular dependence is contained entirely within the $\delta((k-l)^2 - m_\phi^2)$. The $d\cos\alpha$ integral is therefore trivialized through Eq. (B.8). It also follows that, the contribution from

the term featuring D_3 vanishes due to non-overlapping θ -functions. Only the A_3 term is non-vanishing, which results in the double-integral

$$\begin{aligned} \mathcal{M}_{\text{vertex}}^{\mathcal{N}_3} = & \frac{\lambda^4}{2(2\pi)^3} \int_{\mathbb{R} \setminus [-m_\psi, m_\psi]} dk_0 \int_{\mathbb{R} \setminus [p_0 - m_\psi, p_0 + m_\psi]} dl_0 \left\{ \mathcal{P} \frac{1}{p_0(2l_0 - p_0)} \mathcal{P} \frac{1}{p_0(p_0 - 2k_0)} \right. \\ & \times \theta \left(2\sqrt{(k_0^2 - m_\psi^2)((l_0 - p_0)^2 - m_\psi^2)} - |2l_0(p_0 - k_0) - p_0^2 + 2m_\psi^2 - m_\phi^2| \right) \\ & \left. \times [\theta(k_0) + \tilde{n}_\psi(k_0)][\theta(p_0 - l_0) + \tilde{n}_\psi(p_0 - l_0)][\theta(l_0 - k_0) + \tilde{n}_\psi(l_0 - k_0)] \right\} \end{aligned} \quad (\text{B.17})$$

Performing the substitutions $x \equiv -k_0$ and $y \equiv l_0 - p_0$, we get

$$\begin{aligned} \mathcal{M}_{\text{vertex}}^{\mathcal{N}_3} = & \frac{\lambda^4}{2(2\pi)^3} \int_{\mathbb{R} \setminus [-m_\psi, m_\psi]} dx dy \left\{ \mathcal{P} \frac{1}{p_0(p_0 + 2x)} \mathcal{P} \frac{1}{p_0(p_0 + 2y)} \theta(j(x, y)) \right. \\ & \left. \times \epsilon(x)\epsilon(y)\epsilon(x + y + p_0)\tilde{f}_\psi(x)\tilde{f}_\psi(y)(1 + \tilde{f}_\psi(x + y + p_0)) \right\}, \end{aligned} \quad (\text{B.18})$$

where $j(x, y) \equiv 2\sqrt{(x^2 - m_\psi^2)(y^2 - m_\psi^2)} - |2(p_0 + x)(p_0 + y) - p_0^2 + 2m_\psi^2 - m_\phi^2|$. The benefit of this substitution is that the integrand is symmetric under $x \leftrightarrow y$, meaning it does not matter numerically which integral we perform first. This means that if $\theta(j(x_0, y_0)) = 0$ for some (x_0, y_0) , then we also have $\theta(j(y_0, x_0)) = 0$. Unfortunately, we are unable to analytically carry on any further. In order to perform the remaining two integrals numerically, it helps to divide the domain of integration into regions where the integrand is zero due to the $\theta(j(x, y))$ and where it is non-zero. To do this, we solve $j(x, y_\pm(x)) = 0$ for $y_\pm(x)$ as

$$\begin{aligned} y_\pm(x) \equiv & \frac{1}{2(p_0(p_0 + 2x) + m_\psi^2)} \left[(p_0 + x)(m_\phi^2 - 2m_\psi^2 - p_0(p_0 + 2x)) \right. \\ & \left. \pm \sqrt{(x^2 - m_\psi^2) \left(m_\phi^4 + p_0^2(p_0 + 2x)^2 - 2m_\phi^2(2m_\psi^2 + p_0(p_0 + 2x)) \right)} \right]. \end{aligned} \quad (\text{B.19})$$

By integrating over domains bounded by y_\pm , the effect of the $\theta(j(x, y))$ may be accurately accounted for numerically.

Appendix C

Fermionic Two-loop Self-Energy Calculations

Here, we show how to account for angular dependences when inserting a pre-calculated $\Pi_{11}^\psi(k)$ into Eq. (5.27) when ψ is a fermion, where Π_{11}^ψ is the $\psi_+ \rightarrow \psi_+$ self-energy:

$$\Pi_{11}^\psi(k) = \frac{\text{---}\overbrace{\text{---}}^p\text{---}}{\psi \xrightarrow{k-p}} + \mathcal{O}(\lambda^4). \quad (\text{C.1})$$

Calculating quantities like $\Pi_{11}^\psi(k)$ is usually easier if one chooses a reference frame like $k^\mu = (k_0, 0, 0, k_3)$. Unfortunately, since the k^μ in Eq. (5.27) is not connected to external legs, we are not allowed to freely pick such a frame. In the scalar case, this is no issue since all scalar quantities are angularly independent. For fermions, we must either calculate $\Pi_{11}^\psi(k)$ in a frame where $k^\mu = (k_0, k_1, k_2, k_3)$ (which can very quickly become complicated), *or* we must rotate the answer for $k^\mu = (k_0, 0, 0, k_3)$ into an arbitrary frame and insert the rotated expression. This appendix shows how to do the latter.

In the frame where $k^\mu = (k_0, 0, 0, k_3)$, the Dirac structure of $\Pi_{11}^\psi(k)$ takes the form (cf. Section 10 of ref. [46])

$$\Pi_{11}^\psi(k) = \mathcal{U} + \gamma^0 \mathcal{V} + \gamma^3 \mathcal{W} + \not{k} \mathcal{Y}, \quad (\text{C.2})$$

where $\mathcal{U}, \mathcal{V}, \mathcal{W}, \mathcal{Y}$ are some scalar functions of k_0 and $|\mathbf{k}| = k_3$. In order to rotate Eq. (C.2), we consider the rotation matrices

$$\Lambda \equiv \begin{pmatrix} 1 & 0 & 0 & 0 \\ 0 & \cos \beta & \sin \beta \sin \alpha & \sin \beta \cos \alpha \\ 0 & 0 & \cos \alpha & -\sin \alpha \\ 0 & -\sin \beta & \cos \beta \sin \alpha & \cos \beta \cos \alpha \end{pmatrix}, \quad (\text{C.3})$$

where $\alpha \in [0, 2\pi]$, $\beta \in [0, \pi]$ are the angles of rotation around the x - and y -axis, respectively. Since Λ is a spatial rotation, it is also a Lorentz transformation: $\Lambda \in \text{SO}(3) \subset \text{SO}^+(1, 3)$.

Hence, in order to rotate Eq. (C.2), we can utilize that γ^μ transforms under the appropriate Lorentz representation as $\Lambda(\gamma^\mu) = \Lambda_\nu^\mu \gamma^\nu$, while the scalar functions $\mathcal{U}, \mathcal{V}, \mathcal{W}, \mathcal{Y}$ are rotationally invariant. We get

$$\Lambda(\Pi_{11}^\psi) = \mathcal{U} + \Lambda_\mu^0 \gamma^\mu \mathcal{V} + \Lambda_\mu^3 \gamma^\mu \mathcal{W} + \not{k} \mathcal{Y} = \mathcal{X} + \mathcal{U}, \quad (\text{C.4})$$

where

$$\mathcal{X}^\mu \equiv (\mathcal{V} + k_0 \mathcal{Y}, \Lambda^{i3}(\mathcal{W} + |\mathbf{k}| \mathcal{Y})). \quad (\text{C.5})$$

Hence, rather than inserting $\Pi_{11}^\psi(k)$ into Eq. (5.27), we insert $\mathcal{X} + \mathcal{U}$. The trace which appears in Eq. (5.36) then becomes

$$\begin{aligned} & \text{tr} \{ (\not{k} + m_\psi)(\mathcal{X} + \mathcal{U})(\not{k} + m_\psi)(\not{k} - \not{p} + m_\psi) \} \\ & = 4 [\mathcal{U} m_\psi^3 + m_\psi^2 \mathcal{X} \cdot (3k - p) - 2(k \cdot p)(\mathcal{X} \cdot k + \mathcal{U} m_\psi) + k^2(\mathcal{X} \cdot (k + p) + 3\mathcal{U} m_\psi)], \end{aligned} \quad (\text{C.6})$$

where

$$\begin{aligned} \mathcal{X} \cdot k &= k_0(\mathcal{V} + k_0 \mathcal{Y}) - |\mathbf{k}|(\mathcal{W} + |\mathbf{k}| \mathcal{Y}), & \mathcal{X} \cdot p &= p_0(\mathcal{V} + k_0 \mathcal{Y}) + (\mathcal{W} + |\mathbf{k}| \mathcal{Y}) \Lambda_i^3 p^i, \\ k \cdot p &= k_0 p_0 + |\mathbf{k}| \Lambda_i^3 p^i, & k \cdot k &= k_0^2 - |\mathbf{k}|^2. \end{aligned} \quad (\text{C.7})$$

Since Λ_i^3 carries all the angular dependence of the d^4k -integral in Eq. (5.36), we note that if we take $\mathbf{p} = \mathbf{0}$ (i.e. pick the ϕ c.o.m. frame), the trace becomes angularly independent since all terms with Λ_i^3 vanish. This trivializes the angular integrals in Eq. (5.36) and concludes our illustration.

Appendix D

Regularization & Renormalization at Finite Temperature

A complication in calculating Γ_{BW} to $\mathcal{O}(\lambda^4)$ is that it diverges. Specifically, the dy integral in Eq. (5.40) diverges due to the $1/(y + p_0/2)^2$. To assert finiteness of Γ_{BW} , we must employ a renormalization scheme.

Analytically renormalizing thermal QFT is (principally) rather straightforward. It turns out that the counterterms which make the theory finite at $T = 0$ also make the theory finite at $T > 0$ [29]. The reason is that finite temperature effects do not modify the theory at distances $\ll 1/T$, meaning the UV divergences are the same as those at $T = 0$. For a more rigorous treatment of renormalization at finite temperature, see ref. [75] and Chapter 11 of ref. [82].

Numerically, however, matters become more complicated. Although the appropriate counterterms can be calculated, it is not obvious how to treat the cancellation of infinities between diverging loops and counterterms numerically. For example, assuming a $1/\epsilon$ divergence in some loop integral, the analytical cancellation works like

$$\lim_{\epsilon \rightarrow 0^+} \int \left(\text{divergent}_{\text{loop}} \right) - \frac{1}{\epsilon} = \text{finite}. \quad (\text{D.1})$$

How is one supposed to implement this behaviour numerically and extract the singularities when all numerical quantities are inherently finite?

To start, we can write the diverging dy integral in Eq. (5.40) as

$$\mathcal{M}_{\text{SE}}^{(10)}(p_0) \equiv \int_{-\infty}^{\infty} dy F(y, p_0) \mathcal{P} \frac{1}{(y + p_0/2)^2}, \quad (\text{D.2})$$

where $F(y, p_0)$ is implicitly defined through Eq. (5.40).⁴⁹ The divergence appears because the integral is evaluated infinitesimally close to the pole at $y = -p_0/2$ and the integrand is not antisymmetric about this pole. It would converge if we instead integrated over the domains $(-\infty, -p_0/2 - \xi]$ and $[-p_0/2 + \xi, \infty)$, for some arbitrarily small $\xi > 0$. If we can

⁴⁹Instead of having the dy integral be over $\mathbb{R} \setminus [-m_\psi, m_\psi]$, like in Eq. (5.40), we have instead taken the boundaries to be $\pm\infty$ and included a factor of $\theta(y^2 - m_\psi^2)$ in $F(y)$.

parametrize the divergence of Eq. (D.2) for small ξ , we may numerically extract the divergent part through a finite ξ .

This type of regularization is known as *Hadamard regularization* [83, 84], wherein

$$\mathcal{H} \int_a^b dy \frac{f(y)}{(y-c)^2} = \lim_{\xi \rightarrow 0^+} \left\{ \int_a^b dy f(y) \frac{(y-c)^2}{[(y-c)^2 + \xi^2]^2} - \frac{\pi}{2\xi} f(c) - \frac{1}{2} f(c) \left(\frac{1}{b-c} - \frac{1}{a-c} \right) \right\}, \quad (\text{D.3})$$

for any function $f(y)$ that is infinitely differentiable at $y = \xi$ for $a < \xi < b$ and \mathcal{H} denotes the *Hadamard finite-part*. In order to work with dimensionless parameters, we will henceforth pass to $\xi/m_\phi \rightarrow \xi$. For a numerical implementation of Hadamard regularization, we will consider finite a finite $\xi \ll 1$. Like any (correctly implemented) regularization scheme, the Hadamard finite-part should not depend on our choice of ξ . If we pick a ξ that is “too large”, we will be removing not just the divergence from our integral, but also finite, physical contributions. As ξ grows, we therefore expect to eventually observe some ξ -dependence in $\mathcal{H}\mathcal{M}_{\text{SE}}^{(10)}$. Meanwhile, if ξ is “too small” and approaches our numerical working precision, we should observe divergence with no inherent ξ -dependence. This can be seen from Eq. (D.3), since any number smaller than our working precision will be treated numerically as ≈ 0 . Hopefully, we can find a “Goldilocks zone” wherein ξ is small enough for $\mathcal{H}\mathcal{M}_{\text{SE}}^{(10)}$ to be constant in ξ but large enough for $\mathcal{H}\mathcal{M}_{\text{SE}}^{(10)}$ to converge.

This behaviour is exactly what we find if we plot $\mathcal{H}\mathcal{M}_{\text{SE}}^{(10)}(p_0)$ as a function of ξ for different p_0 – see Figure D.1 for $T = 1000m_\phi$ and Figure D.2 for $T = 10m_\phi$. Both figures illustrate that the Goldilocks zone emerges from the chaotic low- ξ zone and that a ξ -dependence appears as ξ grows past this zone. These two plots indicate that only the *upper* bound of the Goldilocks zone is temperature dependent, and that the behaviour towards the lower area of the Goldilocks zone is constant in T . Calculations at other temperatures, working precisions and p_0 seemed to confirm this.

If we take this result as truth, it illustrates our earlier claim about $T = 0$ counterterms renormalizing the theory at all temperatures: Say we had infinite working precision; then the lower bound of the Goldilocks zone would be an infinitesimal. Since changing the temperature may only alter the *upper* bound of the Goldilocks zone, any change in temperature may never exclude an infinitesimal ξ from the Goldilocks zone, giving a temperature-independent regularization. If we take the concept of “infinite working precision” as an analogy to working analytically, we recover that an analytical Hadamard regularization is temperature independent. When performing numerical calculations, we will therefore be picking ξ in the lower area of the Goldilocks zone.

Having asserted the finiteness of our expressions, we must also impose renormalization conditions. Although we are technically only interested in its imaginary component, we will impose the renormalization conditions on the full *physical* self-energy, $\Pi^{\text{phys}}(p_0)$. These

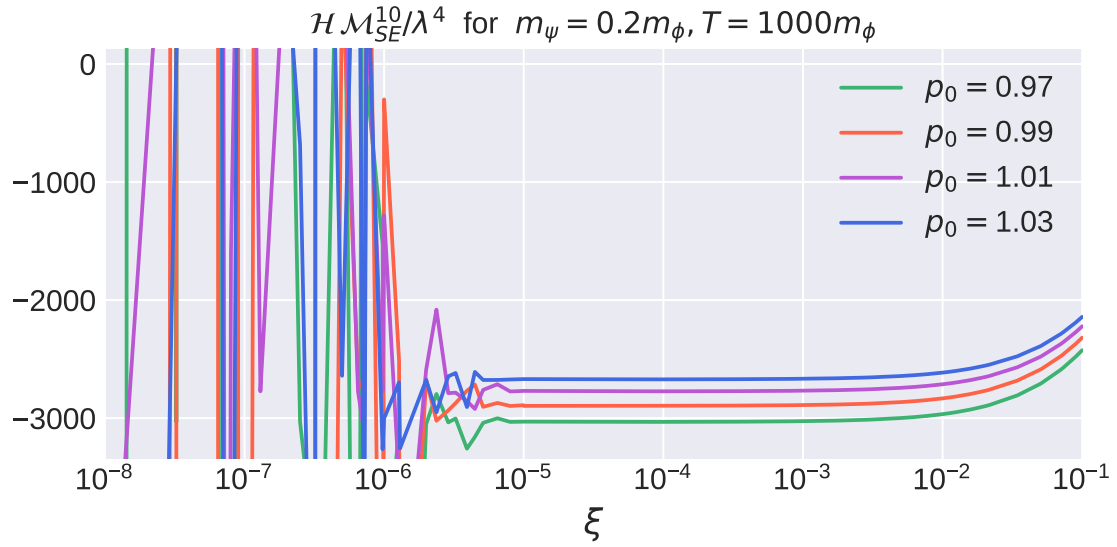


Figure D.1: Plot of the Hadamard finite-part, $\mathcal{H}\mathcal{M}_{SE}^{(10)}/\lambda^4$, from Eq. (5.40), here for $m_\psi = 0.2m_\phi, T = 1000m_\phi$ and four different ρ_0 in the domain of resonance. As ξ^2 becomes smaller than the numerical working precision (which in this case is $\sim 10^{-9}$), the ξ -dependence becomes sporadic and unpredictable due to the ξ^2 in the denominator of Eq. (D.3). The Goldilocks zone seems to start somewhere after $\xi \sim 10^{-5}$, where the Hadamard finite-part is temporarily independent of ξ .

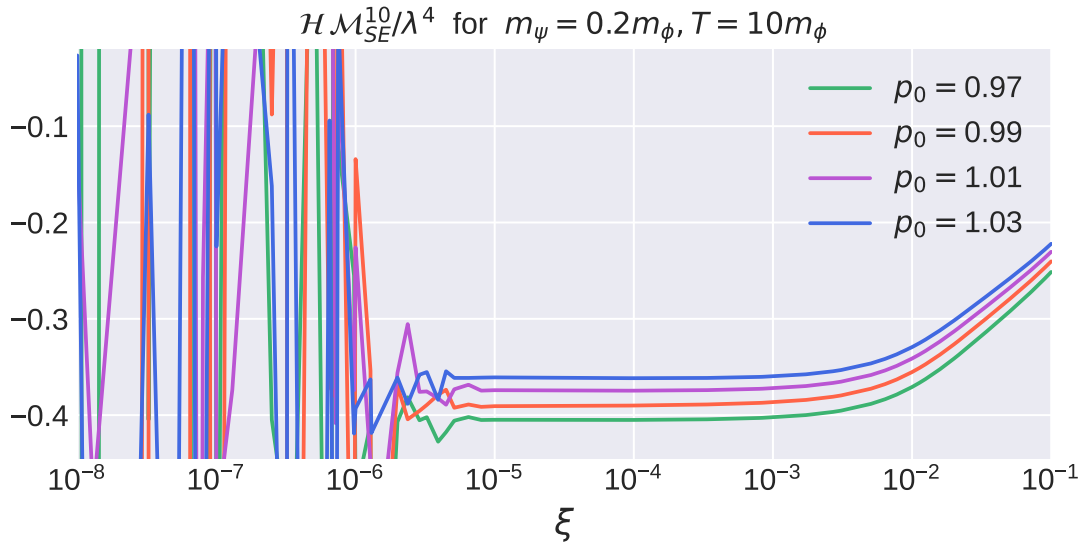
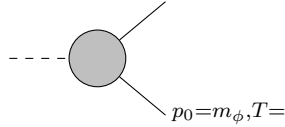


Figure D.2: Plot of $\mathcal{H}\mathcal{M}_{SE}^{(10)}/\lambda^4$, like Figure D.1 but with $T = 10m_\phi$. The Goldilocks zone appears to be smaller at $T = 10m_\phi$ than at $T = 1000m_\phi$. The effect of decreasing the temperature therefore appears to be to lower the upper bound of the Goldilocks zone.

conditions are the same as the ones which we encountered all the way back in Chapter 3:⁵⁰

$$\begin{aligned}\operatorname{Re} \left\{ \Pi^{\text{phys}}(m_\phi) \right\} &= 0, \\ \operatorname{Im} \left\{ \Pi^{\text{phys}}(m_\phi) \right\} &= m_\phi \Gamma_{\text{BW}}^{\text{phys}}.\end{aligned}\tag{D.4}$$

How then is $\Pi^{\text{phys}}(m_\phi)$ related to the quantity $\Pi(p_0)$ which we have been using so far? To answer this, we utilize the above claim that $T = 0$ counterterms also renormalize the theory at $T > 0$: We start by imposing a renormalization condition on the coupling by introducing the renormalized coupling constant, λ_R , defined at $T = 0$ to be



$$\equiv i\lambda_R,\tag{D.5}$$

we then have $\Gamma_{\text{BW}}^{\text{phys}}(m_\phi, 0) \sim \lambda_R^2$. An expression which satisfies the conditions in Eq. (D.4) is then

$$\Pi^{\text{phys}}(p_0, T) \equiv \Pi(p_0, T) - \Pi(m_\phi, 0) + im_\phi \Gamma_{\text{BW}}^{\text{phys}}(m_\phi, 0).\tag{D.6}$$

Denoting by $\Gamma_{\text{BW}}^{(n)}(p_0, T)$ the coefficient of the λ^n -term in the (non-renormalized) BW decay rate, i.e. $\Gamma_{\text{BW}} = \sum_n \Gamma_{\text{BW}}^{(n)} \lambda^n$, we can pass to the renormalized coupling, $\lambda \rightarrow \lambda_R$, and write

$$\Gamma_{\text{BW}}^{\text{phys}}(p_0, T) = \Gamma_{\text{BW}}^{(2)}(p_0, T) \lambda_R^2 + \left[\Gamma_{\text{BW}}^{(4)}(p_0, T) - \Gamma_{\text{BW}}^{(4)}(m_\phi, 0) \right] \lambda_R^4 + \mathcal{O}(\lambda_R^6).\tag{D.7}$$

This is the physical BW decay rate which obeys the renormalization conditions.

⁵⁰Since we are free to pick the bare mass at leisure, we pick it to equal the real pole mass $\tilde{m}_\phi \stackrel{!}{=} m_\phi$.

Appendix E

Imaginary-Time Thermal Quantum Field Theory

In addition to the real-time thermal QFT focused on in this thesis, *imaginary-time* thermal QFT is also a frequently used formalism (sometimes known as the *Matsubara formalism*). In this appendix, we quickly outline the principles behind this formalism – for a more extensive treatment, see the [Reference Guide](#).

The starting point of the imaginary-time formalism is the partition function for a thermalized system

$$Z(\beta) = \text{Tr}\{e^{-\beta\hat{H}}\} = \int dq \langle q | e^{-\beta\hat{H}} | q \rangle, \quad (\text{E.1})$$

where the $|q\rangle$ form an orthogonal basis for the Hilbert space and \hat{H} is the Hamiltonian. Using path formalism, we can write the probability amplitude of a state $|\phi_a\rangle$ at $t = 0$ transitioning into a state $|\phi_b\rangle$ at $t = t'$ as

$$\langle \phi_b | e^{-i\hat{H}t'} | \phi_a \rangle = \int_{\phi(t=0)=\phi_a}^{\phi(t=t')=\phi_b} \mathcal{D}\phi \exp \left\{ i \int_0^{t'} dt \int d^3\mathbf{x} \mathcal{L} \right\}. \quad (\text{E.2})$$

If we naïvely treat the $e^{-\beta\hat{H}} = e^{-i(-i\beta)\hat{H}}$ in Eq. (E.1) as an operator which translates states by an imaginary time $-i\beta$, we are tempted to define a complex time $\tau \equiv it$ and set $t' = -i\beta$ in Eq. (E.2). Using this, we can write $Z(\beta)$ as an integral over transition amplitudes $|\phi(\tau = 0)\rangle \rightarrow |\phi(\tau = \beta)\rangle$, giving

$$Z(\beta) = \int d\phi \langle \phi | e^{-\beta\hat{H}} | \phi \rangle = \int_{\phi(\tau=0)=\phi}^{\phi(\tau=\beta)=\phi} \mathcal{D}\phi \exp \left\{ \int_0^\beta d\tau \int d^3\mathbf{x} \mathcal{L} \right\}. \quad (\text{E.3})$$

This partition function bears a strong resemblance to the generating functional of a Euclidean QFT:

$$\mathcal{Z}_E[j] = \int \mathcal{D}\phi \exp \left\{ - \int d^4x_E (\mathcal{L}_E + j\phi) \right\}, \quad (\text{E.4})$$

evaluated at $j = 0$. Here, $x_E^\mu = (\tau, \mathbf{x})$ and the Euclidean Lagrangian $\mathcal{L}_E \equiv -\mathcal{L}(\tau = it)$ is (minus) the Minkowski Lagrangian evaluated at the imaginary time $\tau = it$. We can therefore make the generating functional and the partition function agree by asserting that the boundary conditions in the $\mathcal{D}\phi$ integrals in Eq. (E.4) and Eq. (E.3) are the same. This implies that

- Bosonic fields are periodic in imaginary-time: $\phi(\tau = \beta) = \phi(\tau = 0)$,
- Fermionic fields are *anti*-periodic: $\psi(\tau = \beta) = -\psi(\tau = 0)$.

The anti-periodicity of fermionic fields follow from their anti-commutativity [29, 30]. To adhere to the $d\tau$ integral in Eq. (E.3), we must also take the imaginary time, τ , to be bounded: $\tau \in [0, \beta]$.

In all, this implies an equality between the partition function (a statistical object) and the generating functional (a QFT object) subject to the above restrictions:

$$Z(\beta) = \mathcal{Z}_E. \tag{E.5}$$

The LHS is related to statistical observables like the *average energy*, $\langle E \rangle = \frac{1}{Z} \text{Tr}\{\hat{H}e^{-\beta\hat{H}}\}$, the *free energy*, $F = -T \ln Z$, and the *entropy*, $S = -\frac{\partial F}{\partial T}$. Meanwhile, the RHS is a field-theoretic object calculated through its Lagrangian, Feynman rules and the S -matrix. Combined, they form a *thermal* theory expressed in the formalism of a *quantum field theory*. Using the generating functional, we can perturbatively calculate these statistical observables, meaning they all have field-theoretic counterparts. For example, the free energy corresponds to the self-energy $\Pi(\omega)$ [30], which has been a central quantity in this thesis.

The biggest difference between imaginary-time thermal QFT and a traditional Euclidean QFT, is that the former is bounded in its time domain. In turn, this implies a discrete energy spectrum. Any 4-dimensional momentum-space integral will therefore instead feature a sum over discrete energies called the *Matsubara frequencies* [85].

Clearly, this formalism is very different from the real-time formalism we derived in Chapter 4. One can, however, show that the two theories are physically equivalent; from the Osterwalder-Schrader theorem [54], it follows that there exists a unique analytical continuation between real- and imaginary-time thermal QFT. The two theories therefore share Green's functions, and by extension, observables. It is therefore a matter of personal taste and situational applicability which formalism one should use. However, due to the complicatedness of having to work with a 2×2 propagator in real-time thermal QFT, the imaginary-time formalism is often the go-to choice for actually performing calculations. Unfortunately, the fact that its physics does not take place in Minkowski space, means that it is more detached from physical principles than the real-time formalism is.

Appendix F

Deriving Conventional Phase Space Suppressions

In this appendix, we use the SSR approach to derive the notion of initial states being suppressed/enhanced by f while final states are suppressed/enhanced by $1 + \tilde{f}$. Of course, QM tells us that this is simply just how the phase spaces of initial and final states behave, but it is nevertheless a bit strange that a plasma cares whether a state is at the beginning or at the end of a process.

To illustrate the relation these factors have with the SSR approach, we will again reproduce a result of Weldon's, similarly to what we did for Γ_d and Γ_p in Section 6.2. According to Weldon [31],⁵¹ in a plasma which contains three sets of particle populations, A, B and C , then the rate at which A “decays” to B when C is also present in the plasma, is

$$\Gamma_d = \frac{1}{2\omega} \int \prod_{i=1}^n \left(\frac{d^3 \mathbf{p}_{B_i}}{(2\pi)^3 2E_{B_i}} (1 + \varepsilon_{B_i} f_{B_i}(E_{B_i})) \right) \prod_{i=1}^m \left(\frac{d^3 \mathbf{p}_{C_i}}{(2\pi)^3 2E_{C_i}} f_{C_i}(E_{C_i}) \right) |\mathcal{M}_{AC \rightarrow B}|^2,$$

while the rate at which A is “produced” is

$$\Gamma_p = \frac{1}{2\omega} \int \prod_{i=1}^n \left(\frac{d^3 \mathbf{p}_{B_i}}{(2\pi)^3 2E_{B_i}} f_{B_i}(E_{B_i}) \right) \prod_{i=1}^m \left(\frac{d^3 \mathbf{p}_{C_i}}{(2\pi)^3 2E_{C_i}} (1 + \varepsilon_{C_i} f_{C_i}(E_{C_i})) \right) |\mathcal{M}_{B \rightarrow AC}|^2,$$

where B and C are n - and m -particle states, respectively. Again, for the sake of brevity, we have absorbed a factor of $(2\pi)^4 \delta^{(4)}(p_A + p_C - p_B)$ into the square matrix element.

In order to reproduce this result in the SSR approach, we must make an assumption that is rather hard to justify. As of now, we will motivate it by the fact that it “simply produces the correct result”, and return to it at the end of this appendix: Consider the BW rate of the process $A \rightarrow BC$, where we let $|B\rangle \in (\mathcal{B}^+)^{\otimes n}$ and $|C\rangle \in (\mathcal{B}^-)^{\otimes m}$, i.e. we let B consist of n states with $p_0 > 0$ and C of m states with $p_0 < 0$. The BW rate for the process $A \rightarrow BC$

⁵¹These are not Weldon's exact words, but an equivalent restatement.

then becomes (using the identities of Eq. (4.24) to rewrite the thermal measures):

$$\begin{aligned}
\Gamma_{\text{BW}} &= \frac{1}{2\omega} \int \prod_{i=1}^n \left(\frac{d^3 \mathbf{p}_{B_i}}{(2\pi)^3 2E_{B_i}} \left(1 + \tilde{f}_{B_i}(E_{B_i}) \right) \right) \prod_{i=1}^m \left(\frac{d^3 \mathbf{p}_{C_i}}{(2\pi)^3 2E_{C_i}} \tilde{f}_{C_i}(E_{C_i}) \right) |\mathcal{M}_{A \rightarrow BC}|^2 \\
&\quad - \frac{1}{2\omega} \int \prod_{i=1}^n \left(\frac{d^3 \mathbf{p}_{B_i}}{(2\pi)^3 2E_{B_i}} \tilde{f}_{B_i}(E_{B_i}) \right) \prod_{i=1}^m \left(\frac{d^3 \mathbf{p}_{C_i}}{(2\pi)^3 2E_{C_i}} \left(1 + \tilde{f}_{C_i}(E_{C_i}) \right) \right) |\mathcal{M}_{BC \rightarrow A}|^2 \\
&= \varepsilon_C \Gamma_d - \varepsilon_B \Gamma_p.
\end{aligned} \tag{F.1}$$

The last equivalence follows from the fact that $|\mathcal{M}_{A \rightarrow BC}|^2 = |\mathcal{M}_{AC \rightarrow B}|^2$.⁵² If we again choose to absorb all factors of ε into the definitions of Γ_d and Γ_p (i.e. we use \tilde{f} instead of f in their definitions), this again recovers $\Gamma_{\text{BW}} = \Gamma_d - \Gamma_p$. This tells us that taking the phase space suppressions of initial and final states to be \tilde{f} and $1 + \tilde{f}$, respectively, is equivalent to considering a scattering process where the final states are not on a single branch. At zero-temperature, inter-branch scattering is not permitted, but at finite temperatures it is perfectly allowed. The initial/final state phase space suppression factors are therefore nothing but the thermal measures, Eq. (4.13), evaluated for states in \mathcal{B}^+ or \mathcal{B}^- , cf. Eq. (4.24).

Of course, this result relies on the assumption that $|B\rangle$ and $|C\rangle$ are states on different branches. At this point in time, we are unable to present a physical reason behind why this produces the phase space suppressions which QM predicts – it simply does. However, keep in mind that this is not the first time that we have had to include unexpected processes which flip our preconceived notions about which states are initial and which are final: In Section 5.1.1, we saw that the approach of ref. [23] overlooked the process $\phi\psi_1 \rightarrow \psi_2$, and that this process differed in its initial- and final states compared to the process we *thought* we were studying, $\phi \rightarrow \psi_1\psi_2$. It is therefore very likely that the requirements $|B\rangle \in (\mathcal{B}^+)^{\otimes n}$ and $|C\rangle \in (\mathcal{B}^-)^{\otimes m}$ are artefacts of some intricate aspect of the plasma containing A, B and C which we have simply not yet considered.

Lastly, we address a supposed discrepancy whose discussion we postponed back in Section 4.2. All of our initial-state suppressions feature \tilde{f}_A instead of f_A , the latter of which is the expected suppression from statistical physics. At first, this may seem to lead to a sign-change in the fermionic case, but it actually turns out that by using \tilde{f}_A instead of f_A , we are accounting for a sign-change that would otherwise happen later down the road. To see this, compare Weldon’s expressions for the discontinuity of the boson and fermion self-energies, Eq. (2.20) and Eq. (2.25), respectively, in ref. [31].⁵³ In these expressions, *all* fermion phase space distribution functions feature an additional minus sign compared to the bosonic functions. Weldon addresses this at the very end of Section II B, where he claims that, in general, fermion initial state suppressions feature an additional minus sign in the final expression for the discontinuity. Since he also proves that this discontinuity is nothing but the imaginary component of the self-energy, it follows that our use of \tilde{f}_A instead of f_A

⁵²To see this for a one-particle state C , note that the only thing that differs in the matrix elements $\mathcal{M}_{A \rightarrow BC}$ and $\mathcal{M}_{AC \rightarrow B}$ is whether the field of C is contracted to an initial or final state. The equality then follows from $(\overline{C|C})^\dagger = \langle C|\overline{C}$, where \overline{C} is the appropriately conjugated field.

⁵³Note that Weldon denotes the thermal phase space distribution functions (our f_A) as n_A .

results in the correct expression. By using the phase space measure in Eq. (4.13) we are preemptively accounting for this sign change.

References and Bibliography

Reference Guide

Several references make themselves noteworthy in the context of this thesis:

- Ref. [23] (*Bringmann et al., 2022*) is the paper which inspired our search for Γ_{BW} at finite temperature. It is recommended to read at least Sections 1 and 2 of this paper in order to understand the context in which we are working.
- The collective content of ref. [29] (*M. L. Bellac, 1996*), ref. [30] (*M. Laine and A. Vuorinen, 2022*) and ref. [75] (*N. P. Landsman and Ch.G. van Weer, 1987*) constitute a comprehensive and detailed introduction to working with thermal QFT, both in the real- and in the imaginary-time formalisms. These are recommended to readers interested in learning the conventional approach to thermal QFT, as well as applications in various areas of physics.
- Ref. [76] (*Ghiglieri et al., 2021*) and ref. [46] (*T. Lundberg and R. Pasechnik, 2021*) are articles which feature a modern review of the field of thermal QFT today. The former focuses on perturbative applications in QCD while the latter performs analytical one-loop calculations in the real-time formalism which can be used to simplify calculations of the two-loop self-energy contributions to Γ_{BW} , as shown in Section 5.2.2.
- Ref. [31] (*H. A. Weldon, 1983*) is a celebrated paper in thermal field theory which lays the groundwork for concepts such as thermal production- and decay rates. A large focus of this thesis is on reproducing Weldon's results through the lens of SSR, as most of modern thermal QFT builds upon his results.
- For a more formal treatment of the finite-temperature cutting rules, see ref. [26] (*R. L. Kobes and G. W. Semenoff, 1986*), and to understand the context which this paper is building upon, see the original derivation of the cutting rules at $T = 0$ in ref. [72] (*R. E. Cutkosky, 1960*).
- For a more comprehensive description of the relevant cosmological background outlined in Chapter 2, see ref. [79] (*E. Kolb and M. Turner, 1990*). Additionally, see ref. [20] (*Bernal et al., 2017*) for a modern review of freeze-in.

Bibliography

- [1] J. C. Kapteyn. “First Attempt at a Theory of the Arrangement and Motion of the Sidereal System”. In: *Astrophysical Journal* 55 (May 1922), p. 302. DOI: [10.1086/142670](https://doi.org/10.1086/142670).
- [2] K. Lundmark. “Über die Bestimmung der Entfernungen, Dimensionen, Massen und Dichtigkeit für die nächstgelegenen anagalactischen Sternsysteme.” In: *Meddelanden fran Lunds Astronomiska Observatorium Serie I* 125 (Jan. 1930), pp. 1–13.
- [3] Alexandre Refregier. “Weak Gravitational Lensing by Large-Scale Structure”. In: *Annual Review of Astronomy and Astrophysics* 41.1 (2003), pp. 645–668. DOI: [10.1146/annurev.astro.41.111302.102207](https://doi.org/10.1146/annurev.astro.41.111302.102207).
- [4] G. Hinshaw et al. “Five-Year Wilkinson Microwave Anisotropy Probe Observations: Data Processing, Sky Maps, and Basic Results”. In: *The Astrophysical Journal Supplement* 180.2 (Feb. 2009), pp. 225–245. DOI: [10.1088/0067-0049/180/2/225](https://doi.org/10.1088/0067-0049/180/2/225).
- [5] Planck Collaboration et al. “Planck 2015 results”. In: *Astronomy & Astrophysics* 594 (2016), A13. DOI: [10.1051/0004-6361/201525830](https://doi.org/10.1051/0004-6361/201525830).
- [6] Planck Collaboration et al. “Planck 2018 results. VI. Cosmological parameters”. In: *Astronomy & Astrophysics* 641, A6 (Sept. 2020), A6. DOI: [10.1051/0004-6361/201833910](https://doi.org/10.1051/0004-6361/201833910).
- [7] Douglas Clowe et al. “A Direct Empirical Proof of the Existence of Dark Matter”. In: *The Astrophysical Journal* 648.2 (2006), pp. L109–L113. DOI: [10.1086/508162](https://doi.org/10.1086/508162).
- [8] M. Aaronson. “Accurate radial velocities for carbon stars in Draco and Ursa Minor :the first hint of a dwarf spheroidal mass-to-light ratio.” In: *Astrophysical Journal* 266 (Mar. 1983), pp. L11–L15. DOI: [10.1086/183969](https://doi.org/10.1086/183969).
- [9] Thomas Hambye. *On the stability of particle dark matter*. 2010. arXiv: [1012.4587 \[hep-ph\]](https://arxiv.org/abs/1012.4587).
- [10] J-W Hsueh et al. “SHARP - VII. New constraints on the dark matter free-streaming properties and substructure abundance from gravitationally lensed quasars”. In: *Monthly Notices of the Royal Astronomical Society* 492.2 (Nov. 2019), pp. 3047–3059. ISSN: 0035-8711. DOI: [10.1093/mnras/stz3177](https://doi.org/10.1093/mnras/stz3177).

- [11] S. Vegetti et al. “Inference of the cold dark matter substructure mass function at $z = 0.2$ using strong gravitational lenses”. In: *Monthly Notices of the Royal Astronomical Society* 442.3 (2014), pp. 2017–2035. DOI: [10.1093/mnras/stu943](https://doi.org/10.1093/mnras/stu943).
- [12] N. Aghanim et al. “Planck 2018 results”. In: *Astronomy Astrophysics* 641 (2020), A6. DOI: [10.1051/0004-6361/201833910](https://doi.org/10.1051/0004-6361/201833910).
- [13] Benjamin W. Lee and Steven Weinberg. “Cosmological Lower Bound on Heavy-Neutrino Masses”. In: *Phys. Rev. Lett.* 39 (4 1977), pp. 165–168. DOI: [10.1103/PhysRevLett.39.165](https://doi.org/10.1103/PhysRevLett.39.165).
- [14] Lawrence J. Hall et al. “Freeze-in production of FIMP dark matter”. In: *Journal of High Energy Physics* 2010.3 (2010). DOI: [10.1007/jhep03\(2010\)080](https://doi.org/10.1007/jhep03(2010)080).
- [15] Giorgio Arcadi et al. “The waning of the WIMP? A review of models, searches, and constraints”. In: *The European Physical Journal C* 78.3 (2018). DOI: [10.1140/epjc/s10052-018-5662-y](https://doi.org/10.1140/epjc/s10052-018-5662-y).
- [16] Patrick J. Fox et al. “Dark matter in light of the LUX results”. In: *Physical Review D* 89.10 (2014). DOI: [10.1103/physrevd.89.103526](https://doi.org/10.1103/physrevd.89.103526).
- [17] Clifford Cheung et al. “Origins of hidden sector dark matter I: cosmology”. In: *Journal of High Energy Physics* 2011.3 (2011). DOI: [10.1007/jhep03\(2011\)042](https://doi.org/10.1007/jhep03(2011)042).
- [18] Clifford Cheung et al. “Origins of hidden sector dark matter II: Collider physics”. In: *Journal of High Energy Physics* 2011 (Mar. 2011), pp. 1–32. DOI: [10.1007/JHEP03\(2011\)085](https://doi.org/10.1007/JHEP03(2011)085).
- [19] Mattias Blennow, Enrique Fernandez-Martínez, and Bryan Zaldivar. “Freeze-in through portals”. In: *Journal of Cosmology and Astroparticle Physics* 2014.01 (2014), pp. 003–003. DOI: [10.1088/1475-7516/2014/01/003](https://doi.org/10.1088/1475-7516/2014/01/003).
- [20] Nicolás Bernal et al. “The dawn of FIMP Dark Matter: A review of models and constraints”. In: *International Journal of Modern Physics A* 32.27 (2017), p. 1730023. DOI: [10.1142/s0217751x1730023x](https://doi.org/10.1142/s0217751x1730023x).
- [21] Vanda Silveira and A. Zee. “Scalar Phantoms”. In: *Physics Letters B* 161.1 (1985), pp. 136–140. ISSN: 0370-2693. DOI: [10.1016/0370-2693\(85\)90624-0](https://doi.org/10.1016/0370-2693(85)90624-0).
- [22] Wan-Lei Guo and Yue-Liang Wu. “The real singlet scalar dark matter model”. In: *Journal of High Energy Physics* 2010.10 (2010). DOI: [10.1007/jhep10\(2010\)083](https://doi.org/10.1007/jhep10(2010)083).
- [23] Torsten Bringmann et al. “Freezing-in a hot bath: resonances, medium effects and phase transitions”. In: *Journal of High Energy Physics* 2022.2 (2022). DOI: [10.1007/jhep02\(2022\)110](https://doi.org/10.1007/jhep02(2022)110).
- [24] Ryogo Kubo. “Statistical-Mechanical Theory of Irreversible Processes. I. General Theory and Simple Applications to Magnetic and Conduction Problems”. In: *Journal of the Physical Society of Japan* 12.6 (1957), pp. 570–586. DOI: [10.1143/JPSJ.12.570](https://doi.org/10.1143/JPSJ.12.570).

- [25] Paul C. Martin and Julian Schwinger. “Theory of Many-Particle Systems. I”. In: *Phys. Rev.* 115 (6 1959), pp. 1342–1373. DOI: [10.1103/PhysRev.115.1342](https://doi.org/10.1103/PhysRev.115.1342).
- [26] Randal L. Kobes and Gordon W. Semenoff. “Discontinuities of green functions in field theory at finite temperature and density (II)”. In: *Nuclear Physics B* 272.2 (July 1986), pp. 329–364. DOI: [10.1016/0550-3213\(86\)90006-4](https://doi.org/10.1016/0550-3213(86)90006-4).
- [27] Paulo F. Bedaque, Ashok Das, and Satchidananda Naik. “Cutting Rules at Finite Temperature”. In: *Modern Physics Letters A* 12.33 (1997), pp. 2481–2496. DOI: [10.1142/s0217732397002612](https://doi.org/10.1142/s0217732397002612).
- [28] François Gelis. “Cutting rules in the real-time formalisms at finite temperature”. In: *Nuclear Physics B* 508.1-2 (1997), pp. 483–505. ISSN: 0550-3213. DOI: [10.1016/s0550-3213\(97\)80023-5](https://doi.org/10.1016/s0550-3213(97)80023-5).
- [29] M.L. Bellac. *Thermal Field Theory*. Cambridge Monographs on Mathematical Physics. Cambridge University Press, 1996. ISBN: 9780521654777.
- [30] Mikko Laine and Aleksi Vuorinen. *Basics of Thermal Field Theory*. Springer International Publishing, 2016. DOI: [10.1007/978-3-319-31933-9](https://doi.org/10.1007/978-3-319-31933-9).
- [31] H. Arthur Weldon. “Simple rules for discontinuities in finite-temperature field theory”. In: *Phys. Rev. D* 28 (8 1983), pp. 2007–2015. DOI: [10.1103/PhysRevD.28.2007](https://doi.org/10.1103/PhysRevD.28.2007).
- [32] James M. Cline et al. “Update on scalar singlet dark matter”. In: *Physical Review D* 88.5 (2013). DOI: [10.1103/physrevd.88.055025](https://doi.org/10.1103/physrevd.88.055025).
- [33] John McDonald. “Gauge singlet scalars as cold dark matter”. In: *Physical Review D* 50.6 (1994), pp. 3637–3649. DOI: [10.1103/physrevd.50.3637](https://doi.org/10.1103/physrevd.50.3637).
- [34] C.P. Burgess, Maxim Pospelov, and Tonnis ter Veldhuis. “The Minimal Model of nonbaryonic dark matter: a singlet scalar”. In: *Nuclear Physics B* 619.1-3 (2001), pp. 709–728. DOI: [10.1016/s0550-3213\(01\)00513-2](https://doi.org/10.1016/s0550-3213(01)00513-2).
- [35] G. Jungman, M. Kamionkowski, and K. Griest. “Supersymmetric dark matter”. In: *Physics Reports* 267 (Mar. 1996), pp. 195–373. DOI: [10.1016/0370-1573\(95\)00058-5](https://doi.org/10.1016/0370-1573(95)00058-5).
- [36] Oleg Lebedev and Takashi Toma. “Relativistic freeze-in”. In: *Physics Letters B* 798 (2019), p. 134961. DOI: [10.1016/j.physletb.2019.134961](https://doi.org/10.1016/j.physletb.2019.134961).
- [37] Simone Biondini and Jacopo Ghiglieri. “Freeze-in produced dark matter in the ultra-relativistic regime”. In: *Journal of Cosmology and Astroparticle Physics* 2021.03 (2021), p. 075. DOI: [10.1088/1475-7516/2021/03/075](https://doi.org/10.1088/1475-7516/2021/03/075).
- [38] Kenneth Intriligator and Nathan Seiberg. “Lectures on supersymmetry breaking”. In: *Classical and Quantum Gravity* 24.21 (2007), S741–S772. DOI: [10.1088/0264-9381/24/21/s02](https://doi.org/10.1088/0264-9381/24/21/s02).
- [39] Are Raklev. *Supersymmetry - Lecture notes for FYS5190/FYS9190 Supersymmetry*. 2021. URL: <https://www.uio.no/studier/emner/matnat/fys/FYS5190/h21/resurser/notes.pdf>.

- [40] M.D. Schwartz. *Quantum Field Theory and the Standard Model*. Quantum Field Theory and the Standard Model. Cambridge University Press, 2014. ISBN: 9781107034730.
- [41] Michael E. Peskin and Daniel V. Schroeder. *An Introduction to quantum field theory*. Reading, USA: Addison-Wesley, 1995. ISBN: 978-0-201-50397-5.
- [42] S. Weinberg. *The Quantum Theory of Fields*. Quantum Theory of Fields, Vol. 2: Modern Applications v. 1. Cambridge University Press, 1995. ISBN: 9780521550017.
- [43] Torsten Bringmann et al. “Electroweak and Higgs boson internal bremsstrahlung. General considerations for Majorana dark matter annihilation and application to MSSM neutralinos”. In: *Journal of High Energy Physics* 2017.9 (2017). DOI: [10.1007/jhep09\(2017\)041](https://doi.org/10.1007/jhep09(2017)041).
- [44] A.E. Siegman. *Lasers*. G - Reference, Information and Interdisciplinary Subjects Series. University Science Books, 1986. ISBN: 9780935702118.
- [45] Naoki Ashida et al. “Diagrammatic algorithm for evaluating finite-temperature reaction rates”. In: *Annals of Physics* 215.2 (1992), pp. 315–371. ISSN: 0003-4916. DOI: [10.1016/0003-4916\(92\)90115-3](https://doi.org/10.1016/0003-4916(92)90115-3).
- [46] Torbjörn Lundberg and Roman Pasechnik. “Thermal Field Theory in real-time formalism: concepts and applications for particle decays”. In: *The European Physical Journal A* 57.2 (2021), p. 71. ISSN: 1434-601X. DOI: [10.1140/epja/s10050-020-00288-5](https://doi.org/10.1140/epja/s10050-020-00288-5).
- [47] E. Wigner. “On Unitary Representations of the Inhomogeneous Lorentz Group”. In: *Annals of Mathematics* 40.1 (1939), pp. 149–204. ISSN: 0003486X.
- [48] Francesco Iachello. “Casimir Operators and Their Eigenvalues”. In: *Lie Algebras and Applications*. Berlin, Heidelberg: Springer Berlin Heidelberg, 2006, pp. 63–74. ISBN: 978-3-540-36239-5. DOI: [10.1007/3-540-36239-8_5](https://doi.org/10.1007/3-540-36239-8_5).
- [49] J.K. Lubański. “Sur la theorie des particules élémentaires de spin quelconque. I”. In: *Physica* 9.3 (1942), pp. 310–324. ISSN: 0031-8914. DOI: [10.1016/S0031-8914\(42\)90113-7](https://doi.org/10.1016/S0031-8914(42)90113-7).
- [50] Gunnar Källén. “On the definition of the Renormalization Constants in Quantum Electrodynamics”. In: *Helv. Phys. Acta* 25.4 (1952). Ed. by Cecilia Jarlskog, p. 417. DOI: [10.1007/978-3-319-00627-7_90](https://doi.org/10.1007/978-3-319-00627-7_90).
- [51] H. Lehmann. “Über Eigenschaften von Ausbreitungsfunktionen und Renormierungskonstanten quantisierter Felder”. In: *Il Nuovo Cimento* 11.4 (Apr. 1954), pp. 342–357. DOI: [10.1007/BF02783624](https://doi.org/10.1007/BF02783624).
- [52] L S Schulman. “UNSTABLE PARTICLES AND THE POINCARÉ SEMIGROUP.” In: *Ann. Phys. (N. Y.)* 59: 201-18(Jul 1970). (Jan. 1970). DOI: [10.1016/0003-4916\(70\)90400-8](https://doi.org/10.1016/0003-4916(70)90400-8).
- [53] F. J. Dyson. “The S Matrix in Quantum Electrodynamics”. In: *Phys. Rev.* 75 (11 1949), pp. 1736–1755. DOI: [10.1103/PhysRev.75.1736](https://doi.org/10.1103/PhysRev.75.1736).

- [54] Konrad Osterwalder and Robert Schrader. “Axioms for Euclidean Green’s functions”. In: *Communications in Mathematical Physics* 31.2 (1973), pp. 83–112.
- [55] H. Lehmann, K. Symanzik, and W. Zimmermann. “Zur Formulierung quantisierter Feldtheorien”. In: *Il Nuovo Cimento (1955-1965)* 1.1 (1955), pp. 205–225. ISSN: 1827-6121. DOI: [10.1007/BF02731765](https://doi.org/10.1007/BF02731765).
- [56] H. Arthur Weldon. “Thermal phase space”. In: *Annals of Physics* 214.1 (1992), pp. 152–159. ISSN: 0003-4916. DOI: [10.1016/0003-4916\(92\)90065-T](https://doi.org/10.1016/0003-4916(92)90065-T).
- [57] R. P. Feynman. “Space-Time Approach to Non-Relativistic Quantum Mechanics”. In: *Rev. Mod. Phys.* 20 (2 1948), pp. 367–387. DOI: [10.1103/RevModPhys.20.367](https://doi.org/10.1103/RevModPhys.20.367).
- [58] Jacob A. Barandes. *Manifestly Covariant Lagrangians, Classical Particles with Spin, and the Origins of Gauge Invariance*. 2019. DOI: [10.48550/ARXIV.1911.08892](https://doi.org/10.48550/ARXIV.1911.08892).
- [59] Shoji Ozaki. “Selection Rules for Interaction Types in Quantum Field Theory: ” in: *Progress of Theoretical Physics* 23.2 (Feb. 1960), pp. 221–228. ISSN: 0033-068X. DOI: [10.1143/PTP.23.221](https://doi.org/10.1143/PTP.23.221).
- [60] Domenico Giulini. *Superselection Rules*. 2007. DOI: [10.48550/ARXIV.0710.1516](https://doi.org/10.48550/ARXIV.0710.1516).
- [61] G. C. Wick, A. S. Wightman, and E. P. Wigner. “The Intrinsic Parity of Elementary Particles”. In: *Phys. Rev.* 88 (1 1952), pp. 101–105. DOI: [10.1103/PhysRev.88.101](https://doi.org/10.1103/PhysRev.88.101).
- [62] C. S. Wu et al. “Experimental Test of Parity Conservation in Beta Decay”. In: *Phys. Rev.* 105 (4 1957), pp. 1413–1415. DOI: [10.1103/PhysRev.105.1413](https://doi.org/10.1103/PhysRev.105.1413).
- [63] A. Alavi-Harati et al. “Observation of Direct CP Violation in $K_{S,L} \rightarrow \pi\pi$ Decays”. In: *Physical Review Letters* 83.1 (1999), pp. 22–27. DOI: [10.1103/physrevlett.83.22](https://doi.org/10.1103/physrevlett.83.22).
- [64] V. Fanti et al. “A new measurement of direct CP violation in two pion decays of the neutral kaon”. In: *Physics Letters B* 465.1-4 (1999), pp. 335–348. DOI: [10.1016/S0370-2693\(99\)01030-8](https://doi.org/10.1016/S0370-2693(99)01030-8).
- [65] O. W. Greenberg. “CPT Violation Implies Violation of Lorentz Invariance”. In: *Physical Review Letters* 89.23 (2002). DOI: [10.1103/physrevlett.89.231602](https://doi.org/10.1103/physrevlett.89.231602).
- [66] W. Pauli. *General Principles of Quantum Mechanics*. Springer-Verlag, 1980. ISBN: 9783540098423.
- [67] P.A.M. Dirac. *The Principles of Quantum Mechanics*. Comparative Pathobiology - Studies in the Postmodern Theory of Education. Clarendon Press, 1981. ISBN: 9780198520115.
- [68] F. J. Dyson. “Heisenberg Operators in Quantum Electrodynamics. I”. In: *Phys. Rev.* 82 (3 1951), pp. 428–439. DOI: [10.1103/PhysRev.82.428](https://doi.org/10.1103/PhysRev.82.428).
- [69] P Danielewicz. “Quantum theory of nonequilibrium processes, I”. In: *Annals of Physics* 152.2 (1984), pp. 239–304. ISSN: 0003-4916. DOI: [10.1016/0003-4916\(84\)90092-7](https://doi.org/10.1016/0003-4916(84)90092-7).
- [70] N.P. Landsman. “Consistent real-time propagators for any spin, mass, temperature and density”. In: *Physics Letters B* 172.1 (1986), pp. 46–48. ISSN: 0370-2693. DOI: [10.1016/0370-2693\(86\)90213-3](https://doi.org/10.1016/0370-2693(86)90213-3).

- [71] R. Mills. *Propagators for Many-particle Systems: An Elementary Treatment*. Gordon and Breach, 1969. ISBN: 9780677020402.
- [72] R. E. Cutkosky. “Singularities and Discontinuities of Feynman Amplitudes”. In: *Journal of Mathematical Physics* 1.5 (Sept. 1960), pp. 429–433. DOI: [10.1063/1.1703676](https://doi.org/10.1063/1.1703676).
- [73] P. Aurenche and T. Becherrawy. “A comparison of the real-time and the imaginary-time formalisms of finite-temperature field theory for 2, 3 and 4-point Green functions”. In: *Nuclear Physics B* 379.1 (1992), pp. 259–303. ISSN: 0550-3213. DOI: [10.1016/0550-3213\(92\)90597-5](https://doi.org/10.1016/0550-3213(92)90597-5).
- [74] T. S. Evans and A. C. Pearson. “Reexamination of the path-ordered approach to real time thermal field theory”. In: *Phys. Rev. D* 52 (8 1995), pp. 4652–4659. DOI: [10.1103/PhysRevD.52.4652](https://doi.org/10.1103/PhysRevD.52.4652).
- [75] N.P. Landsman and Ch.G. van Weert. “Real- and imaginary-time field theory at finite temperature and density”. In: *Physics Reports* 145.3 (1987), pp. 141–249. ISSN: 0370-1573. DOI: [10.1016/0370-1573\(87\)90121-9](https://doi.org/10.1016/0370-1573(87)90121-9).
- [76] Jacopo Ghiglieri et al. “Perturbative thermal QCD: Formalism and applications”. In: *Physics Reports* 880 (2020). Perturbative Thermal QCD: Formalism and Applications, pp. 1–73. ISSN: 0370-1573. DOI: [10.1016/j.physrep.2020.07.004](https://doi.org/10.1016/j.physrep.2020.07.004).
- [77] Martinus Veltman. *Diagrammatica: The Path to Feynman Diagrams*. Cambridge Lecture Notes in Physics. Cambridge University Press, 1994. DOI: [10.1017/CB09780511564079](https://doi.org/10.1017/CB09780511564079).
- [78] R. L. Workman and Others. “Review of Particle Physics”. In: *PTEP* 2022 (2022), p. 083C01. DOI: [10.1093/ptep/ptac097](https://doi.org/10.1093/ptep/ptac097).
- [79] Edward W. Kolb and Michael S. Turner. *The Early Universe*. Vol. 69. 1990. ISBN: 978-0-201-62674-2. DOI: [10.1201/9780429492860](https://doi.org/10.1201/9780429492860).
- [80] Leonid V Keldysh et al. “Diagram technique for nonequilibrium processes”. In: *Sov. Phys. JETP* 20.4 (1965), pp. 1018–1026.
- [81] Mathias Wagner. “Expansions of nonequilibrium Green’s functions”. In: *Phys. Rev. B* 44 (12 1991), pp. 6104–6117. DOI: [10.1103/PhysRevB.44.6104](https://doi.org/10.1103/PhysRevB.44.6104).
- [82] John C. Collins. *Renormalization: An Introduction to Renormalization, the Renormalization Group and the Operator-Product Expansion*. Cambridge Monographs on Mathematical Physics. Cambridge University Press, 1984. DOI: [10.1017/CB09780511622656](https://doi.org/10.1017/CB09780511622656).
- [83] J. Hadamard. *Le problème de Cauchy et les équations aux dérivées partielles linéaires hyperboliques*. French. 1932.
- [84] Marcel Riesz. “L’intégrale de Riemann-Liouville et le problème de Cauchy”. In: *Acta Mathematica* 81.none (1949), pp. 1–222. DOI: [10.1007/BF02395016](https://doi.org/10.1007/BF02395016).

- [85] A.A. Abrikosov et al. *Methods of Quantum Field Theory in Statistical Physics*. Dover Books on Physics. Dover Publications, 2012. ISBN: 9780486140155.